Optical methods for structure elucidation of protein-ligand interactions

Tardioli, S.

2011

Optical methods for structure elucidation of protein–ligand interactions: fluorescence and ultraviolet resonance Raman spectroscopy

Reading committee:

prof.dr.	A. González Ureña
prof.dr.	M.H.M. Janssen
prof.dr.	M. Smit
dr.	F. Ariese
dr.	A. Mank

Printed by Ipskamp Drukkers B.V., The Netherlands

VRIJE UNIVERSITEIT

Optical methods for structure elucidation of protein–ligand interactions: fluorescence and ultraviolet resonance Raman spectroscopy

ACADEMISCH PROEFSCHRIFT

ter verkrijging van de graad Doctor aan
de Vrije Universiteit Amsterdam,
op gezag van de rector magnificus
prof.dr. L.M. Bouter,
in het openbaar te verdedigen
ten overstaan van de promotiecommissie
van de faculteit der Exacte Wetenschappen
op dinsdag 15 november 2011 om 13.45 uur
in de aula van de universiteit,
De Boelelaan 1105

door

Silvia Tardioli

geboren te Assisi, Italië

promotor:	prof.dr. C. Gooijer
copromotor:	dr. G. van der Zwan

To those who supported me along the way

Happiness only real when shared

Chris McCandless
Into The Wild

Contents

Preface **V**

List of abbreviations, symbols, and prefixes **IX**

1 Introduction **1**

1.1 What is optical spectroscopy? 1

1.2 Characteristic features of fluorescence, phosphorescence, and Raman spectroscopy 2

1.3 Instrumentation 9

1.4 HSA —the protein 13

1.5 H_1 Antihistamines —the ligands TRP, MEP and BPA 16

2 UVRR spectroscopy: a distinctive probe of protein-ligand binding in solution **21**

2.1 Introduction 22

2.2 The technique 24

2.3 UVRR of proteins 29

2.4 Applications in protein–ligand binding 33

2.5 Conclusions 43

3 Anomalous photophysics of H_1 antihistamines in aqueous solution 49
3.1 Introduction . . . 50
3.2 Experimental . . . 53
3.3 Results and Discussion . . . 55
3.4 Conclusions . . . 74

4 Structure elucidation of fluorescent H_1 antihistamines by UVRR spectroscopy 77
4.1 Introduction . . . 79
4.2 Experimental . . . 82
4.3 Results and Discussion . . . 84
4.4 Conclusions . . . 101

5 Complementary fluorescence and phosphorescence study of the interaction of BPA with HSA 107
5.1 Introduction . . . 108
5.2 Experimental . . . 111
5.3 Results and Discussion . . . 113
5.4 Conclusions . . . 123

6 pH dependent complexation of antihistamines and HSA by UVRR spectroscopy 127
6.1 Introduction . . . 129
6.2 Experimental . . . 131
6.3 Results and Discussion . . . 135
6.4 Conclusions . . . 147
6.5 Supplementary Information . . . 149

Summary 155

Samenvatting 159

List of publications **163**

Acknowledgments **165**

Bibliography **167**

Preface

How ligands bind to proteins under physiological conditions is of key importance to essentially all biomolecular processes in the field of pharmacology and biochemistry. The question is quite challenging because it is not only limited to the determination of the (overall) association equilibrium constants, preferably information is obtained about the structure and kinetics of binding as well. Furthermore, molecular and spatial structural information is welcome since one usually deals with a multitude of sites in the protein, all potentially accessible to the ligand.

Much structural information is generally provided by computational methods and X–ray spectroscopy. For measurements under physiological conditions in principle various molecular spectroscopic methods are more appropriate. Among them are absorption in the ultraviolet and visible range, and fluorescence; those are routine techniques in protein–ligand analysis with the greatest versatility of applications, but unfortunately they generally do not provide many structural details. For this purpose, spectroscopic techniques with a much higher information content are desirable, such as nuclear magnetic resonance and the optical vibrational infrared and Raman spectroscopies. This in particular applies to resonance Raman spectroscopy, a sensitive and selective mode of conventional Raman spectroscopy active in the deep ultraviolet region

(< 260 nm) and therefore suitable for the study of proteins, which show ultraviolet absorption in that wavelength range. All of these techniques, however, have their inherent advantages and disadvantages.

This thesis presents a study of the use of fluorescence and ultraviolet resonance Raman spectroscopy, as means of elucidating molecular structures and aspects of protein–ligand interaction in solution. Three relevant pharmacological compounds —the H_1 antihistamines tripelennamine, mepyramine, and brompheniramine— and their interaction with the blood protein human serum albumin have been investigated for the first time by these techniques. H_1 antihistamines are used for supportive care of allergic manifestations and are selective binders to the H_1 G–protein coupled receptor. They also act in the central nervous system causing sedation because of weak binding ability to human serum albumin, which is the main transporter of these antihistamines in the blood to the receptors. The fundamental question on how those ligands act on the H_1 G–protein coupled receptor still remains unsolved. At the same time there is a lack of information on the kind of interaction occurring with serum proteins. The structure elucidation of those binding mechanism has obviously a relevance for the development of new drugs and therapies.

The aim of this thesis is therefore investigating the feasibility of using these H_1 antihistamines as intrinsic optical probes for structure elucidation in protein binding studies, since they exhibit native fluorescence and furthermore their electronic absorption spectrum extends far enough to the red so that they can be selectively excited, separately from the fluorescing amino acid residues in the protein. It allows us to make use of both native fluorescence and resonance Raman enhancement in the deep ultraviolet region (below 260 nm).

The thesis is divided into three parts. The introductory part is composed of Chapter 1 and Chapter 2. In **Chapter 1** some characteristic features of the spectroscopic methods used in the thesis, *i.e.* fluorescence, phosphorescence —though less prominent— and resonance Raman spectroscopy are first discussed with focus on the aspects related to the results provided in the subsequent chapters. In addition, a concise description of the instrumentation

is presented. Finally, the structure and properties of human serum albumin and the antihistamines are described briefly. In **Chapter 2** emphasis is put on the role of ultraviolet resonance Raman spectroscopy as a distinctive —but not yet well established— tool in protein–ligand analysis, through a survey of current analytical applications. The second part is devoted to the spectral characterization of the selected H_1 antihistamines in solution as a function of pH. In **Chapter 3** a detailed description of the complex photophysical properties of tripelennamine and mepyramine is given, based on conventional ultraviolet absorption and fluorescence excitation and emission spectroscopy, as well as time–resolved fluorescence spectroscopy. In **Chapter 4** the solution structures of tripelennamine and mepyramine were investigated by ultraviolet resonance Raman spectroscopy by utilizing reference compounds and a molecular modeling approach. In the third part binding of H_1 antihistamines to human serum albumin is explored under physiological and basic pH conditions (*i.e.* 7.2 and 9.0), in order to investigate the influence of ligand protonation on the binding affinity to the protein. A comparison is made with the H_1 antihistamine brompheniramine, which has a molecular structure similar to that of tripelennamine and mepyramine but but rather different spectroscopic behavior. In **Chapter 5** the binding of brompheniramine to human serum albumin is studied by measuring the quenching of tryptophan fluorescence and room temperature phosphorescence. Finally, in **Chapter 6** the binding behavior of tripelennamine, mepyramine, and brompheniramine to human serum albumin is successfully monitored by means of ultraviolet resonance Raman spectroscopy, and structural elucidation is achieved.

List of abbreviations, symbols, and prefixes

2AP	2–Aminopyridine
2DMP	2–(*N,N*–dimethylamino)pyridine
AP	Aminopyridine
BPA	Brompheniramine Maleate
C	Carbon
CNS	Central Nervous System
DAS	Decay Associated Spectrum
DMA	*N,N*–Dimethylaniline
F	Phenylalanine
FRET	Förster Resonant Energy Transfer
FTIR	Fourier Transform Infrared
GPCR	G–Protein Coupled Receptor
H	Hydrogen
HSA	Human Serum Albumin
IR	Infrared
IRF	Instrument Response Function
M	Molarity
MEP	Mepyramine Maleate
N	Nitrogen
NIR	Near Infrared

NMR	Nuclear Magnetic Resonance
O	Oxygen
PMT	Photomultiplier Tube
RR	Resonance Raman
RS	Raman Spectroscopy
RTP	Room Temperature Phosphorescence
TCSPC	Time Correlated Single Photon Counting
TRP	Tripelennamine Hydrochloride
UV	Ultraviolet
UVRR	Ultraviolet Resonance Raman
VIS	Visible
Y	Tyrosine
W	Tryptophan
λ	wavelength
μ	micro (10^{-6})
ν	frequency
$\tilde{\nu}$	wavenumber
m	milli (10^{-3})
n	nano (10^{-9})
p	pico (10^{-12})

Chapter 1

Introduction

1.1 What is optical spectroscopy?

The interaction of electromagnetic radiation with atoms and molecules is the process behind any spectroscopic method. Electromagnetic radiation, of which visible light is an example, is a wave of oscillating electric and magnetic fields propagating through space. The smallest possible units are elementary particles called photons, each traveling in a wave–like pattern at the speed of light (c) and carrying a discrete amount of energy ϵ which depends on the frequency or wavelength of the radiation according to

$$\epsilon = h\nu = \frac{hc}{\lambda} = hc\tilde{\nu}$$

where h is Planck's constant, ν the frequency of the electric and magnetic field oscillation, λ the wavelength of the oscillation, and $\tilde{\nu}$ is the corresponding wavenumber, in units of inverse length (cm^{-1}). Optical methods make use of electromagnetic radiation having wavelengths from about 200 nm to a few μm. This interval comprises the UV (200–400 nm), the VIS (400–700 nm) and the

NIR region (above 700 nm). UV absorption, fluorescence, and phosphorescence involve phenomena concerned with radiation in the region from 200 to 800 nm; UVRR spectroscopy is primarily related to the UV spectral range. The methods used in this thesis deal with valence electrons —the electrons of an atom that can participate in the formation of chemical bonds— that have the ability to absorb, emit, and scatter energy of electromagnetic radiation in the form of photons.

1.2 Characteristic features of fluorescence, phosphorescence, and Raman spectroscopy

The processes that occur with the absorption and emission of light are usually illustrated by the Jablonski diagram, where the electronic states of molecules are quantized according to energy levels and spin multiplicity (singlet, S, and triplet, T, states). In Figure 1.1 a simplified Jablonski diagram for an organic molecule is depicted, showing the lower singlet electronic states S_0, S_1, and S_2 and the lowest triplet electronic state T_1. Additionally, some vibrational states are included (denoted by v= 0, 3) and furthermore the radiative transitions operative in fluorescence, phosphorescence, and conventional RS are indicated. However, some features should be noted.

Absorption of an UV or VIS photon promotes a valence electron of a molecule from its ground state, usually an S_0 state, to an excited state with conservation of the electrons spin. For an electronic transition to occur the photon energy must be equivalent to the energy difference between the initial and the final electronic state. Transitions occur in about 10^{-15} s, a time too short for significant displacement of nuclei. This is the Franck–Condon principle. After excitation of the molecule, the first part of the decay path (via vibrational relaxation and internal conversion) is non–radiative, down to the lowest vibrational state of S_1. It implies that the excitation spectra in fluorescence and phosphorescence have identical shapes. They are also equal in shape to the

absorption spectrum if there are no other sample constituents available and inner filter effects are negligible.

Fluorescence is observed if the molecule takes the radiative $S_1 \rightarrow S_0$ route for deactivation. So the quantum yield of fluorescence, which is the fraction of excited molecules returning to the ground state by fluorescence, is given by

$$\phi_f = \frac{\kappa_f}{\kappa_f + \kappa_{nf} + \kappa_{isc} + \sum \kappa_q[Q]} = \kappa_f \tau_f$$

where κ_f, κ_{nf}, and κ_{isc} are the monomolecular rate constants of the fluorescence decay, non–fluorescence decay and inter–system crossing, respectively, and κ_q is the bimolecular rate constant for quenching by a compound Q [1]. The fluorescence lifetime is given by τ_f and represents the mean time during which the molecule remains in the excited singlet state before returning to the ground state. This time ranges from nanoseconds (10^{-9} s) to picoseconds (10^{-12} s) and it is dependent on the effectiveness of the competing relaxation processes leading to decay of the emitting state. The decay from the excited state is a random process that in most cases follows a single exponential behavior and is dependent on its lifetime via:

$$I_f(t) = I_0 \exp(-t/\tau_f)$$

where I_0 is the fluorescence intensity at time $t = 0$. $I_f(t)$ is the intensity decay or the time distribution of emitted photons [1]. According to the intensity decay distribution, the fluorescence lifetime is defined as the time in which the population of the excited state is reduced to $1/e$ of the initial population and defines the window in which dynamic phenomena can be observed. After about $10\tau_f$ observation of fluorescence is no longer possible. On the other hand, processes slower than $1/10\tau_f$ will not affect the decay at all.

Phosphorescence is observed if the molecule follows the inter–system crossing pathway $S_1 \rightarrow T_1$ and subsequently the radiative $T_1 \rightarrow S_0$ transition for deactivation. Since both transitions are spin forbidden they can be strengthened by including heavy atoms in the molecular system. The phosphorescence

lifetime τ_p is the lifetime of the T_1 state given by

$$\tau_p = \frac{1}{\kappa_p + \kappa_{np} + \sum \kappa_q[Q]}$$

where κ_p and κ_{np} are the monomolecular rate constants of phosphorescence and non–radiative decay respectively, and κ_q the bimolecular rate constant of quenching by a compound Q [1]. Since κ_p is much lower (at least 10^6 times) than κ_f, bimolecular quenching is much more effective in phosphorescence than in fluorescence. To obtain efficient liquid state RTP sample deoxygenation is a prerequisite.

As regards excited state energy transfer to an acceptor, in fluorescence the Förster mechanism

$$D^*(S_1) + A(S_0) \longrightarrow D(S_0) + A^*(S_1)$$

dominates, in which D and A represent donor and acceptor, and transfer occurs through long–range dipole dipole interactions [1].

In phosphorescence the Förster mechanism is usually not operative since

$$D^*(T_1) + A(S_0) \longrightarrow D(S_0) + A^*(T_1)$$

is doubly spin–forbidden. In phosphorescence one therefore deals with the collisional–induced Dexter transfer mechanism, only operative at short distances [1]. Contrary to what might be expected on the basis of Figure 1.1, in absorption, fluorescence, and phosphorescence spectra in frozen or liquid solutions, no sharp transitions are observed. They are inhomogeneously broadened: because of interaction with the immediate surroundings any particular molecule has its own electronic state energy so that in a spectroscopy experiment one deals with a distribution of slightly different S_0, S_1, S_2 and T_1 energies. In RS such inhomogeneous line broadening plays a much less important role so that the S_0 state vibrations are clearly seen and high–resolution spectra are obtained.

As can be seen in Figure 1.1, in conventional RS the incident photon energy is too low to accomplish an electronic transition. For absorption and emission of a photon to occur, radiation of a specific energy —corresponding to a

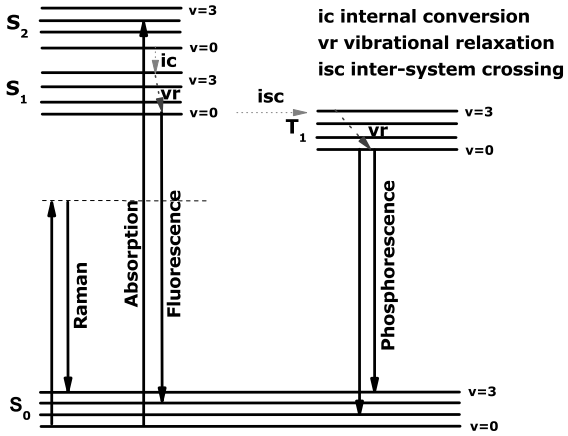

Figure 1.1: Jablonski Diagram.

particular electronic transition within the molecule— is required. The Raman effect is not caused by absorption or emission of radiation of specific energy (resonance), but relies on a different mechanism of interaction between radiation and molecules, named scattering, and takes place at any wavelength (non resonance). Raman scattering is a general property of matter dependent on its electric polarizability (α) and probes the characteristic vibrational bands of chemical groups as the atoms move with respect to one another in response to the oscillating electromagnetic field ($\vec{E}$). It is therefore a type of vibrational spectroscopy. A simple classical electromagnetic field description of Raman scattering can be used to explain the important features of Raman band intensities and position [2, 3, 4]. When a molecule interacts with the the incident radiation, the electric field $\vec{E}$ of the beam induces a dipole moment $\vec{\mu}$ in the

Relaxation process	Details
Vibrational relaxation	Involves transitions between a vibronically excited state and the v=0 state within a given electronic state when an excite molecule collides with solvent molecules. The excess vibrational energy is dissipated as heat.
Internal conversion	Involves radiationless transitions between vibronic states of different electronic transitions and same multiplicity.
Inter–system crossing	Intra–molecule spin forbidden radiationless transitions between isoenergetic states of different multiplicity.
Fluorescence	Photon emission from the lowest vibrational level of the lowest excited singlet state.
Phosphorescence	Photon emission from states of different multiplicity, usually from the lowest vibrational level of the lowest excited triplet state.

Table 1.1: Summary of the absorption and emission properties shown in Figure 1.1.

molecule related to $\vec{E}$ by a linear relationship:

$$\vec{\mu} = \alpha\vec{E}$$

where α is the polarizability tensor, an element indicating the ease with which the electron cloud in a bond can be distorted. The induced dipole will radiate with intensities proportional to $|\mu|^2$ in all directions at the frequency (energy) of the incident radiation $\vec{E}$. This is the basis for the elastic or Rayleigh scattering process. If the polarizability of the molecule changes as the bond distorts,

non–linear effects give rise to dipole oscillation at frequencies other than the imposed frequency and the induced frequency (energy) of the dipole oscillation is reduced/increased by an amount corresponding to the normal mode vibration in the molecule itself. Hence, the resulting frequency of the scattered radiation will be shifted because some energy is used to excite/de-excite the molecular vibration. This shift in frequency (Stokes/Anti–Stokes shift) is the basis for RS. If a vibration does not greatly change the polarizability the intensity of the Raman bands will be low.

The plot of the intensity of the scattered light versus the Raman shift, *i.e.* the energy difference between the incident and the scattered light expressed in wavenumbers ($\tilde{\nu}$) is called a Raman spectrum. Numerically, the Raman shift is calculated through

$$\tilde{\nu} = \frac{1}{\lambda_{incident}} - \frac{1}{\lambda_{scattered}}$$

in which $\lambda_{incident}$ and $\lambda_{scattered}$ are the wavelengths —expressed in centimeter (10–2 meter— of the incident radiation and Raman scattered photons respectively.

1.2.1 Resonance Raman spectroscopy

Conventional RS is a process with an inherently very low probability, (*ca.* 1 in 10^7 photons is scattered inelastically) but the scattered intensity can be increased by several order of magnitudes if the wavelength (energy) of the incident radiation matches an electronic transition of the molecule (resonance) [5, 6]. In other words if it coincides with an electronic absorption band, as in fluorescence and phosphorescence. This is visualized in Figure 1.2, assuming that the excitation energy is close to the $S_0 \longrightarrow S_2$ transition.

In fact the molecular polarizability α depends on the excitation wavelength. It is inversely proportional to the difference between the energy of the incident photon ν_0 and the energy of a certain electronic transition $S_n \rightarrow S_0$ according

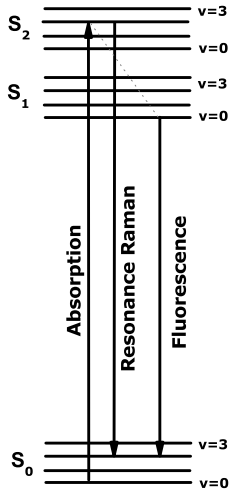

Figure 1.2: Energy diagram of UVRR spectroscopy.

to:

$$\alpha \sim \frac{1}{(S_n \rightarrow S_0) - \nu_0}$$

The intensity of the Raman signal is proportional to the square of α and the fourth power of ν_0 according to:

$$I \sim I_0 {\nu_0}^4 \alpha^2$$

It follows that when the incident photon energy approaches the energy of an electronic transition the intensity of the Raman signal increases dramatically (with a factor up to 10^6) for totally symmetric vibrations in resonance with the radiation energy.

With resonance excitation the energy of the incident radiation is large enough to promote the molecule dealt with to an excited electronic state. Contrary to

fluorescence, in RRS the non–radiative decay path via vibrational relaxation and internal conversion to the lowest vibration of the S_1 state plays no role. Scattering is an instantaneous process taking place on a faster than femtoseconds time scale (10^{-15} s).

1.3 Instrumentation

1.3.1 Steady–state fluorescence and phosphorescence

The basic design of instrumentation for monitoring molecular fluorescence and phosphorescence comprises three basic items: a source of light, a sample holder, and a detector. However, for phosphorescence to be discriminated from fluorescence, a delay between excitation and measuring phosphorescence emission has to be set. Fluorescence and phosphorescence excitation is achieved by a Xenon lamp, with a continuum output allowing any wavelength through the UV–VIS region of the spectrum to be selected. In the phosphorescence mode the xenon lamp sends a μs pulse of light at selected time intervals (16 ms). To isolate a particular wavelength from the source, monochromators are used for both the excitation and emission wavelengths. Photons impinge on the excitation monochromator, which selectively transmits light in a narrow range centered about the specified excitation wavelength. The transmitted light passes through adjustable slits that control the intensity and resolution by further limiting the range of transmitted light. The filtered light passes into the sample cell causing fluorescence emission by molecules within the sample. Emitted light enters the emission monochromator, which is positioned at a 90° C from the excitation light path and exits through adjustable slits, finally reaching the photomultiplier tube. The signal is amplified and creates a voltage difference that is proportional to the measured emitted intensity. An emission spectrum is the wavelength distribution of an emission measured at a single excitation wavelength. Conversely an excitation spectrum is the dependence

of emission intensity, measured at a single emission wavelength upon scanning the excitation wavelength.

1.3.2 Time–resolved fluorescence

A schematic representation of the setup used to record fluorescence lifetimes is shown in Figure 1.3. The sample is irradiated with a very short–duration light pulse (3 ps) of a Mira 900-P Ti:Sapphire laser to ensure any molecule will only be excited once during the pulse. At the repetition rate of the laser is applied (76 MHz) an excitation pulse would occur every 13 ns, which is too short a time span in view of the relevant fluorescence lifetimes. Therefore the repetition rate is reduced twenty fold to 3.8 MHz using a pulse picker (APE PulseSelect, Berlin, Germany). The laser is pumped by an Innova–300 argon ion laser (Coherent) to provide laser light that is tunable from 700 to 1000 nm. To enable excitation at 245 nm and 295 nm a frequency tripler (Oplaz Technologies fs-tripler, Chatsworth CA, USA) is used. Fluorescence emission is collected at a 90° angle and dispersed by a monochromator (TVC JarrellAsh Monospec 18, Grand Junction CO, USA). A multichannel-plate photomultiplier (Hamamatsu, R3809U-50) collects the fluorescence emission, and data are recorded through a SPC-630 module (Becker & Hickl GmbH, Berlin, Germany) with a time resolution of 15 ps.

The TCSPC technique is used to determine fluorescence intensity decays. The principle of detection is based on the timespan between a start and a stop photon. For a full description of the TCSPC method we refer to [7]. The start photon coming directly from the laser source is detected by a photodiode producing an electrical signal that starts charging a capacitor. The same laser pulse excites the sample, which will emit a photon after a certain delay time. This photon is detected on a photomultiplier tube and provides the stop signal. The charge is then read out, and related to the time between the start and stop signal . After recording many of these start–stop cycles, a histogram of individual photon arrival times can be constructed. This histogram is the intensity

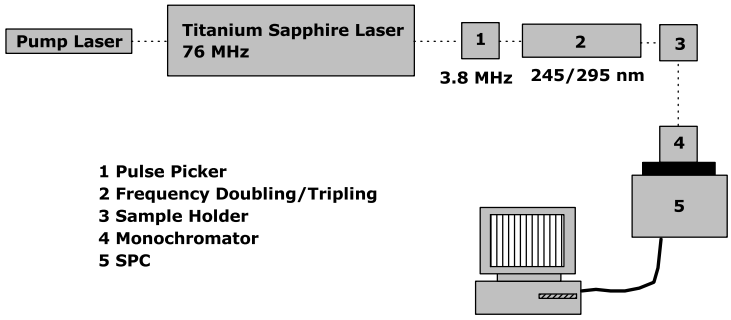

Figure 1.3: Scheme of the setup used for time–resolved fluorescence measurements.

decay curve and is fitted to an exponential function, or a sum of exponential functions, to obtain fluorescence lifetimes. In order to obtain the fluorescence lifetime, the profile of instrument response function (excitation pulse) has to be measured in addition to the fluorescence decay. This is because the laser pulse has a finite temporal width, which distorts the intrinsic fluorescence response from the sample. In addition the instrument response (about 25 ps)needs to be taken into account by a process called deconvolution. In a typical experiment, two decays are measured: the instrument response function (IRF) using a scatterer solution, and the decay curve. Analysis is then performed by convoluting the IRF with a model function (*e.g.* a single or double exponential decay, or some other function) followed by comparison with the experimental decay. This is done by an iterative numerical procedure until the best agreement with the experimental decay curve is achieved.

1.3.3 UVRR spectroscopy

A sketch of the setup used to record UVRR spectra is shown in Figure 1.4. A line of an Innova FreD 90C (Coherent, Utrecht, The Netherlands) continuous frequency–doubled argon ion laser (typical power: 6 mW at 229 nm; 40 mW at 244 nm; 40 mW at 257 nm) is projected on to a Pellin-Broca prism, to remove the fundamental laser line. The beam is then enlarged by a factor of 6 using a telescope consisting of two plano convex lenses L1 (focal length f = 50 mm) and L2 (f = 300 mm) Via a beam splitter BS (model MUVBS45-FS-1D; Acton Research) the laser line is projected onto a sample holder. The scattered radiation is then collected via the same objective (backscattering geometry). Removal of the laser line was achieved by using a dielectric stack filter HPF

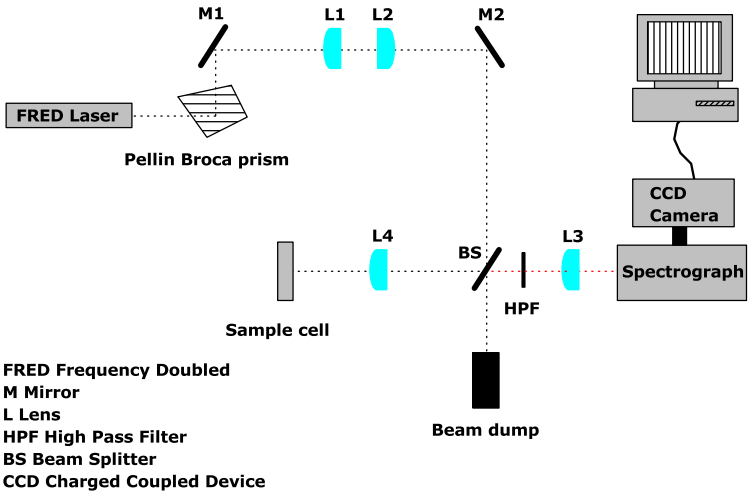

Figure 1.4: Scheme of the setup used for UVRR measurements.

(Omega Optical, Brattleboro, VT). Finally the scattered light was projected via a focusing lens (f = 100 mm) to a single-stage 0.5 m spectrograph (Spex model 1870, Edison, NJ) equiped with a grating of 3600 grooves/mm. The Raman spectra were recorded with a cooled (-50° C) Andor Technology model DV420-OE CCD camera (Belfast, Northern Ireland). For spectral calibration, the spectrum of cyclohexane was used according to [8]. For the protein measurements the set–up was modified as described in Chapter 5.

1.4 HSA —the protein

1.4.1 Structure and binding sites

HSA is an abundant plasma protein (35–50 mg/ml) that binds a remarkably wide range of drugs, thereby restricting their free, active concentrations. Its role is recognized as an important factor in disposition of H_1 antihistamines to the H_1 receptor and to the central nervous system, thereby causing sedation [9]. HSA comprises a chain of 585 amino acids containing a single tryptophan (W214) and a large number of charged amino acids, which provide a calculated net charge of −15 at pH 7.0 [10]. The three-dimensional structure of HSA is composed of three α-helical homologous domains (I, II and III) that assemble to form a heart–shaped molecule as shown in Figure 1.5.

Each domain is a product of two subdomains (A and B) that possess common structural motifs. Crystallographic analysis of seventeen different complexes of HSA with a wide variety of drugs and small-molecule toxins has revealed the precise architecture of the two primary drug-binding sites on the protein, identifying residues that are key determinants of binding specificity, and illuminating the capacity of both pockets for flexible accommodation. The principal regions of ligand binding are located in hydrophobic cavities in subdomains IIA (Drug site 1) and IIIA (Drug site 2), which exhibit similar chemistry. The single tryptophan residue is located in sub–domain IIA, which is a pocket with the

inside wall being formed by hydrophobic side chains and the entrance of the pocket being surrounded by positive charge residues. Drug site 2 entrance is more exposed to solvent and has a single main polar patch located close to one side of the entrance centered on tyrosine residue Y411 [11]. HSA contains eighteen tyrosine residues and among them Y411, located in sub–domain IIIA has been implicated in the binding process by several studies [12]. Numerous secondary binding sites for drugs distributed across the protein have also been identified.

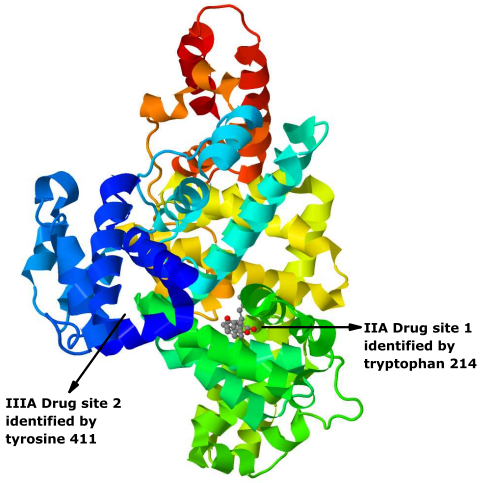

Figure 1.5: Crystal structure of HSA complexed with warfarin in binding site I. The structure was obtained from the Protein Data Bank (ID code 1ha2) [11]. Protein structure is shown in the ribbon model identifying the three domains I, II, and III, labeled in red, green, and blue, respectively.

1.4.2 Spectral properties of HSA

Proteins contain three amino-acid residues responsible for fluorescence, *i.e.* tryptophan, tyrosine, and phenylalanine, but only tyrosine and tryptophan fluorescence are used experimentally because their quantum yield is high enough to give a good fluorescence signal. Tyrosine emission is easily quenched as a result of energy transfer (FRET) to surrounding tryptophan residues or excited state dissociation of the hydroxyl group at neutral pH. This explains why the emission spectrum of HSA resembles the emission of tryptophan, despite the presence of eighteen tyrosine residues. The tryptophan residue of HSA emits with more than one lifetime due to either multiple conformations or the intrinsic heterogeneity of tryptophan itself [1]. The general aspects of protein fluorescence have been described extensively elsewhere [1, 13]. The tryptophan residue of HSA also exhibits room temperature phosphorescence [14] with a multiexponential decay. The most valuable feature of the intrinsic fluorescence/phosphorescence of tryptophan is the high sensitivity to its local environment [1]. Interaction with a ligand can in fact induce perturbation or modification in intensity and/or lifetimes of tryptophan if binding occurs within the range of the fluorescence/phosphorescence lifetimes. In the present thesis we show how use can be made of the intrinsic HSA fluorescence/phosphorescence to monitor ligand binding. The analysis is aided by the fact that the protein only possess one single tryptophan and so we can be confident about the origin of the signal and on the area implicated in binding. This situation is not typical and often methods must be devised to discriminate the fluorescence/phosphorescence originating from several tryptophans within a protein.

Another important peculiarity of tryptophan is its sensitivity to collisional quenching, a contact phenomenon that results in the loss of excitation energy as heat instead of as fluorescence/phosphorescence [15]. Molecular contact between the protein and the ligand is required for collisional quenching to occur, therefore measurements of collisional quenching can be useful for determining the accessibility of the fluorescent moiety within the protein. This method

will be used in this thesis for the evaluation of BPA association constant, from intrinsic fluorescence/phosphorescence quenching of HSA.

The aromatic amino acids —phenylalanine, tyrosine and tryptophan— and the peptide bonds of proteins are responsible for UV electronic absorption. Therefore by resonance excitation in this spectral region the vibrations of those molecular groups dominate the Raman spectra of proteins. The analysis of aromatic amino acids contribution to UVRR spectra of proteins and their application for the study of protein–ligand interactions will be reviewed in Chapter 2.

1.5 H_1 Antihistamines —the ligands TRP, MEP and BPA

1.5.1 The H_1 receptor

Histamine, a major mediator of allergic disorders such as rhinitis, asthma, urticaria, and anaphylaxis, exerts its specific effects through interaction with one of four distinct GPCR's (H_1 to H_4). The histamine H_1 receptor plays an important role in allergic conditions and counts the largest number of human drug targets under its members. The H_1-GPCR is a single seven–helical integral membrane protein. Activation of the receptor by binding of histamine leads to a conformational change in receptor topology that propagates through the membrane domain and, in turn, binds and activates a G-protein at the intracellular side, that mediates follow-up cellular responses [16, 17]. Ligands that competitively block effects of histamine on corresponding receptor regions are called antihistamines. In particular, H_1 antihistamines, or H_1 inverse agonists, competitively bind to H_1–GPCR thus preventing histamine from binding and activity (antagonism).

The crystal structure of the H_1 receptor complex with a first generation H_1 antagonist, doxepin, and the atomic details of binding were recently revealed [18]. Doxepin sits deep in the ligand–binding pocket and directly inter-

acts with tryptophan 428, a highly conserved key residue in GPCR activation with mostly hydrophobic nature. In addition, it is the tryptophan residue 167 in transmembrane domain 6 (TM 6) of the receptor to be indicated as probable interaction point with the H_1 antihistamines investigated in this study [19], (see subsection 1.5.3).

1.5.2 Structure

The general formula of the H_1 antihistamines studied in this thesis is presented in Figure 1.6 where comparison is made with histamine, in view of their structural similarity. H_1 antihistamines are composed of two aromatic rings, *i.e.* the AP chromophore and a substituted benzene. These rings are connected via a nitrogen N, carbon C, or oxygen O, linkage X to the ethylamine group $(CH_2)_2NR_1R_2$. Unlike that of histamine, the nitrogen of the ethylamino group is tertiary with two alkyl substituent groups R_1 and R_2, usually methyl groups. The substituted ethylamine side chain is protonated under physiological conditions and the groupis essential for H_1 antihistamine binding to the receptor. The three ligands investigated in this study are shown in Figure 1.7. We will show in Chapter 3 and 4 that the presence of the nitrogen atom at the linkage position with the ethylamino group is fundamental for the existence of TRP and MEP isomers in solution.

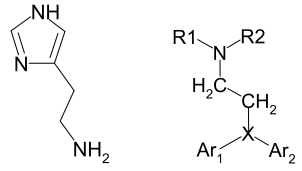

Figure 1.6: (Left) Structure of histamine and (Right) general structure of H_1 antihistamines. Ar_1 and Ar_2 are carbocyclic or heterocyclic aromatic rings.

Three features of H_1 antihistamines are essential for agonism. First, the

presence of multiple aromatic or heterocyclic rings and alkyl substituents in these agonists results in liphophilic properties, in contrast to histamine, which is a hydropilic compound. Second is the basicity of the nitrogen groups the closer the pK_a is to 8.6 the more potent the compound is. Third is the nature of the linkage atom X. Unique stereo chemistry of interaction is recognized as the requirement for optimum activity upon drug–receptor interactions. H_1 antihistamines cause CNS side effects upon drug ingestion. The highly lipophilic nature of the H_1 antihistamines allows them to penetrate well into the CNS where they induce sedation. This is thought to be related to weak binding to serum proteins [9]. Binding of those ligands to plasma proteins is therefore an important issue for their biological efficacy, since it modulates drug availability to the intended target. This topic will be discussed in Chapters 5 and 6.

1.5.3 Binding mechanism. Role of the tail.

The aspartic acid residue conserved within the third transmembrane domain (TM 3) of the H_1 receptor is crucial for the binding of histamine and H_1 antihistamine to the H_1 receptor. For both ligands, binding is mediated by the ionic interaction of the protonated primary or tertiary amine function side chain and the negatively charged aspartate residue [20]. For the binding of H_1 antihistamines, mutational studies have further identified other amino acids in TM 6, like tryptophan and phenylalanine, as binding partners of the AP ring [19, 21]. These large conformational changes of TM 3 and TM 6 are considered to be an important step in the process of GPCR activation and have received experimental support from various biophysical and mutational studies.

1.5.4 Spectral properties

TRP and MEP show native fluorescence owing to the aromatic bonds of the π systems characterizing their structure (Figure 1.7). Those ligands can be

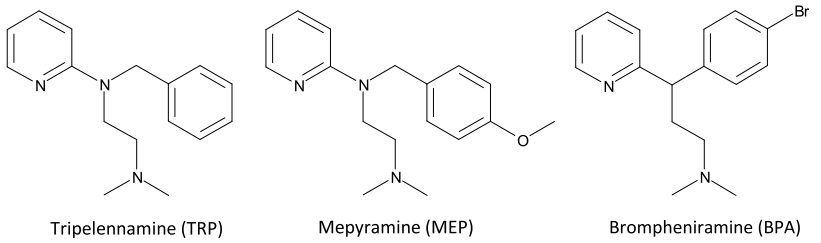

Figure 1.7: The chemical structure of H_1 antihistamines investigated in this study. They share a common structure consisting of an AP chromophore (intracyclic ring nitrogen) and a substituted benzene ring connected to the ethylamino side chain by a linkage atom (N or C).

selectively excited in the presence of a protein at longer wavelengths (≥ 310 nm) than tryptophan. In contrast BPA does not show any fluorescence in solution presumably because of the presence of the heavy atom Br that quenches ligand fluorescence.

Despite the potential applicability of TRP and MEP as intrinsic fluorescent probes, little definite spectroscopic information was available when we started to investigate their photophysics in solution. Our study will demonstrate that the absorption/fluorescence properties of TRP and MEP are rather complex due to the presence of three protonable nitrogens, intramolecular H–bonding, possibility of excited state electron transfer, quenching due to the formation of a charge transfer state, and intramolecular FRET (see Chapter 3). In addition, the three ligands show electronic absorption in the UV region, which therefore enables to make use of UVRR spectroscopy. It will be shown in Chapter 4 that RR enhancement below 260 nm originates from the vibrations of the AP group of the three ligands investigated, and that several vibrations of the moiety will be affected by binding to HSA (see Chapter 6).

Chapter 2

UVRR spectroscopy: a distinctive probe of protein-ligand binding in solution[2]

[2] The contents of this Chapter were submitted for publication by Silvia Tardioli, Cees Gooijer, and Gert van der Zwan.

Abstract Ultraviolet resonance Raman (UVRR) spectroscopy —a technique based on laser light with a wavelength shorter than 260 nm— is an exceptionally sensitive and selective tool for studying protein–ligand binding in solution. More importantly at these laser wavelengths fluorescence background hardly plays a role. Despite the distinctive power of the technique only a few studies are available in literature. Hence this review aims at exhibiting how much specific structural information can be inferred from UVRR spectroscopy on protein–ligand binding mechanism, through survey of representative applications of the technique in this field. Basic principles of UVRR spectroscopy and experimental aspects on the recording and assignment of protein–ligand spectra will be covered. The resonance enhancement mechanism of internal chromophores within proteins will be discussed, as well as their sensitive environmental markers.

2.1 Introduction

Experimental methods that give structural information about binding of ligands and substrates to proteins in aqueous solution are of paramount importance and UVRR spectroscopy represents a distinctive analytical tool for direct elucidation of protein structure in its native environment. The potential of UVRR in analytical chemistry has been clearly outlined by Asher already more than fifteen years ago [5, 6]. In recent years the technique was successfully employed in several bioanalytical applications, as reported elsewhere [22, 23]. However, the acceptance of the method by the analytical community has been relatively slow in view of the high cost and the poor tunability of lasers in the deep UV. In particular laser tunability or even more demanding scannability, would be quite attractive in UVRR since the resonance enhancement achieved is related to the extinction coefficient (ϵ) of the analyte. As a rule of thumb it is proportional to ϵ^2. In fact, for resonance enhancement of the Raman signal to occur, the energy of the laser radiation has to overlap with an electronic ab-

sorption of the molecule investigated, and since the vast majority of molecules do absorb in the spectral range below 260 nm, UVRR spectroscopy in principle has a very wide applicability. At the resonance condition Raman vibrations related to specific electronic transition are tremendously enhanced compared to other molecular vibrations so that, in case of big molecules comprising various chromophoric groups, selective examination of parts of the molecule can be obtained. Internal chromophores within proteins absorbing UV light are certain amino acids and peptide groups, which resonate with the UV Raman excitation and are amenable to study with UVRR. This selectivity has some rather important consequences in the study of protein–ligand binding in solution since via selective enhancement of the amino acid residues their hydrophobic/hydrophilic surroundings as well as H–bonding and π–cation interactions can be probed. Furthermore, enhancement of the polypeptide backbone vibrations is directly related to the secondary structure of proteins.

The principal objective of this chapter is to survey representative applications (among the few available from literature) of UVRR to protein–ligand binding to show how much specific structural information can be inferred on the binding mechanism and to discuss its future prospects as a trend in analytical chemistry. Emphasis is also given to those basic principles of the technique related to selectivity and sensitivity and to those experimental aspects directly involved in recording and assignment of protein–ligand spectra. The resonance enhancement mechanism of internal chromophores within proteins will be discussed, as well as their sensitive environmental markers. As will be outlined below, UVRR spectroscopy is a prospective analytical technique providing a wealth of structural information about protein–ligand interactions. Of course it is not the only tool. It should be considered as complementary to X–ray crystallography (applicable if the protein can be crystallized) and NMR if liquid solution (applicable if sufficiently high concentrations can be handled in liquid solution).

2.2 The technique

2.2.1 Basic aspects of UVRR

Raman spectroscopy (RS) probes the vibrational modes of molecules and relies on the inelastic scattering of light. Principles of Raman theory have been extensively reviewed in the past and for a in–depth examination we refer to references [5, 24, 25]. In the scattering process quanta of energy are transferred from a beam of intense monochromatic radiation (laser photons) to the target molecule with which the photons interact. The transferred energy is typically a small fraction of the total energy of the incident photon. The quanta are gained by the molecule in the form of discrete vibrational energies, which constitute the Raman frequencies. These frequencies, along with their relative scattering probabilities (Raman intensities) and tensor characteristics (Raman polarizations), constitute the Raman spectrum of the molecule. The changes in molecular geometry or conformation that characterize many molecular biological phenomena can produce relatively large changes in Raman band intensities and positions (frequency shifts). Such changes are the basis for applications of the technique to analyze the vibrational structure of molecules and their interactions.

In conventional RS the excitation wavelength of the laser is in the green—near infrared spectral region above 400 nm. Conversely UVRR employs short wavelength UV lasers (below 260 nm) that are coincident (resonance condition) with the electronic absorption band of many molecules. The resonance Raman effect leads to well established advantages over conventional RS in terms of sensitivity, selectivity and —in the deep UV range— there is negligible fluorescence background interference [5, 6]. In resonance excitation, the induced dipole moment of the chromophore becomes much larger compared to conventional RS, causing an increase (10^6 or more) in intensity of the Raman scattering signal [26]. The sensitivity reached at the resonance condition has led to record vibrational Raman spectra of dilute protein solution in the range 0.5–2 mg/mL [27]. The enhancement of the Raman signal happens for a few

of the molecular vibrations, giving resonance Raman much greater selectivity than conventional RS. In fact, only the Raman bands of the chromophores that are in resonance at the wavelength of excitation, are significantly enhanced. Raman bands of non–absorbing species are not enhanced and do not interfere with those of the chromophore. It should be emphasized that —contrary to both RR spectroscopy in general and to conventional Raman spectroscopy where fluorescence interference frequently overwhelms the signal— in UVRR such a problem hardly plays a role. As it has been pointed out already as early as 1984 [28] there are two main reasons for this diminished fluorescence background. Firstly, fluorescent molecules typically emit at wavelengths longer than 300 nm, long enough not to interfere with the UVRR spectra. Molecules exclusively absorbing below 260 nm usually have a negligible fluorescence quantum yield, because most do not have a rigid structure. Such molecules undergo significant molecular rearrangement upon excitation and return to the ground state via non–radiative processes.

2.2.2 Instrumentation

For optimum UVRR spectroscopy, low–cost continuous–wave (CW) lasers should be available (to avoid photodegradation as much as possible), easily tunable or even scannable, over the 190–270 nm range (to fully exploit UVRR inherent selectivity). These conditions are not yet fully met at this very moment, but important progress has been achieved over the last decades. In the early 1980's laser wavelengths below 300 nm required optical nonlinear conversion processes and numerous excitation frequencies in the deep UV were obtained combining frequency tripling, quadrupling, and quintupling of low duty cycle Nd:YAG lasers with H_2 gas Raman shifting [29]. More recently, higher duty cycle XeCl excimer lasers were adopted. Nevertheless, shot–to–shot laser intensity fluctuations and ground state depletion were inherent to their use [30, 31]. An even higher barrier for UVRR spectroscopy to be accepted as an anlytical tool is the sample photodegradation problem. In particular

low duty cycle lasers characterized by high peak powers cause serious effects; photodegradation is strongly reduced if CW lasers or pulsed lasers with high repetition rate (up to 80 MHz) are used [32], preferably in combination with continuous flow stirring or spinning of the sample [5, 33]. That is why revolutionary advance in Raman excitation sources occurred with the development of the CW intracavity frequency-doubled Ar^+ (257, 248, 244, 238, 229 nm) and Kr^+ (234, 206.5 nm) lasers because of the improvement in spectral signal to noise ratio [34]. These and low peak power Ti:sapphire lasers are currently the most applicable laser sources in UVRR spectroscopy. Deep UV tunable spectrometers based on fourth harmonic generation of a Ti:sapphire laser have been presented in 2005 and allow selective excitation in the range 193–210 nm [35] and 193–270 nm [36].

UVRR is performed on gases, liquids and solids and the setups employed for signal collection optics are correspondingly diverse. The review of Kelley [24] is largely dedicated to UVRR instrumentation both in a historical context and in its present and future implementations. The vast majority of modern Raman instruments utilize a grating spectrometer to separate the scattered wavelengths and a multichannel detector, usually a charge-coupled-device (CCD) with thermoelectric or liquid nitrogen cooling. This multichannel detector is essential for simultaneous collection of the entire spectrum. Different schemes are used for removing interference from the usually strong scattered laser light. Dielectric filters, holographic notch filters, and colored glass filters are commonly used for laser light rejection but each relatively expensive filter normally works at only a single laser wavelength and Raman spectra can be obtained to within only a few hundred cm^{-1} of the laser line. A double spectrograph functioning in subtractive mode is often used as a Rayleigh filter when broadly tunable excitation is required and/or small Raman shifts need to be observed. This is typically followed by a single dispersive spectrograph with the drawback of a low throughput because of the large number of optical elements requiredd [5].

The high cost of lasers and optics for the UV spectral region have limited

UVRR spectroscopy and its use in the past. The development and availability of lower cost portable and compact deep UV spectrometer has found a place in the world of analytical instrumentation.

2.2.3 Internal standards

UVRR spectroscopy can be used for quantitative analysis since the area of a Raman band is proportional to the concentration of the vibrating species. In order to correlate intensity and concentration the Raman cross section of the molecule must be known [5]. The absolute intensity of a Raman band is dependent on several factors like laser power, sample refractive index and optical sample geometry. Therefore nearly all quantitative UVRR methods make use of relative measurements with respect to an internal standards [5]. UVRR studies of proteins generally employ the ν_1 band of common salts, such as $SO4^{2-}$ (982 cm^{-1}) and $ClO4^-$ (934 cm^{-1}) at a concentration of ca. 0.1 M (under off–resonance conditions). The major requirement for an internal standard is that it does not interact with the analyte molecule. For quantitative analysis the cross sections of the salts have to be known [37]. Those are reported for 193, 197, 200, 203, 206, and 210 nm excitation wavelength in [35]. Cross section measurements were also reported at wavelengths longer than 220 nm [38] and down to 192 nm [39].

2.2.4 Band assignment

Identification of the Raman bands upon UV excitation is not always straightforward. Conventional Raman spectra can no longer be exclusively used for fingerprint identification and reference spectra recorded under the same resonance excitation conditions are required. Theoretical calculation of excited state potentials can be an important tool for assignment purposes. However, significant progress is still necessary for correct prediction of enhancement factors [23]. Band assignment of UVRR spectra of proteins has been principally

achieved by means of model compounds, *i.e.* amino acids and short peptides since those chromophores contribute to resonance enhancement of proteins in the deep UV region below 260 nm. Comparisons of the UVRR spectra of phenylalanine, tyrosine, and tryptophan to those of toluene, phenol, and indole has shown that all of the features in the spectra may be assigned to normal modes of the aromatic rings of the amino acids [40]. These aromatic amino acid, as discussed in the next section, can be used to predict the selectivity of aromatic amino acid enhancement in proteins [30]. Also, important insights into the nature of the amide modes of the peptide group in proteins has been provided by UVRR studiesof N-methyl acetamide (NMA), which is an appropriate model for the peptide bond [41].

2.2.5 Raman difference spectra

The evaluation of changes in intensity and frequencies of the protein vibrations upon binding of a ligand is generally accomplished in UVRR by means of difference spectra: 1) (protein–ligand) – (protein) when the ligand has no UVRR enhancement or if the free ligand concentration is negligible with respect to the bound one; 2) (protein–ligand) – (protein) – (ligand) when the ligand shows UVRR enhancement. Spectral calibration is performed using the known internal standard band. Essentially the unchanged protein and ligand features in the bound protein spectrum are subtracted and the difference profile is exclusively generated by those molecular group vibrations of either the protein or the ligand (if resonance enhanced) affected by binding. The crucial point of the method is that parent spectra must be very accurate so that small differences between them show up without experimental error in the difference spectrum.

2.3 UVRR of proteins

In proteins internal chromophores giving rise to electronic absorption bands in the UV region of the spectrum are the aromatic amino acids, tryptophan (trp), tyrosine (tyr), phenylalanine (phe), and histidine (his) that contribute with electronic bands in the range 220–300 nm. In addition, the amide backbone absorbs light below 220 nm. With deep UV excitation those groups show resonance enhancement dependent on the excitation wavelength used and furthermore, their band intensities and frequencies are directly connected to their local environment and the protein conformation, as discussed below.

2.3.1 Amino acids

Enhancement mechanism The UV absorption spectra of trp, tyr, and phe in the range 180–280 nm are characterized by three bands and are closely related to the parent benzene chromophore. The first intense band in the deep UV is assigned to the benzene-like $B_{a,b}$ transition (π–π^*) and the two lower energy weaker bands assigned to the benzene-like L_a and L_b transitions (π–π^*) [30, 42]. The description of the enhancement pattern of amino acids at different excitation wavelengths was carefully described elsewhere [30, 31, 42, 43] and the changes observed at different excitation wavelengths were interpreted in terms of dominant vibronic (B term) scattering in resonance with L_a and L_b transition states, and Franck–Condon (A term) scattering via the allowed $B_{a,b}$ states [25]. From those studies it is derived that for trp the strongest scattering is seen at 218 nm in resonance with the $B_{a,b}$ transition. For tyr and tyrosinate at 200 nm excitation is close to resonance with the tyr $B_{a,b}$ transition and for phe it is found at 218 nm close to resonance with the L_a transition. In addition deprotonation of the phenolic hydrogen (tyrosinate) shifts the L_a absorption maximum from 222 to 249 nm so that tyr and its deprotonated form can be selectively enhanced and discriminated by changing excitation wavelengths [42, 43]. This is a remarkable advantage of UVRR spectroscopy in comparison with

fluorescence spectroscopy, for which tyr and tyrosinate emission spectra are hardly detectable in view of the high quantum yield of trp [1]. The prominent ring mode fundamentals of the aromatic amino acids at several excitations are presented in Table 2.1. The Raman bands arising from trp, tyr and phe, residues are labeled W, Y, and F respectively.

2.3.2 Structure sensitive vibrations

Tryptophan A systematic investigation of the effects of H–bonding and hydrophobic interactions on the UVRR spectrum of a model compound of the indole ring of trp was conducted by Matsuno *et al.* [44] in the range 230–270 nm. Their study showed that UVRR bands enhanced through resonance with $B_{a,b}$ transition become strongest when the indole ring is H–bonded in a hydrophobic environment. Raman bands enhanced via the L_a transition give the highest intensity when the indole NH site is not involved in H–bonding. Notable vibrations of trp correlated with the local environment and geometry of the trp side chain in proteins are: 1) W3, the peak position of which is indicative of the absolute value of the side chain torsion angle [45]; 2) the Fermi doublet intensity ratio W7 (I_{1360}/I_{1340}) increases with increasing hydrophobicity of the indolyl ring environment and thus serves as an indicator of local hydrophobicity [46]; 3) W17 and W18 produce Raman bands near 880 and 755 cm^{-1}, the frequency of which is sensitive to indole NCH H-bond donation [44]; 4) W16, W3 and W7 may be used to detect the H–bond at the NH site of trp located in hydrophobic environments. Recently, an analysis of trp derivatives was reported by Schlamadinger *et al.* [47] at 230 nm excitation. One of the new findings of trp Raman markers are: the intensity ratio I_{W10}/I_{W9}, which according to authors may be used for H–bonding discrimination, and the change in W18 and W16 probing the occurrence of cation–πinteractions within proteins.

Tyrosine Tyr has been reported repeatedly in the past, as part of UV resonance Raman studies, to be a good probe for investigating the local environ-

ment of a protein. Specifically, vibrational bands associated with the phenolic ring seem to be particularly sensitive to the change in local environment and to H–bonding of the phenolic OH. The tyr side chain generates a pair of distinctive Raman bands —a Fermi doublet near 850 and 830 cm^{-1}. In conventional RS, variation in the ratio for different tyr entities is attributed to changes in the Fermi interaction associated with the state of the OH proton, thus the ratio is diagnostic for H–bonding of the phenol ring. This ratio, however, seems to be much less discriminating in the UVRR spectra [42, 43]. In the work of Hildebrandt *et al.* [48] tyr and its sensitivity to H–bond donation was investigated by UVRR at 229 nm excitation. Their results suggest that the strength of tyr H–bonding interactions in proteins can be assessed from the ring modes Y8a and Y8b, which optimum selectivity is obtained at 229 nm. Exploiting the H–bond sensitivity of the Y8a band a quantitative determination of the pK_a of two tyr residues in an 11–residue peptide fragment from transthyretin could be achieved by titration of the band intensity as a function of pH [49].

Phenylalanine Phe shows an intense band at 1002 cm^{-1} generally overwhelmed by trp and tyr Raman scattering signals [50], as their Raman cross sections are almost 10 times stronger. In addition since its structure is unable to form H–bonds, this Raman band is not a sensitive marker of protein environment.

Histidine The imidazole side chain of his often plays an important role in protein function. The his residue has a π–π^* transition in the deep UV and is a candidate for UV resonance enhancement. An extensive discussion of it modes is given by Caswel *et al.* [51]. Although the Raman bands of his are weak compared to those of trp, tyr, and phe, it is possible to identify some his Raman bands in visible and UV Raman spectra of proteins, in particular when the protein does not contain many aromatic residues. In D_2O solution, however, his generates a moderately intense Raman band near 1408 cm^{-1}, which is assigned to an in–plane vibration of the N-deuterated imidazolium ring. The band is particularly useful for monitoring histidine H/D exchange

dynamics as well as histidine-histidinium equilibria (in D_2O). This band was exploited for monitoring the protonation state of histidine residues in proteins as described in reference [51].

2.3.3 Peptide backbone

Enhancement mechanism There are two relevant absorption bands in the UV spectrum of NMA, the appropriate model compound for the study of the peptide bond in proteins [41]. A weak band at ca. 210 nm (n–π^* transition) and a stronger one at the 186 nm (π–π^* transition). The latter plays the main role in UVRR studies [27]. The amide groups of a protein have characteristic vibrational frequencies, which typically come in particular ranges [52]: 3280 cm^{-1} (amide A), 3090 cm^{-1} (amide B), 1653 cm^{-1} (amide I), 1567 cm^{-1} (amide II), 1299 cm^{-1} (amide III), 627 cm^{-1} (amide IV), 725 cm^{-1} (amide V), 600 cm^{-1} (amide VI), and 206 cm^{-1} (amide VII). Among them amides I, II, and III show large enhancement upon resonance excitation below 210 nm. In addition to the three classical amide modes another vibration gives rise to a detectable band between 1390 and 1400 cm^{-1} (Amide S) in the UVRR spectra of non–helical peptides and attributed to the C_α-H deformation mode that mixes with amide III [27].

2.3.4 Protein secondary structure

Amide bands are sensitive to changes in the dihedral angles (ϕ, ψ) and provide direct quantitative information about the secondary structure of proteins [53, 54]. Secondary structure can be monitored via the intensities of resolved UVRR components of the amide III and S spectral envelopes, or by least squares fitting, over all four amide regions, with secondary structure spectra determined from crystallographically characterized protein sets. Methods were discussed elsewhere [27, 55, 56, 57, 58].

2.4 Applications in protein–ligand binding

2.4.1 Plasma proteins

Among the plasma proteins, human serum albumin (HSA) is the most important carrier for many endogenous and exogenous ligands [12]. In view of the clinical and pharmacological importance of the protein, its molecular interactions have been studied extensively. HSA has two principal binding regions: site I, which contains the unique trp residue (trp214), and site II with tyr411, the chromophore directly involved in the binding of several ligands in the pocket [11]. Site I and site II accommodate a copious number of ligands, though for many of them the detailed binding mechanism has not yet been clarified. For this objective, UVRR spectroscopy of a HSA–ligand system represents a very efficient tool. Detailed structural information can be inferred since trp and tyr vibrations are sensitive markers for H–bonding, hydrophobic and π–cation interactions. Furthermore, since HSA has a unique trp in site I this can be used for binding site identification. In fact, any modification in the enhancement pattern of trp upon ligand binding in the UVRR spectrum of HSA is directly correlated with the accommodation of the ligand in the site. This does not work for site II because HSA has 18 tyr residues and the bands enhanced in the UVRR spectrum of HSA represent their average state. Therefore changes of the tyr bands cannot be attributed to site II unequivocally.

The interactions of warfarin and ibuprofen (typical drugs that binds to site I and II) and palmitate (fatty acid), with HSA at 244 nm excitation was investigated by Hashimoto *et al.* [50]. Their work represents the first attempt to use UVRR for probing protein–ligand interactions. At 244 nm excitation several bands of the hydroxycoumarin part of warfarin were enhanced in the UVRR spectrum of the HSA–ligand complex. Their identification was accomplished by means of a model compound, 4–hydroxycoumarin. Warfarin binds to site I and accordingly, the difference spectrum shows positive features from the trp vibrations W1 and W3, the latter being shifted in frequency. The intensity increase is ascribed to a red–shift of the $B_{a,b}$ transition [30] compatible with an

increased hydrophobicity of the trp environment. The frequency up shift of the W3 mode reveals a change of the torsion angle around the trp side chain [45]. Negative features in the difference spectrum derive from a more hydrophobic environment experienced by warfarin in site I. Those observations were interpreted by the authors as evidence for a direct hydrophobic interaction between the trp indole ring and the benzene ring of the ligand. Also ibuprofen is resonance enhanced at 244 nm but no changes in its spectrum upon binding were observed. The ligand binds to site II, and in line with this, only tyr vibrations, Y8a Y7a Y9a and the Fermi doublet, contributed to the difference spectral profile. The 10% intensity increase of those bands gives support to the formation of a H–bond between the tyr411 phenolic OH and the carboxylate of the ligand. Palmitate vibrations are not resonance enhanced at 244 nm. Therefore all the features in the difference spectrum are ascribed to HSA. Upon binding, a 30% intensity increase of the original tyr bands, Y8a, Y3, Y7a, Y9a and Y1, was unveiled in the difference spectrum. The bound palmitate molecule makes the environment of tyr residues more hydrophobic. It is concluded that the ligand binds HSA through hydrophobic interactions with tyr residues.

We have recently investigated the binding of tripelennamine, mepyramine and brompheniramine (first generation of Histamine H1 receptor antagonists) to HSA at pH 7.2 and 9.0 because under those conditions the extent of protonation of the ethylamino side chain of the ligands is different [59]. This group, when protonated, has been shown to cause an intramolecular H–bond, which could explain the weak affinity of those ligands to HSA at physiological conditions. By means of 244 nm excitation resonance enhancement is obtained for both the protein and each ligand. Spectral modifications in the difference spectra derive from the trp214 and the tyr residues within HSA and the aminopyridine chromophore of the ligands, which therefore are directly involved in the binding. Furthermore binding affinity is greater at pH 9.0, when the ethylamino side chain is deprotonated, than at pH 7.2.

Transferrins are a group of iron binding proteins that bind iron only in the presence of synergistic anions. The capture and release of Fe^{3+} are mediated

by the binding of anions. The application of UVRR spectroscopy with 244 nm excitation to examine the sulphate binding to apo-human serum transferrin (apohTf) has been worked out by Clarkson *et al.* [60]. At this excitation wavelength UVRR spectra of a tyrosinate residue within the protein could be detected by changing the pH of the protein solution, see Figure 2.1. The intense tyrosinate bands at pH 8.75 are observed to significantly reduce in intensity upon addition of sulphate. From the difference spectrum, negative features from tyrosinate appeared (see Figure 2.2). By monitoring the dependence of the Y8a band as a function of pH a pK_a of 7.8 for the tyr residue involved in the binding with the anion was determined. This work represents the first conclusive evidence that the addition of sulphate ions to apohTf causes an elevation in the pK_a of a tyr residue, which is generally around 9. Those results support the hypothesis that tyrosinate is the electronic reporter of anion binding.

2.4.2 Enzymes

It is well established that Raman spectroscopy provides very precise structural information on active-site bound substrates to enzymes [61, 62]. The resonance Raman effect in the visible region has been used to probe selectively the vibrational spectrum of the substrate in an enzyme-substrate complex. The strategy is to form an enzyme-substrate species, wherein the substrate (or the enzyme-substrate bonds themselves) forms a chromophore which absorbs above 300 nm. UV laser sources in the near and deep UV have greatly extended the range of systems that can be probed selectively exciting inner chromophores of the enzymes.

The paper from Couling *et al.* [63] represents a nice example of the use of UVRR spectroscopy for elucidating aspects of protein–ligand interactions. The systems investigated in their study are dihydrofolate reductase (DHFR) with its inhibitor trimethoprim (TMP), gyrase with novobiocin, and catechol O-methyltransferase (COMT) with dinitrocatechol (DNC). Selective excitation

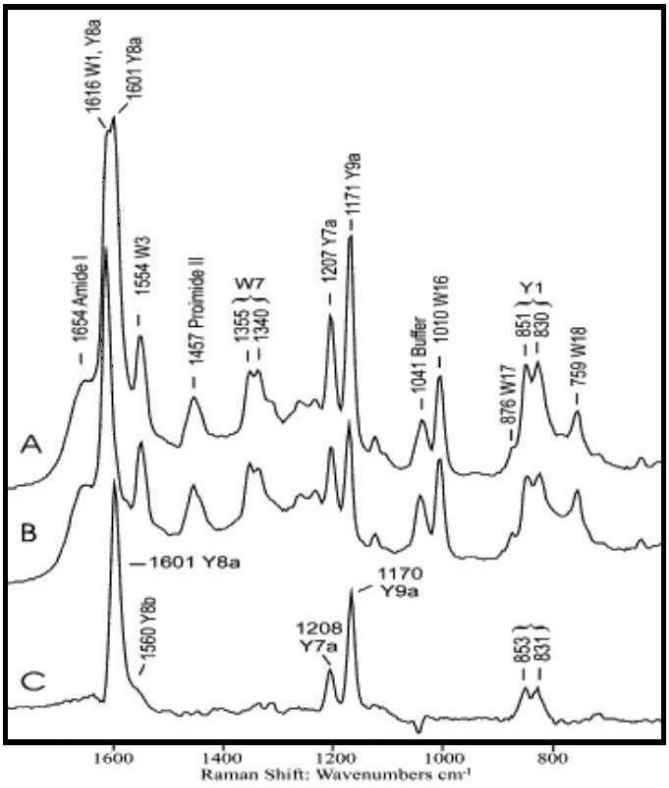

Figure 2.1: 244 nm UVRR spectra of apohTf at (A) pH 6.25 and (B) 8.75. C: Difference spectrum of A minus B showing tyrosinate UVRR bands only, with minor features due to changes in buffer species [60].

at 244 nm is used to enhance the sensitivity of trp and tyr vibrations. DHFR has three tyr and two trp residues close to the binding site. Because the TMP ligand is not resonantly enhanced at 244 nm, only changes in the spectrum of the protein were detected. Those showed a change in the environment–sensitive

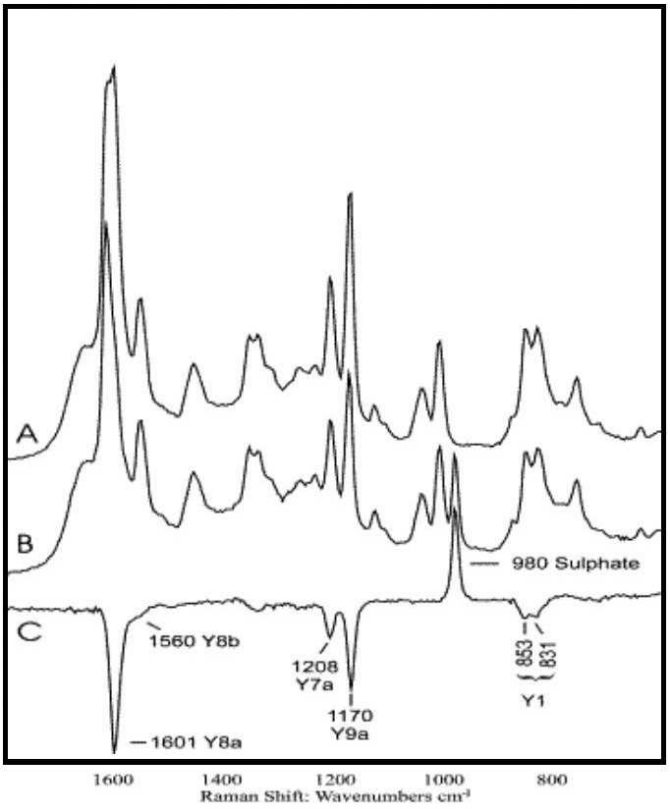

Figure 2.2: 244 nm UVRR spectra of apohTf at pH 8.75 before (A) and after (B) addition of sulphate. C: Difference spectrum of A minus B showing negative tyrosinate bands and positive sulphate band [60].

ratio I_{1340}/I_{1356} of the trp doublet (see Figure 2.3), which arises from the trp located in the binding pocket and that comes in contact with the aromatic TMP upon binding. At 244 nm both gyrase and novobiocin are resonance enhanced and difference spectra were calculated to distinguish between spectral

changes of the enzyme and of the ligand. The binding site of gyrase contains neither trp or tyr residues, the nearest tyr being 10 Å away and the nearest trp being 20 Å away from the binding site. Changes in the tyr and trp Fermi doublet were detected and were attributed to dipole–dipole and dipole–polarizability interactions between the enzyme and its ligand in view of the spatial distance between them. UV resonance enhancement of novobiocin has shown that a substantial structural changes of the ligand occurs upon binding. COMT has two trp residues, Trp143, which is close to the binding site and involved in conformational changes, and Trp38 located edge to face with the planar structure of DNC. Binding with DNC led to changes in the doublet ratio I_{1340}/I_{1356} of the two Trp residues. The changes indicate that the trp residues are initially exposed to the aqueous solvent, and subsequently find themselves in a hydrophobic environment. The study on COMT also indicates that it is possible to observe agonist–antagonist interactions with the protein.

In the work of Villancourt *et al.* [64] the utility of UVRRS as a probe of substrate binding in catechol-transforming enzymes, including ring-cleaving dioxygenases is established. UVRR data presented in this study provided direct, unambiguous evidence that an extradiol dioxygenase, DHBD, binds its preferred substrate, DHB, as a monoanion. The conclusion was achieved in view of the position of the tyr Y8a mode of the bound substrate in the difference spectrum, which was investigated in solution in its dianionic, monoanionic and neutral state.

2.4.3 Receptors

Cyclic AMP receptor protein (CRP) is a regulatory protein in *Escherichia coli*. This protein binds cAMP, which causes a conformational change that allows the protein to bind tightly to a specific DNA sequence in the promoters of the genes it controls [65]. Conformational changes of CRP induced by binding of cAMP are considered to be the key event in the activation pathway of CRP. The work of Fujimoto *et al.* [66] describes the application of UVRR

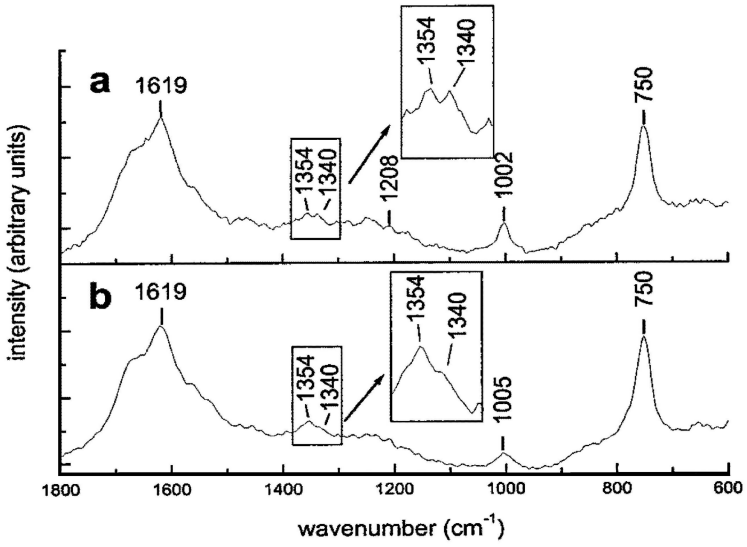

Figure 2.3: UVVRR spectra of the DHFR/TMP system with (a) free DHFR and (b) DHFR:TMP (1:1). For clarity, the trp doublet regions are shown enlarged. From [63]

spectroscopy to study the binding modes of cAMP to CRP with excitation at 257 and 229 nm. To investigate structural changes of CRP when bound to cAMP, UVRR spectra of CRP–cAMP complex were recorded with 229 nm excitation, which produces strong Raman scattering from two trp residues (trp13 and trp85) but no detectable scattering from cAMP. The H–bonding state of the indole NH site is unaffected by the binding of cAMP, as demonstrated by identical wavenumbers of trp mode W17 in its bound and free state. Therefore, the intensity decrease observed for the trp Raman scattering is attributed to an increase in the environmental hydrophobicity. Trp85 is proposed to bind to cAMP since NMR and fluorescence studies demonstrated that trp13 is insensitive to binding. With 257 nm excitation the conformational change of

the cAMP ligand upon binding was successfully monitored. The adenine chromophore of cAMP has a strong absorption at 258 nm and the excitation around this wavelength produces a resonance enhancement of the Raman scattering from cAMP. Binding to CRP causes a wavenumber downshift for some adenine ring vibrations. Applications of RS and UVRR spectroscopy to investigate nucleic acids an their complexes were reviewed elsewhere [29, 67]. In conclusion, from the UVRR results and the comparison with available X–ray crystal data it was suggested that the environmental change of trp85 residues of the protein, is consistent with an opening of the cleft between the N–terminal cAMP and C–terminal DNA binding domains in the process of CRP activation by binding of a single cAMP molecule. The ligand, which exists as a mixture of the anti and syn forms in H_2O solution, adopts only the anti orientation in the binding with CRP. This work illustrates the advantage of UVRR for examining the structures of protein–nucleic acid complexes. Because proteins and nucleic acids have UV absorption bands in different wavelength regions, tuning the Raman excitation wavelength to an absorption band of either a protein or a nucleic acid produces much stronger Raman signals from the targeted component than from the other.

2.4.4 Heme–proteins

Heme proteins recognize a specific small diatomic molecule by its binding to the heme iron, and subsequent conformational changes of a protein result in a functional reaction at the catalytic site [68]. Interestingly, for those proteins both RR in the visible and in the deep UV region are extremely informative. Because of the presence of the heme iron, in the visible range where the porphyrin group absorbs light, background fluorescence plays no role (heavy–atom effect). The RR spectra in the visible region are dominated by the porphyrin ring modes and provide detailed information about the interaction with ligands [69]. In UV excitation contributions from the tyr and trp residues are enhanced, while contributions from the heme group are suppressed. Thus,

the protein moiety can be investigated independently of the prosthetic group. Myoglobin and hemoglobin are without doubt the two most widely studied heme proteins. The investigation of the molecular mechanisms of oxygen binding, storage, and release in these systems has involved the efforts of a wide range of scientists and a variety of physical, chemical, and biochemical techniques for many years. Nevertheless, many questions still remain unanswered, particularly regarding the detailed mechanism controlling the oxygen-protein interaction. UVRR spectroscopy has brought significant progress in the comprehension of those mechanisms because of its distinct structural elucidation capability.

In the work of Haruta *et al.* [70] conformational change of sperm whale and horse Mb accompanied by CO binding was investigated with 244 nm excitation, through spectral changes of tyr and trp bands. Some RR bands of the heme group unexpectedly appeared with 244 nm excitation causing an overlap with the trp doublet W7 around 1360/1340 cm^{-1}, which could not be used as a marker band. The trp W3 band and Y9a of tyr were not affected and could therefore be used for structural consideration. Sperm whale Mb has two trp residues, trp7 and trp14. To determine which of them undergoes environmental changes upon ligand binding two mutants, W7F and W14F, of individual trp residues were prepared. It was shown that upon CO binding the most part of the change of the trp W3 band of native Mb comes from trp7. The position of W3 has a good correlation with the torsion angle of the indole side chain. By comparison of the UVRR enhancement of Y9a in sperm whale Mb (tyr103, tyr146, and tyr151) and horse Mb (tyr103 and tyr146) in their CO bound and free forms, it was concluded that the environment of tyr151 in sperm whale Mb is largely affected by binding with CO. Its frequency is lower and its intensity higher in the deoxy state compared to the CO-bound state. This means that tyr151 in the deoxy state is placed in more hydrophobic environments and works as a H–bond donor rather than in the CO–bound state. Mb consists of eight helices, and the heme is embedded between the E and F helices, while trp7 and tyr151 are contained in the A and H helices, which are interacting

with the E and F helices, respectively. The appearance of the ligand binding effects only on trp7 and tyr151 residues might be partly due to the fact that these side chains are located near the surface of the protein and accordingly are favorable for the detection of conformational change.

The deoxy and oxy forms of Hemoglobin (Hb) have distinct quaternary structures, which are associated with the low and high affinity states, T and R. Cooperative oxygen binding to Hb has been interpreted in terms of a reversible switch between the R and T states. A detailed understanding of Hb cooperativity at the molecular level remains elusive. Structural studies on Hb deoxy- and CO-Hb have have been performed with deep UV excitation at 212 and 200 nm [71] and 230 nm [72]. Several studies point to a second H–bond to the heme-bound dioxygen originating from tyrB10 as the source of this unusual reactivity. In the study of Huang *et al.* [73] UVRR spectroscopy was used to directly observe the formation of the H–bond upon oxygen binding to Hb (from *Ascaris suum*) by monitoring sensitive markers like Y8a and Y8b. The study reveals that both O_2 and CO induce similar local tertiary changes upon binding to the heme in the globin region of Hb. However, in the case of O_2, a strong H–bond involving a tyrB10 is also observed.

2.4.5 DNA–binding proteins

In conventional Raman measurements, it is difficult to distinguish nucleic acid residues of the same species at different sequence positions of a DNA duplex because Raman bands arising from such residues severely overlap each other.Thanks to the advent of the UV laser, UVRR spectroscopy of nucleoproteins became feasible. Packaged single–stranded DNA (ssDNA) and the aromatic side chains of coat protein subunits in filamentous viruses show UV absorption below 260 nm and can be selectively enhanced, even though those residues represent only a small fraction of the total virion mass.

The first report on the use of UVRR spectroscopy to probe DNA base and coat protein tyr environments in the filamentous virus Pf1 assembly is from

Wen *et al.* in 1999 [74]. They made use of UVRR spectroscopy to detect differences in the structure assembly of Pf1 and another class of filamentous virus, fd. Several excitation wavelengths (257, 244, 238, and 229 nm) were employed in their study. Selective excitation of the coat protein tyr residues (tyr25 and tyr40) was performed at 229 nm. Instead the 257 nm excitation wavelength enhanced Raman bands of the packaged ssDNA [57]. UVRR markers of Pf1 and fd tyr differ dramatically from those of the free amino acid. The components of the phenolic ring Fermi doublet I_{850} and I_{830} for free tyr are supplanted in Pf1 and fd by a singlet at 853 cm^{-1}. The result is attributed to an unusual hydrophobic environment for the phenolic ring within the native virion assembly. Comparison of UVRR spectra of Pf1 in H_2O and D_2O with 229 nm excitation has indicated two H–bond markers of tyr side chain orientation, tyr modes Y7a and Y9a, see Figure 2.4. When UVRR spectra of Pf1 and fd are compared significant differences are found in the tyr H/D markers, which suggest strong H–bonding interactions between DNA bases and coat subunits of Pf1 but not between those of fd.

2.5 Conclusions

The examples outlined and discussed in the present chapter underline the main issues of UVRR spectroscopy in terms of strong sensitivity and structural selectivity for protein–ligand binding. In particular the introduction of the CW frequency–doubled Ar^+ ion and Kr^+ ion UV lasers has helped to increase the number of studies on proteins and thanks to the pioneering work of several groups, UVRR has now being recognized and appreciated as a distinctive analytical tool for quantitative and qualitative protein analysis. Its relevance in analytical chemistry will undoubtedly further increase since portable and less expensive multichannel spectrometers (applicable in the UV range) have become available. Upon UV excitation (below 260 nm) amino acid residues, like tyr and trp, and peptide backbone show strong resonance Raman enhancement

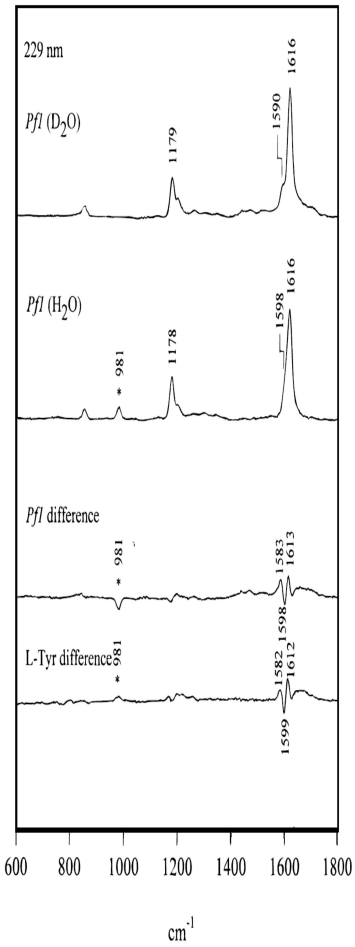

Figure 2.4: UVRR spectra (229 nm) of Pf1 in D_2O (top) and H_2O (second from top) and their difference spectrum (second from bottom). Also shown for comparison (bottom) is the D_2O-minus-H_2O difference spectrum of L-tyrosine. From [57].

among the very large number of protein vibrations. Those groups are extremely sensitive markers of H–bonding, hydrophobic and π–cation interactions, and binding to ligands can be therefore detected by UVRR if those residues are located near the protein binding site. It should be mentioned that the UVRR approach does not provide information on large protein structures but exclusively on small regions. In that sense UVRR complements techniques such as X–ray crystallography which provide the overall picture.

Tryptophan		
Frequency cm^{-1}	Assignment	Description
758	W18	symmetric benzene/pyrrole in phase breathing mode
881	W17	indole ring vibration with NH bending
1012	W16	symmetric benzene/pyrrole out-of-phase breathing
1132	W13	i-p benzene CH bend, 9b
1238	W10	i-p benzene CH bend 3
1308	W8	pyrrole ring vibration 5π
1340–1360	W7 Fermi Doublet	pyrrole ring vibration
1438	W6	pyrrole ring vibration 6π
1462	W5	benzene 19b
1495	W4	benzene 19a
1553	W3	C_2–C_3 stretching of the pyrrole ring
1578	W2	i–p benzene ring stretch 8b
1621	W1	i–p benzene ring stretch/pyrrole NC stretching
Tyrosine		
Frequency cm^{-1}	Assignment	Description
830	Fermi Doublet	2x16 o–p
853	Y1	ring breathing
1182	Y9a	i-p CH bend, C6H5–C stretch
1210		para sub. benzene totally symmetric stretch
1265	Y7a	symmetric ring deformation
1600	Y8b	i–p ring stretch
1618	Y8a	i–p ring stretch
Phenylalanine		
Frequency cm^{-1}	Assignment	Description
1003	F1	ring breathing
1032	F12	ring deformation
1185	F9a	i-p CH bend
1208	F7a	phenyl–C stretch
1586	F8b	i–p ring stretch
1606	F8a	i–p ring stretch

Table 2.1: UVRR bands of the aromatic amino acids. Benzene mode numbering from [75]. Frequencies from [35] and assignment/description from [30, 39, 42]. Abbreviations: i–p in–plane; o–p out of plane.

Study of H_1 antihistamines

Chapter 3

Anomalous photophysics of H_1 antihistamines in aqueous solution[3]

[3] The contents of this Chapter were published by Silvia Tardioli, Cees Gooijer, and Gert van der Zwan in the Journal of Physical Chemistry B 113(19):6949-6957 (2009).

Abstract Electronic absorption, emission, and excitation spectra, and fluorescence lifetimes of two H_1 antihistamines —tripelennamine and mepyramine— are investigated in detail to ascertain their usefulness as fluorescent probes for ligand binding to G–Protein Coupled receptors. The photophysical behavior of these compounds in aqueous solution is complex due to the presence of three protonable nitrogens, intramolecular hydrogen bonding, possibility of excited state proton transfer, quenching due to the formation of a charge transfer state, and intramolecular FRET. At physiological pH values anomalous photophysical behavior is observed: the compounds are found to be in a ground state equilibrium mixture of two species, one with the alkylamine tail involved in an intramolecular hydrogen bond and a second without such a bond. This internal hydrogen bonded tail has a profound effect on the ground and excited state properties of both tripelennamine and mepyramine, which is further elucidated by comparing them to reference compounds 2–aminopyridine and 2–(*N,N*–dimethylamino)pyridine.

3.1 Introduction

Histamine plays a major role in allergic inflammation by combining with and stabilizing the activated conformation of the histamine H_1 receptor [16, 17]. H_1 antihistamines also bind to this receptor, but they act as so–called inverse agonists by shifting the equilibrium toward the inactive state and preventing histamine from activity.

The H_1 receptor belongs to the group of G–Protein coupled receptors (GPCR's). They constitute a large and functionally diverse family of transmembrane proteins and are among the most targeted proteins in drug discovery. However, the molecular mechanism of inverse agonist deactivation is in many cases not clear and more detailed information is desirable for developing appropriate therapies, for studying drug selectivity, and for elucidation of the signaling pathway within the receptor.

Of particular interest are the conformational changes of the H_1 receptor upon complexation with inverse agonists and the dynamics of that process. Besides more conventional biochemical and modern *in silico* methods, studies on GPCR conformation have been performed using fluorescent markers since the mid–1970's [76]. Those external dyes provide a wealth of information regarding the mechanism of ligand binding, the localization of receptors in living cells, and the physical nature of the binding pocket. But this usually involves introduction of a bulky structure, which is hard to combine with retention of the biological activity [76].

Among the ~forty currently used H_1 antihistamines there are only a few that show native fluorescence. Examples are tripelennamine (TRP) and mepyramine (MEP), which have the added advantage that they can be selectively excited in the presence of protein, since they absorb at longer wavelengths (> 300 nm) than tryptophan. So far these compounds have not been used in optical studies of ligand binding and little definite spectroscopic information is available. In this Chapter we hope to remedy that situation by presenting a detailed study of the photophysical properties of TRP and MEP in aqueous solution as a function of pH.

The two ligands are shown in Figure 3.1. They are provided as salts and share a common structure consisting of a butylamino chain with a strongly basic amine nitrogen atom at the end, and two aromatic groups connected to a central aromatic amine nitrogen. The butylamino nitrogen is protonated under physiological conditions. An aminopyridine moiety is common to both and the second aromatic group, a benzene in TRP and and anisole in MEP, differentiates their structures. In an earlier study of the fluorescence properties of these molecules [77], complex pH–dependent behavior was observed, and an interpretation of the results was presented by invoking reference compound 2–aminopyridine (2AP), see Figure 3.2. This compound has the same chromophore, and was therefore expected to have optical properties similar to TRP and MEP. Unfortunately that study and interpretation suffer from some serious omissions, as will be shown below. At neutral pH, TRP and MEP

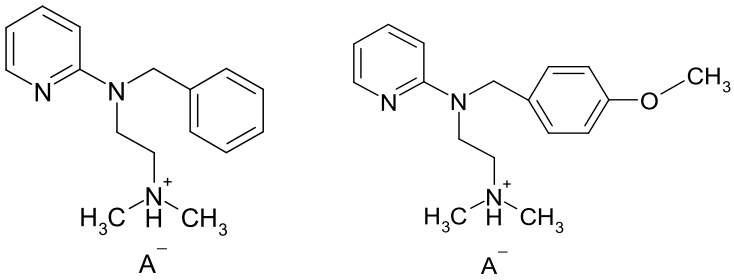

Figure 3.1: H_1 antihistamine salts investigated in this study. Left: tripelennamine hydrochloride A^-=Cl^-. Right: mepyramine maleate A^-=maleate.

actually have properties that are quite different from those of 2AP under the same conditions, which turns out to be mainly a consequence of the protonated butylamino side chain. Careful analysis of the spectra indicates that this side chain plays an important role by allowing an internal hydrogen bond with the pyridine nitrogen, affecting the electronic structure of the pyridine moiety in both its ground– and excited states.

Both TRP and MEP show complex pH–dependent fluorophoric properties since various protonation equilibria occur in aqueous solution. This property makes them suitable for probing protein binding because the protonation state of a particular functional group will determine the charge and the possibility of intermolecular hydrogen bond formation of these antihistamines. We will also show that the absorption and emission characteristics, (*e.g.* spectral position and intensity), and fluorescence lifetimes depend on their conformation. In addition, it is not unlikely that the presence of an intramolecular hydrogen bonded tail in TRP and MEP affects the binding properties to a receptor [78].

Various aspects such as the electronic coupling of the chromophores, struc-

tural rearrangements, and influence of the protonated amine side chain are discussed in this Chapter. Particular attention is given to the possible parent structures for the aminopyridine part of TRP and MEP (Figure 3.2), which appears to be the only chromophore responsible for the fluorescence emission. An analysis based on 2AP and another possible reference compound 2–(*N*,*N*–dimethylamino)pyridine (2DMP), which has an absorption spectrum closer to that of the aminopyridine moiety in TRP and MEP, is presented.

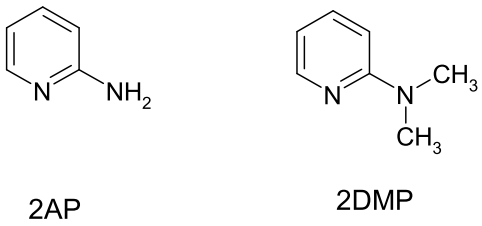

Figure 3.2: Parent structures for the aminopyridine group of TRP and MEP. 2AP was previously proposed [77], whereas 2DMP is also investigated in this study.

3.2 Experimental

3.2.1 Chemicals

Tripelennamine hydrochloride (TRP), mepyramine maleate (MEP) and the reference compounds 2–aminopyridine (2AP), 2–(*N*,*N*–dimethylamino)pyridine (2DMP), and anisole, were purchased from Sigma Aldrich and used without further purification. Aqueous solutions were prepared dissolving the antihistamine salts in Milli–Q distilled water. All

measurements were performed at room temperature in a 1 cm quartz cuvette at a sample concentration of 4 μM. Under these conditions the optical density is kept below 0.1 to minimize inner filter effects. The pH of the aqueous solution at a sample concentration of 4 μM was 6.3. The solutions were then adjusted to more acidic or alkaline pH with analytical grade sulfuric acid or sodium hydroxide, respectively.

3.2.2 Apparatus

Absorption spectra were measured on a Varian Cary 50 Bio UV-vis spectrophotometer. Steady–state emission and excitation spectra were recorded at a number of different excitation and emission wavelengths with a Perkin-Elmer LS50B luminescence spectrometer. The time correlated single photon counting (TCSPC) technique was used to determine fluorescence intensity decays. The excitation source is a Coherent Mira 900 Ti:Sapphire laser with a pulse width of 3 ps. The output of the laser is frequency tripled to get the excitation wavelength of 250 nm. A multichannel–plate photomultiplier (Hamamatsu, R3809U–50) collected the fluorescence emission and data were recorded through a SPC–630 module (Becker&Hickl GmbH, Berlin, Germany) with a time resolution of 15 ps. Fluorescence decay curves were analyzed using a global fitting procedure based on the Levenberg–Marquardt algorithm. This method uses the instrument response function (determined by collection of scattered light from a suspension of silica particles) for deconvolution of the recorded decays and for determination of lifetimes and wavelength–dependent amplitudes. Each intensity curve was fitted by mono– and multi–exponential decay and the goodness of the fit was assessed on the basis of χ^2, and the distribution of residuals.

3.2.3 Determination of Decay Associated Spectra

Decay-associated spectra (DAS) provide information on the fluorescence emission per lifetime component. DAS are constructed by distributing the total intensity per decay curve over the lifetimes that make up the total intensity according to their amplitudes obtained by the above fit procedure. The relative fluorescence intensity $I_{\tau_j}(\lambda)$ of lifetime component τ_j at wavelength λ with amplitude $A_j(\lambda)$ can be expressed by the following equation

$$I_{\tau_j}(\lambda) = \frac{A_j(\lambda)\tau_j}{\sum_i A_i(\lambda)\tau_i} \tag{3.2.1}$$

The sum in the denominator of this expression is equal to the steady state emission spectrum.

3.3 Results and Discussion

3.3.1 Photophysics of H_1 Antihistamines in Aqueous Solution

The antihistamines under investigation (Figure 3.1) both possess two chromophores absorbing in the near–UV part of the spectrum. The aminopyridine–like part, denoted as AP, (note that we distinguish between this as part of the molecule, and 2AP, which denotes 2–aminopyridine itself) is common to both, whereas the second chromophore is a benzene (R=C_6H_5) in TRP and an anisole group (R=$C_6H_4OCH_3$) in MEP.

Unbuffered aqueous solutions of the antihistamine salts have a pH around 6.3. Under this condition the absorption spectra of the two ligands show similar bands centered at 245 nm and 306 nm (Figure 3.3) ascribed to the AP group [77].

Two additional bands are observed in the spectrum of MEP, a rather weak band with some vibrational structure centered at 275 nm and a stronger band at 225 nm, both of which can be assigned to the anisole moiety, although they are slightly blue shifted compared to the free anisole absorption spectrum.

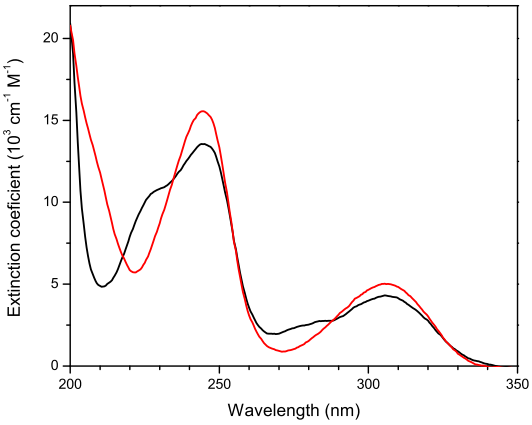

Figure 3.3: Extinction coefficients of TRP —— and MEP —— at pH 6.3. The MEP spectrum was corrected for the maleate counter–ion absorption.

Below 240 nm the maleate counter–ion has a strong pH dependent absorption and the spectrum of MEP has to be corrected for it. The extinction coefficient of the benzene group in TRP is very low above 220 nm ($< 10^2 \mathrm{M}^{-1}\mathrm{cm}^{-1}$); it becomes only significant at shorter wavelengths which is not relevant for the experiments reported here.

Both antihistamines exhibit native fluorescence with more or less identical emission spectra independent of the excitation wavelength. The spectra are shown in Figure 3.4, together with the fluorescence emission of anisole. Emission of MEP is slightly red–shifted compared to TRP emission. Differences in fluorescence intensity are due to dissimilar extinction coefficients at the excitation wavelength of 240 nm. The emission band, with a maximum at 364 nm, is located approximately where 2AP fluorescence emission takes place (not shown), whereas it is obvious that anisole emission is much further blue–

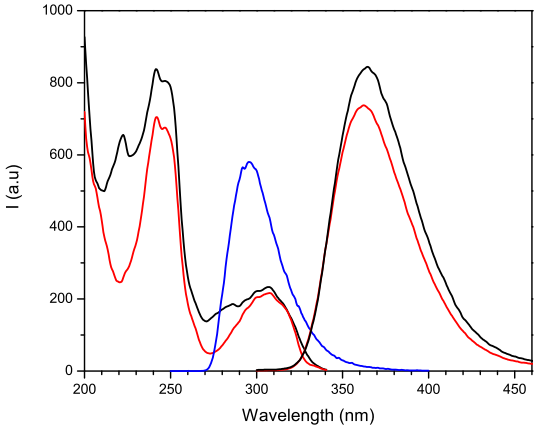

Figure 3.4: Emission and excitation spectra of TRP —— and MEP —— at pH 6.3. Excitation wavelength (for emission spectra) λ_{exc}=240 nm. Emission wavelength (for excitation spectra) λ_{em}=363 nm. Anisole fluorescence emission —— is also shown with excitation at 220 nm.

shifted with a maximum at 295 nm. We only find emission starting from 325 nm even for excitation at wavelengths where the anisole group absorbs. This result suggests that in MEP a strong coupling between the two chromophoric units leads to total energy transfer due to a FRET mechanism.

This is corroborated by the excitation spectra of the same compounds also shown in Figure 3.4. the anisole bands show up in the excitation profile taken at the emission wavelength of AP. We can therefore conclude that the AP chromophore is responsible for the fluorescence emission of both TRP and MEP and that anisole emission is absent.

Wilson *et al.* [77] investigated the luminescence properties of MEP in aqueous solution. On the basis of their results they concluded that no energy transfer occurs between the anisole and the AP group. However, they only

used excitation wavelengths of 242 nm, 254 nm, and 306 nm where mainly the AP moiety absorbs, and anisole barely has absorption.

For excitation at 230 nm and 280 nm, where anisole absorption is significant, we recorded the same emission spectrum and no trace of emission around 300 nm is found. Although the anisole emission might be slightly shifted when embedded in the MEP molecule (the absorption is shifted somewhat to the red compared to that of the free molecule), there is considerable overlap between the emission of anisole (around 300 nm) and the long wavelength absorption band of AP (around 295 nm) needed for efficient excited state energy transfer (FRET).

3.3.2 Photophysics of H_1 antihistamines as a function of pH

The three protonation centers in the structure of the compounds studied —the butyldimethylammonium nitrogen (N_1), the heterocyclic ring nitrogen (N_2) and the exocyclic nitrogen (N_3)— implicate the existence of acid–base equilibria depending on the pH of the solution (Figure 3.5). The effect of pH on the ground and excited state electronic properties of both TRP and MEP was investigated and a summary of absorption and fluorescence data is presented in Table 3.1.

The ground state acidity constant pK_1 for the de–protonation at the N_1 position is 8.9 [79]. Therefore in neutral aqueous solution N_1 is protonated and positively charged while only in strongly alkaline solutions (above pH≈11) MEP and TRP are completely de–protonated.

As the pH is decreased a second protonation most likely takes place at the N_2 position, similarly to substituted nitrogen heterocycles [80, 81], where the heterocyclic nitrogen atom is found to be more basic than the amino substituent. We determined the ground state acidity constant pK_2 of the AP group in TRP and MEP by means of UV absorption titration measurements. A value as low as 4.0 was found, in agreement within 0.2 pK units with the value reported by Wilson *et al.* [77]. In neutral solution we therefore expect the N_2 to be

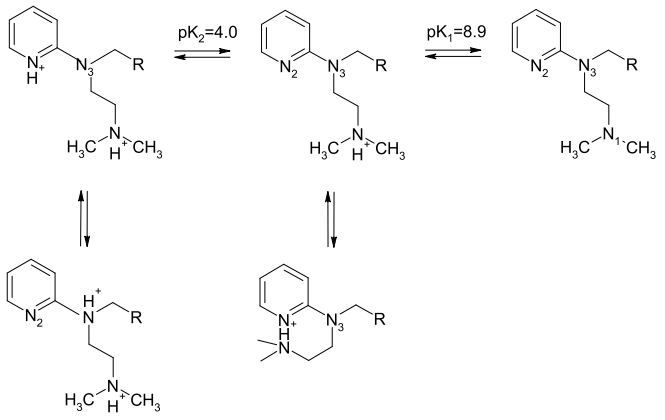

Figure 3.5: Structure of TRP and MEP as a function of pH. Each nitrogen is identified by a number: N_1 is the butylammonium nitrogen; N_2 is the heterocyclic ring nitrogen, N_3 is the exocyclic nitrogen. The second chromophore in both TRP and MEP, denoted by R, does not have (de)protonable groups.

de–protonated. The pK_2 value of 4.0 is in sharp contrast with the pK values of the parent compounds 2AP and 2DMP, which are found to be close to 7.0 [82, 83]. This has serious consequences when comparing the photophysics of TRP and MEP with that of 2AP or 2DMP at a pH in the range 4.5 to 6.5, since the former will have a neutral chromophore while the latter will be mainly protonated. The origin of the three orders of difference of magnitude in K_a value will be discussed in detail later in this Chapter.

Protonation of the exocyclic nitrogen atom ($pK_3 = -10.21$ according to Wilson *et al.* [81]) does not take place in the pH range investigated in this study.

	TRP		MEP	
pH	λ_{abs} nm	λ_{em} nm	λ_{abs} nm	λ_{em} nm
2.0	238, 315	418	238, 315	366
3.0	240, 312	370	239, 313	365
4.0	244, 308	362	243, 308	365
6.3	245, 306	362	245, 306	364
8.0	245, 306	362	245, 307	364
10.0	249, 313	371	249, 313	371
13.0	249, 313	374	249, 313	376

Table 3.1: Absorption and emission data of TRP and MEP as a function of pH. Listed are maximum absorption intensities of the two main bands. Excitation wavelength was 240 nm for all emission spectra.

Under our most acidic conditions (pH 2.0), the absorption and fluorescence properties of the two antihistamines originate from the di–cation in which both the ammonium nitrogen N_1 and the heterocyclic nitrogen N_2 are protonated. To explain their results at low pH, Wilson *et al.* [77] suggested the presence of a triple protonated species at pH 2.0. In view of the above mentioned pK_3 value we consider this hypothesis extremely unlikely. Instead we entertain the possibility of protonation at N_3, instead of N_2, in the double protonated species to explain some of the results of MEP fluorescence as indicated in Figure 3.5.

Based on the pK values, the species of TRP and MEP molecules present at different pH values should be clear (first row of Figure 3.5). Spectroscopic consequences are clearly visible: there is a small blue–shift (6–7 nm) of both the absorption and emission spectrum going from the completely neutral to the singly protonated species, followed by a red–shift when the ring also becomes protonated, *c*f. Table 3.1. On closer inspection, however, we can report a number of unexpected and significant spectroscopic properties.

3.3.3 Unexpected results: neutral–alkaline solution

In view of the pK_2 value for the second protonation, the ring nitrogen in TRP and MEP is not protonated above pH 6.3. Since the AP moiety is the optically active part in both these molecules, the absorption and fluorescence properties of the antihistamines between pH 6.3 and pH 13.0 must therefore be attributed to a neutrally charged AP group. Consequently, spectra are expected to be similar in intensity and position over this pH range. However, for both compounds a 7 nm bathochromic shift of the absorption and fluorescence emission bands is observed, *c*f. Table 3.1, coupled to a considerable decrease in fluorescence intensity, as can be seen in Figure 3.6 for MEP. Identical results, with a slightly larger bathochromic shift, were obtained for TRP.

Fluorescence excitation spectra were recorded to characterize the nature of

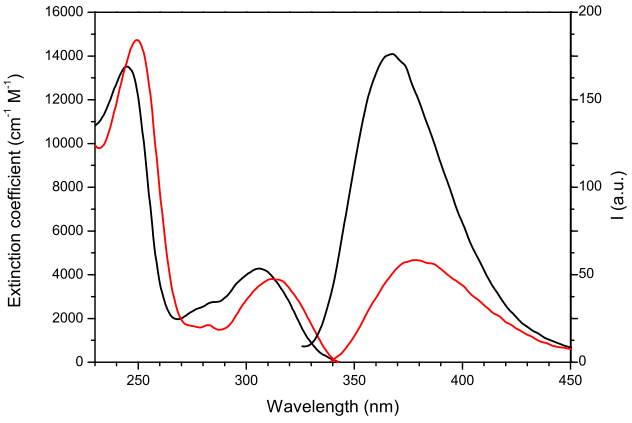

Figure 3.6: Extinction coefficient and fluorescence spectra of MEP at pH 6.3 —— and pH 13.0 ——. The MEP spectrum was corrected for the maleate absorption. TRP shows an identical behavior but the spectra are not shown.

the fluorescing species at different pH conditions well above and below pK_1. At pH 6.3 and at pH 13.0 the excitation bands overlap with the absorption bands measured under the same conditions. Again we only see AP emission and in the excitation spectrum in alkaline media the anisole bands are also present, as in neutral aqueous solution, indicating energy transfer between anisole and AP in MEP. At pH values close to pK_1, the excitation spectra of the investigated compounds become emission wavelength dependent. Excitation spectra of TRP and MEP recorded at the blue–edge of the fluorescence band (350–370) nm match the excitation profile recorded in aqueous solution, whereas the excitation spectra measured at the red–edge (390–420) nm match the excitation profile recorded at pH 13.0, as expected.

Since the only structural change in this pH range is the protonation state of the nitrogen side chain, these absorption and fluorescence data strongly suggest that (de)protonation at N_1 position seriously affects the spectroscopy of the AP group. A likely option to explain this influence, which will be further investigated below, is an interaction between the protonated tail and the pyridine ring. Electrostatic interaction, or intramolecular hydrogen bonding, may be energetically favored [84]. The polarity of the solvent could also play a role in this [85].

3.3.4 Unexpected results: acidic solution

The two antihistamines exhibit similar absorption and fluorescence behavior at neutral and alkaline pH. However, a large spectral change is observed in their excitation and fluorescence emission profile below pH 4.0, where the AP group starts to be protonated at the ring nitrogen N_2 in addition to protonation of the molecules at N_1, see Figure 3.5. The absorption spectra of TRP and MEP at pH 3.0 are shown in Figure 3.7 and compared with the spectrum of MEP at pH 6.3. The TRP spectrum at pH 6.3 (not shown) overlaps with that of MEP under the same conditions except of course for the absence of the anisole bands. The bands ascribed to the anisole chromophore at pH 6.3 are found

at the same position at pH 3.0. Therefore, as expected, this moiety is not influenced by a change of pH in the range investigated in this study. The two absorption bands ascribed to the AP group are indeed shifted for both TRP and MEP, and this result is taken to indicate protonation at the heterocyclic nitrogen N_2 . According to the Henderson–Hasselbalch equation, 90% of TRP and MEP is expected to be protonated at the N_2 position at pH 3.0, but 10% is still de–protonated. The equivalence between the absorption spectra of TRP and MEP in terms of position of the bands indicates that the same percentage of ground sate species is optically active. In line with this fact, in emission MEP shows a single and weak fluorescence band at the location of the fluorescence in aqueous solution (Figure 3.8, top) but, unexpectedly, TRP displays an additional longer wavelength band around 420 nm.

As the pH is further decreased to pH 2.0 the long wavelength component becomes clearly visible in the fluorescence spectrum of TRP, whereas MEP just shows a weaker band than at pH 3.0, still centered at the position of the band at neutral pH (Figure 3.8).

Excitation spectra of TRP and MEP were recorded to elucidate this behavior. In MEP the anisole absorption again shows up in the excitation spectrum (Figure 3.8, top), similar to the behavior in neutral and alkaline solution. Energy transfer from anisole to AP is apparently still taking place. At pH 3.0 and pH 2.0 the excitation spectra of MEP are not emission wavelength dependent, indicating that only a single species is responsible for the fluorescence emission. However, in both cases the position of the excitation bands does not match the absorption profile at the same pH but overlaps with the spectrum recorded at pH 6.3 where the AP group is not protonated. This is indicates that the only population emitting at these acidic pH values is the small percentage of still mono–protonated molecules, while for the double protonated species the fluorescence is quenched. These results point to a very weakly or non–fluorescent di–cation when protonation is at the N_2 site.

Similar pH dependent emission behavior is observed for TRP, except for the appearance of an additional long wavelength emission. At pH 3.0 the excitation

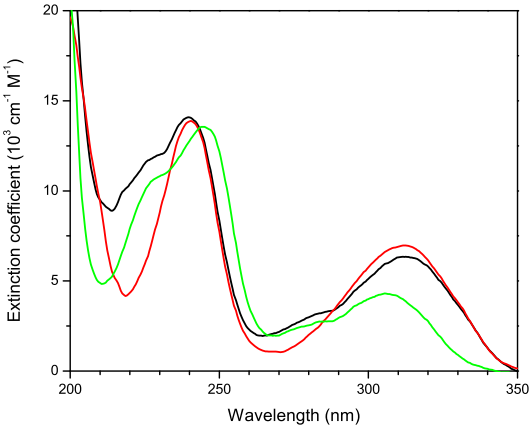

Figure 3.7: Extinction coefficient of TRP —— at pH 3.0. Extinction coefficient of MEP corrected for the counter–ion absorption both at pH 3.0 —— and at pH 6.3 ——.

spectra are wavelength dependent. The profiles recorded below 360 nm match with the absorption at pH 6.3. Similarly to MEP, those spectra are ascribed to the 10% of molecules not protonated at the AP group. The excitation bands recorded above 400 nm are close in position to the absorption bands taken at pH 3.0, but not completely overlapping. At pH 2.0 TRP clearly shows a long wavelength fluorescence component at 420 nm, and the corresponding excitation spectrum is the same as the one recorded at pH 3.0. When the excitation spectrum at pH 2.0 is compared with the absorption profile at the same condition the position of the bands is shifted and their relative intensities are different (Figure 3.9). It is possible that for both TRP and MEP excited state proton transfer takes place leading to a tautomeric form in the S_1 state. For MEP this tautomer shows negligible fluorescence due to efficient electron transfer quenching caused by the methoxy substituted benzene moiety.

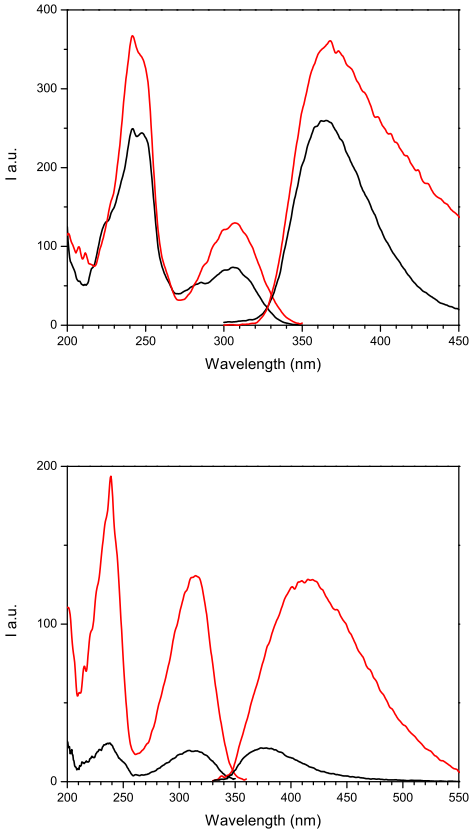

Figure 3.8: Top: Fluorescence excitation (λ_{em}=360 nm) and emission (λ_{exc}=240 nm) of TRP —— and MEP —— at pH 3.0. Bottom: Fluorescence excitation and emission of TRP —— (λ_{em}=420 nm λ_{exc}=310 nm) and MEP —— (λ_{em}=360 nm λ_{exc}=310 nm) at pH 2.0.

The result is consistent with the behavior of MEP where the di–cation is found to be almost non–fluorescent, and in line with the fluorescence quenching

of 2DMP upon protonation of the pyridine nitrogen [83]. We thus propose the presence of a new species responsible for this long wavelength emission, protonated at the N_1 and N_3 positions rather than at N_1 and N_2. It is currently unclear if such a tautomeric process is only relevant in the excited state, or in the ground state as well.

An exocyclic amino group on a pyridine ring is a weaker base than a pyridine nitrogen. The resonance effect of the substituent leads to delocalization of the non–bonding electron pair of the dimethyl nitrogen into the aromatic ring thus allowing the electron density to be positioned at the cyclic nitrogen, which becomes a stronger Brönsted base. As a consequence, the ring nitrogen of the AP group is the first to be protonated [80, 86], but under stronger acidic conditions protonation at the exocyclic nitrogen should also become possible. Therefore at pH 2.0, there could be a ground state equilibrium between protonation at the N_3 and at the N_2 position with a minor contribution of the protonated amino N_3. The species protonated at N_1 and N_3 are likely to be fluorescent, in contrast to the one protonated at N_1 and N_2. Obviously in the excited state this equilibrium can be shifted leading to excited state proton transfer, which also explains the larger Stokes shift [1]. Time resolved measurements at pH 6.3 also point in this direction, as discussed in the next section. For the reaction to be thermodynamically favored, the excited state of the di–cation should be a stronger acid. According to Wilson *et al.* [77] establishment of an excited state prototropic equilibrium is too slow to compete with the fluorescence emission. The excited state pK^* estimated from the Förster cycle is about 2 pK units more basic than the ground state, therefore the protonation of an excited di–cation in the pH region corresponding to the ground state pK_2 to give an excited tri–cation could be thermodynamically favored. But this pK^* was evaluated from change in absorption spectra by taking the absorption maximum of the mono-cation at neutral pH, where hydrogen bond indeed influences the ground state properties of the AP chromophore. If the absorption maximum recorded at pH 13.0 is used in the cycle, a pK^* of 4.4 is found. Apparently excitation does not seem to have a strong influence when compared to the ground

state value of 4.0. The Förster cycle method often yields valuable information about intramolecular charge transfer accompanying excitation. However, owing to the approximations concerning equal entropies of protonation in the ground and excited states and similarities of the vibrational modes, pK^* values should be used with caution [1].

Thus, at these low pH values, TRP and MEP have dissimilar photophysical properties. MEP does not show emission at 420 nm and either the maleate counter–ion or the anisole chromophore may be responsible for it. The interaction with maleate for instance might affect the basicity of the exocyclic nitrogen N_3 as a potential proton acceptor and thus the efficiency of proton transfer. To exclude this influence, fluorescence excitation and emission spectra of MEP were recorded in 1 mM KCl to replace the maleate ion with a chloride ion, but the spectroscopic properties of MEP under these conditions are not different from the previous measurements. Apparently the maleate counter–ion does not influence the fluorescence emission properties of MEP. The difference in behavior at low pH between TRP and MEP should therefore be attributed to the presence of the anisole moiety, which can then be held responsible for fluorescence quenching via electron transfer.

3.3.5 Fluorescence lifetimes of H_1 antihistamines

The fluorescence lifetimes of TRP and MEP were determined by TCSPC at pH 2.0, 6.3, and 13.0. Data are summarized in Table 3.2 and DAS spectra are shown in Figure 3.10. Results are consistent with the steady state results.

Two well–resolved fluorescence lifetimes of comparable magnitude were found for TRP and MEP at pH 6.3. The DAS for each lifetime component and the total intensity derived from them, see equation (3.2.1), are shown in Figure 3.10 and compared with the steady state fluorescence emission spectrum. The sum of the DAS of MEP perfectly matches the steady state fluorescence emission, whereas TRP slightly diverges from it starting from 400 nm. For TRP above this wavelength a third lifetime component might be present,

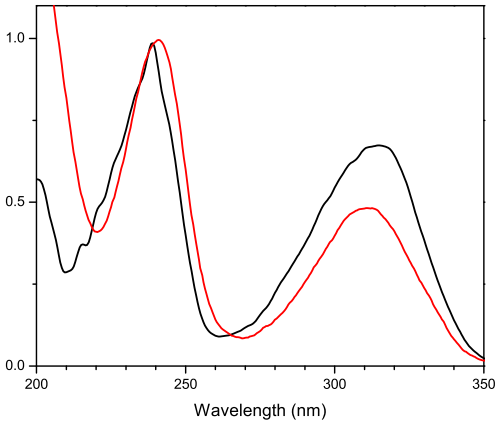

Figure 3.9: Fluorescence excitation of TRP —— (emission wavelength 420 nm) and absorption —— at pH 2.0.

which, however, could not be resolved accurately by the fit procedure. Its possible origin is discussed below.

The observed fluorescence lifetimes at pH 6.3 are consistent with an emission of TRP and MEP originating from two ground state conformations of the AP chromophore. Steady state data already indicated an effect of the protonated side chain to the AP group, which is expected to decrease as the pH of the solution becomes more strongly alkaline. At pH 13.0 where TRP and MEP certainly are fully de–protonated only a fast component remains. Consequently we ascribe the fast decay (0.3 ns) to the linear (trans) molecular conformation where the tail is not interacting with the AP moiety, and the longer lifetime (1.5 ns) to the gauche conformation where the tail interacts with AP, see Figure 3.5.

Upon protonation at N_2 position the di–cation of the two antihistamines

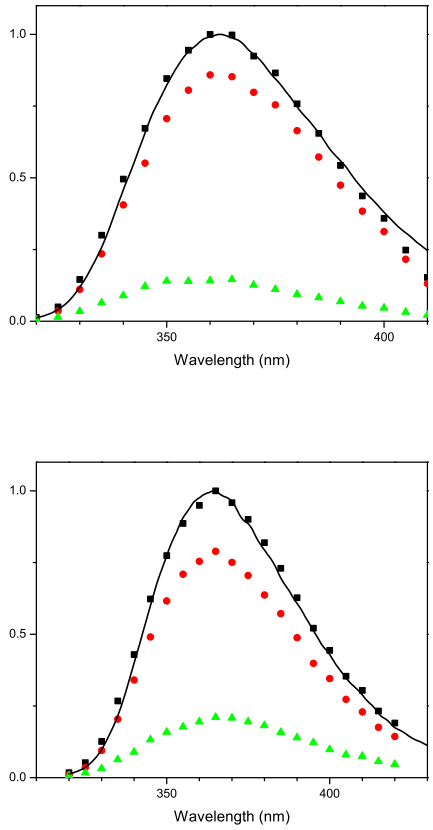

Figure 3.10: Top: Comparison between the total fluorescence of TRP —— and the sum of the decay associated spectra ■ constructed from amplitudes obtained from fit procedure at pH 6.3. The separate DAS are also given: τ_1=1.6 ns ● and τ_2=0.3 ns ▲. Bottom: Comparison between the emission flurescence of MEP —— and the total decay associated spectrum ■ constructed from amplitudes obtained from fit procedure at pH 6.3. The separate DAS are also given: τ_1 =1.6 ns ● and τ_2 =0.3 ns △.

	Tripelennamine		Mepyramine	
pH	τ_1 (λ_{em})	τ_2 (λ_{em})	τ_1 (λ_{em})	τ_2 (λ_{em})
2.0	0.4ns (420nm)			
6.3	1.6ns (363nm)	0.3ns (360nm)	1.5ns (365nm)	0.3ns (369nm)
13.0		0.3ns (374nm)		0.3ns (375nm)

Table 3.2: Fluorescence lifetimes and associated DAS maxima for various pH values.

was found to be essentially non–fluorescent. The very weak fluorescence emission of MEP at pH 2.0 then originates from the small fraction of molecules, which are not yet protonated at N_2 position. The decay time of MEP at this condition could not be measured with any accuracy. The steady state fluorescence emission of TRP was also quenched at acidic condition, but a new long emission wavelength band started to be clearly visible. Is is attributed to tautomeric emission caused by excited state proton transfer, and characterized by a lifetime of 0.4 ns.

In line with steady state data in acidic solution, this long emission band could now be the resultant emission of the minor fraction of di–protonated molecules at N_1 and N_3 position. Further investigations using other techniques and DFT calculations are presented in Chapter 4, *c*f. [87].

3.3.6 Parent structure for the AP chromophore

Wilson *et al.* indicate 2AP (Figure 3.2) as the appropriate model compound to describe the fluorescence emission of TRP and MEP [77]. Their choice was made on the basis of similarities between the number of bands in the excitation spectra of TRP and MEP compared to the reference molecule and on the occurrence of their fluorescence emission exactly where the 2AP fluorescence takes place. There are, however, remarkable differences between the behavior of AP as part of TRP and MEP and 2AP as an independent molecule.

The absorption spectra of the antihistamines studied are strongly red–shifted compared to 2AP, which is relevant since the position of the long wavelength absorption band plays a crucial role in possible FRET. Furthermore the pK value for the protonation of the pyridine nitrogen is almost three units higher with a pK of 6.8. This also means that a comparison between the spectra of the two molecules has to be made with care: at pH 6.3 2AP is protonated, but TRP and MEP are only protonated to the extent that the butylamino tail interacts with the pyridine N_2, something that was not taken into account in [77].

For a proper understanding of the photophysics of TRP and MEP, in particular the energy transfer mechanism between the chromophores, the geometry of the molecule is important, as well as the electronic states of the chromophores. For benzene in TRP and anisole in MEP this is not a problem: the spectra show that the electronic properties are close enough to those of the isolated molecules to be useful. For the second chromophore, AP, the situation is much less obvious.

Clearly 2AP is not the appropriate candidate: its absorption spectrum is too far to the blue, and the K value for acid–base equilibrium differs by three orders of magnitude. That is why we decided to investigate a second compound, 2DMP, the structure of which may be closer to the AP group of the antihistamines.

The spectroscopic behavior of 2AP and 2DMP was examined as a function of pH. In general we observe a bathochromic shift of 2DMP spectra when compared to those of 2AP. The same result is reported for aniline and dimethylaniline due to a combination of steric and substitution effects typical of ortho–derivatives [88].

Establishing which parent molecule better resembles the electronic structure of the AP group in TRP and MEP should be done in the absence of interaction with the protonated side chain, since that clearly influences the spectroscopic properties. Therefore in Figure 3.11 (left) the absorption spectra of the reference compounds at pH 9.0, where they are not protonated, is compared to the

extinction coefficient of a de–protonated TRP and MEP.

The strong bathochromic shift of TRP absorption bands with respect to 2AP could be indicative of a significant exciton coupling with benzene. However, these two chromophores do not have close lying excited states around 300 nm, and the observed shift of more than 30 nm, which corresponds to an energy difference of more than 3000 cm^{-1} leads to unlikely high excitonic interaction energies. In MEP the effect on the spectrum should be even larger, since for that molecule there are closer lying electronic states of anisole and 2AP, but no such effect is found. For that reason the close similarity of 2DMP spectrum with TRP in terms of intensity and position of the bands may prove to be more indicative of the expected weak electronic rearrangement the AP group undergoes upon coupling with the second chromophore. This result is valid for MEP as well. Applying the same arguments regarding protonation states in acidic solution, the spectrum of a mono–protonated 2DMP better matches the profile of a di–protonated TRP and MEP (Figure 3.11, right). In addition upon protonation of the heterocyclic nitrogen 2DMP becomes non–fluorescent, similar to what happens to the two antihistamines under the same condition.

The fluorescence quenching mechanism of mono–protonated 2DMP is ascribed to an excited state electron transfer reaction from the lone pair at the dimethylamino–N to the heterocyclic ring [83]. The same type of mechanism may account for the absence of fluorescence emission of the di–protonated antihistamines. In complete contrast, the $2APH^+$ cation is more fluorescent than the neutral form. The reason for that could be the following: inversion of the two lowest excited singlet states n-π^* and π–π^* removes any n-π^* character of the emitting state upon protonation of the pyridine nitrogen [89]. Therefore use of 2AP as reference compound cannot explain the lack of fluorescence emission that we observe in acidic solution for the di–protonated antihistamines. The different spectroscopic behavior of the two parent compounds in acidic solution is explained in terms of the charge transfer character of 2DMP with respect to 2AP.

2AP is an aromatic heterocyclic molecule where excitation occurs at the pyri-

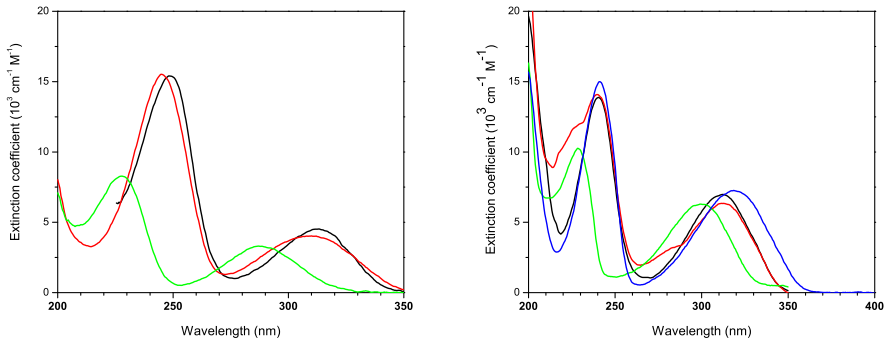

Figure 3.11: Left: Extinction coefficient of a de–protonated TRP —— (pH 13.0) compared with the extinction coefficient of the de–protonated parent compounds 2AP —— (pH 9.0) and 2DMP —— (pH 9.0). Right: Extinction coefficient of di–protonated antihistamines at pH 3.0: TRP —— and MEP ——. Extinction coefficient of mono–protonated reference structure at pH 3.0: 2AP —— and 2DMP ——.

dine nitrogen and interactions between close lying n-π^*, π–π^* states depends upon the polarity of the solvent [89]. It is well–known that the ionization potential of *N*–alkyl substituted aromatic amines are lower than those of the unsubstituted molecule and that they are better electron donors [90]. Therefore 2DMP can be regarded as an intramolecular donor–acceptor pair with the dimethylamine part of the molecule as the electron donor and the pyridine as acceptor in the excited state [1, 83]. In the case of TRP and MEP, upon protonation of the pyridine nitrogen it is then the delocalization of the lone pair at the N_3 position over the pyridine ring to explain the absence of fluorescence emission similar to mono–protonated 2DMP.

These observations lead to the conclusion that 2DMP is a more reliable reference structure than 2AP for the ground and excited state properties of a neutral and protonated AP group in TRP and MEP, respectively in alkaline and acidic pH. However, the high fluorescence emission of TRP and MEP in

neutral solution when compared to alkaline pH, still needs to be explained together with the strong difference in pK between the AP group of TRP and MEP and 2DMP (pK=7.5).

Both 2AP and 2DMP have high fluorescence yields in H–bonding solvents due to a significant π–π^* character of the pyridine nitrogen in the excited singlet state [82]. Similarly we may attribute the high fluorescence yield of the two antihistamines at neutral pH to a π–π^* character of the excited singlet enhanced by the electrostatic interaction between the AP group and the protonated side chain. The proposed interaction is negligible in alkaline solution and consequently a decrease in fluorescence emission is observed. As an effect of the protonated side chain, the basicity of the heterocyclic nitrogen at N_2 position is drastically reduced, thus accounting for the strong pK difference that can now be taken as an evidence of the proposed intramolecular interaction.

We therefore conclude that the 2AP molecule *cannot* be considered a plausible parent chromophore because it completely lacks the charge–transfer character that explains the absence of fluorescence from di–protonated TRP and MEP. 2DMP is a much better parent chromophore but it should be emphasized that at neutral condition the AP group of the two antihistamines cannot be described by a de–protonated 2DMP because in TRP and MEP the chromophore is electronically interacting with the protonated side chain.

3.4 Conclusions

In this Chapter we clarified the photophysics of TRP and MEP and the relation between structure and spectroscopy in solutions of varying pH. Although the complete pH range investigated is not likely to be important for biological systems, measurements at very low (pH 13.0) and very high (pH 2.0) acidity did help to understand the behavior of TRP and MEP at physiological pH values.

The main result of this Chapter is that there is a definite influence of the

protonated butylamino chain on the chemical and photophysical properties of these molecules. The change of pK value, from about 7 in related compounds like 2AP and 2DMP to about 4 in TRP and MEP is related to the presence of an internal hydrogen bond between the protonated butylamino tail and the pyridine nitrogen, changing the accessibility of this nitrogen for external protons. Decay associated spectra at these pH values indicate an equilibrium mixture between two species. The difference in spectroscopic properties makes it possible to use fluorescence techniques in binding studies.

At lower pH, upon protonation of the heterocyclic nitrogen N_2, MEP becomes non–fluorescent. However, a long emission band centered at 420 nm shows up in the TRP emission spectrum, possibly as a result of excited state proton transfer from the N_2 to the N_3 position. The absence of this long wavelength emission band in MEP indicates that fluorescence quenching via electron transfer startinng at the anisole group accounts for the difference.

Another effect that contributes to the specific spectroscopic properties of MEP is the interaction between the two chromophores. In MEP it is obvious from the excitation and emission spectra that excitation energy is transfered completely from the anisole to the AP moiety. There are two ways that can be used to describe this phenomenon. The FRET mechanism can be invoked or it can be viewed as excitonic interaction between the chromophores. In both cases the result is related to the geometric structure, in particular the relative orientations of the chromophores [91]. A description by excitonic interaction may be the most appropriate in this case. There are several reasons for this. First of all the chromophores are rather close, probably closer than 1 nm [92]. In addition the spectrum of the anisole moiety in MEP is shifted slightly to the blue and the spectrum of AP is more to the red than those of the corresponding isolated molecules, something that could be explained by excitonic interaction.

Whatever the exact mechanism is, a consistent picture requires, apart from the geometry of the full molecule for the calculation of angular factors (κ in the FRET mechanism), spectral overlap or positions of the energy levels, and the distance. For this reason the most appropriate reference compound for the

AP moiety is very relevant, something we discussed at length in section 4.

A spectral shift of the band ascribed to the AP group is recorded for both TRP and MEP when going from neutral to alkaline solution. At this condition it is the protonation state of the side chain that changes, which affects the absorption and the emission properties of the chromophore responsible for the fluorescence emission, *i.e.* a deprotonated AP. It has been suggested that self–association of TRP and MEP could also play a role in explaining spectral shifts [93], but complexation starts to be important in aqueous solution at much higher concentrations than the ones used in this study.

NMR and IR measurements in solution suggest the coexistence of a number of gauche and trans conformations both for histamine [94] and antihistamines [85, 95] due to an extreme flexibility of the sigma bonds in the aliphatic chain, which gives appreciable structural freedom. NMR data also show that the cationic ethylenediamine derivatives TRP and MEP exist in water predominantly as equivalent mixtures of gauche and trans conformers [78]. Therefore the intramolecular tail–AP interaction is the most likely option to explain the unexpected spectral shift we observe.

Different conformers may have different activities because they are are not equally complementary to the 3D structure of a target protein. For example, the trans form of H_1 antihistamines appears to be essential for activity at the H_1 receptor, whereas the gauche form does not interact [95]. Characterization of the various conformational forms of agonists and antagonists is an important step in elucidating the molecular background to the biological versatility. Our results show that the two different conformations can be distinguished by means of fluorescence spectroscopy, which has interesting consequences for the protein binding studies.

Acknowledgement We would like to thank M. Smit and R. Leurs of the Department of Medicinal Chemistry for support and discussions.

Chapter 4

Structure elucidation of fluorescent H_1 antihistamines by ultraviolet resonance Raman spectroscopy. Solvent structures of tripelennamine and mepyramine[4]

[4] The contents of this Chapter were published by Silvia Tardioli, Cees Gooijer, and Gert van der Zwan in the Journal of Raman Spectroscopy 42(5):1016-1024 (2011).

Abstract Ultraviolet resonance Raman (UVRR) spectroscopy —a Raman technique that combines high sensitivity with high selectivity and does not suffer from background fluorescence— is applied to the fluorescent H_1 antihistamines tripelennamine (TRP) and mepyramine (MEP) in aqueous solution to elucidate their molecular structure as a function of pH. In a previous investigation of these compounds [*J. Phys. Chem. B*, **113**, (2009), 6949] the presence of gauche conformers caused by intramolecular interaction of the protonated alkylamine tail with the pyridine nitrogen was assumed to explain the pH dependence of the fluorescence properties. In order to validate this assumption use is made of resonant excitation of the aminopyridine chromophore in TRP and MEP. In that way structural information associated with the vibrations of that moiety can be obtained, and changes it undergoes upon protonation can be monitored. Assignment of the vibrations was achieved with the help of a number of other compounds, and quantum chemical calculations. *N*,N–dimethylaminopyridine (2DMP) and its mono–protonated form ($2DMPH^+$) were investigated, since this molecule was shown to have optical properties closely resembling those of the aminopyridine moiety in TRP and MEP. Assignment of the vibrations of 2DMP was accomplished by comparison with resonant Raman spectra of two other reference structures, 2–aminopyridine and dimethylaniline —for which ordinary Raman data are available —and by Gaussian calculations. UVRR spectra of TRP and MEP could be readily interpreted on the basis of vibrational assignments of the parent chromophores, *i*.e. 2DMP and $2DMPH^+$. Vibrations of the aminopyridine chromophore in TRP and MEP at neutral pH, where the aminoalkyl chain is protonated, are modified when compared to the vibrational pattern recorded for a fully neutral molecule in alkaline solution. This implies an electronic redistribution in the ring originating from internal hydrogen bonding between the aminoalkyl tail and the aminopyridine chromophore.

4.1 Introduction

Experimental methods which give structural information about binding of ligands and substrates to proteins in aqueous solution are of paramount importance for understanding the behavior of receptors and enzymes, and provide much needed information for validation of computational binding studies. Vibrational spectroscopies are potentially powerful techniques to obtain direct information about the structure of ligands in the binding site. In particular resonance Raman spectroscopy can provide detailed data on how exactly a ligand is bound. This is made easier if it is possible to selectively excite the ligand. It is, however, necessary to understand the vibrational structure of the ligands themselves to a sufficient degree before attempting to relate structural changes that may occur in the vibrational spectra upon binding.

Raman spectroscopy in aqueous solution has an inherent advantage over infrared vibrational spectroscopy since water is not Raman active in the relevant wavenumber range. An equally inherent disadvantage, however, is its low sensitivity. High concentrations are needed, and fluorescence can easily swamp the much weaker Raman signal. In Resonance Raman (RR) spectroscopy, where electronic transitions are used to substantially increase the signal, sensitivity is much better. Concentrations of the solute can be well below 100 μM, sufficient to avoid effects of association [23]. Selectivity is also increased dramatically, since only vibrations of the chromophore are enhanced in intensity. The positions of the lines do not change. Using resonance with higher electronic states, by excitation in the UV, the remaining problem —fluorescence— can also be avoided, since it is shifted far enough to the red to allow a complete Raman spectrum to be recorded before fluorescence starts to play a role. This makes UVRR spectroscopy a quite attractive analytical tool for structure elucidation [5, 6].

In view of the electronic absorption spectra of the compounds of interest (see Figure4.2), deep UV wavelengths are appropriate to achieve resonance with a higher electronic transition between 220 and 270 nm. Not many CW laser

lines are available in that wavelength region. In fact only a few lines of the frequency–doubled Argon ion laser, of which the two wavelengths at 229 nm and 257 nm are in resonance with the absorption of the 2–aminopyridine (AP) moiety in tripelennamine (TRP) and mepyramine (MEP). At these wavelengths the molecules are excited to different electronic states, which gives interesting additional information due to differences in enhancement. This makes our results also useful for validation of computational techniques for calculating RR spectra [96].

In Chapter 3 we showed by means of fluorescence spectroscopy that two naturally fluorescent reverse agonists of the histamine H_1 receptor, TRP and MEP, occur in aqueous solution at neutral pH in two possible conformations, the trans form and the gauche form, *c*f. Figure 4.1. It is rather likely that binding to the H_1 receptor will occur only for one of these forms [94], and consequently the thermodynamics and kinetics of binding will be dependent on the equilibrium between the trans and gauche forms of these compounds. In addition the complicated behavior of TRP and MEP provides interesting possibilities for a detailed look at the binding properties. We showed that the steady state and time–dependent fluorescent properties are different for the two forms, which potentially give the possibility to see which of the forms of these compounds is bound in the active site of a protein.

Most of the pH–dependent electronic properties of the antihistamines could be understood by comparing them to those of *N,N*–dimethylaminopyridine (2DMP) [97]. Though 2DMP is very similar to the chromophoric moiety of these antihistamines (*c*f. Figure 4.1a), their spectroscopic properties in neutral–alkaline aqueous solution were shown to be significantly different. To explain these differences in the electronic spectra it was proposed that in the antihistamines interaction of the protonated aminoalkyl chain with the neutral pyridine ring is responsible for the different behavior. The aminoalkyl nitrogen has a pK_a value of about 9 and is therefore protonated at physiological conditions. The presence of these structures might play an important role in understanding the binding properties to the histamine receptor.

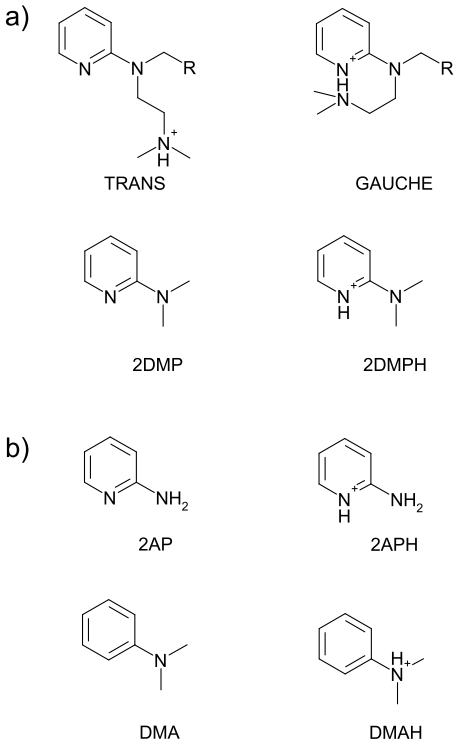

Figure 4.1: Chemical structure of the compounds investigated in this study. (a) Trans and gauche conformers in aqueous solution of tripelennamine (R=benzene) and mepyramine (R=anisole) at physiological pH. Structurally the aminopryidine chromophore of TRP and MEP is close to 2DMP [97]. (b) The vibrational assignment of 2DMP and its mono–protonated form $2DMPH^+$ was achieved by comparison to two other reference structures, 2AP and DMA, both in their neutral and mono–protonated forms, $2APH^+$ and $DMAH^+$.

The present Chapter aims at further testing this assumption by means of UVRR spectroscopy. The effect of protonation on the parent chromophore of the aminopyridine (AP) group, *i.e.* 2DMP, is studied with the purpose to pro-

vide a vibrational assignment useful to derive detailed structural information about the AP group of antihistamines and the way it is affected by protonation.

RR spectra of 2DMP, $2DMPH^+$, and the antihistamines are not available in the literature. To facilitate the vibrational assignment of 2DMP and $2DMPH^+$ two other reference compounds were also studied: 2–aminopyridine (2AP) and dimethylaniline (DMA) both in their neutral and mono–protonated forms (see Figure4.1b). For these compounds ordinary Raman spectra of the unprotonated forms are available [98]. The first compound, 2AP, is used to show the effect of protonation on the vibrations of the pyridine ring. The RR spectra of DMA show vibrations of the $-N(CH_3)_2$ or $-N(CH_3)_2H^+$ group in resonance with a benzene ring. The complete assignment of the 2DMP vibrations was achieved by correlation with the vibrational bands of these reference compounds.

Spectral modifications resulting from protonation of the pyridine ring in $2DMPH^+$ are discussed on the basis of the RR spectra of the mono–protonated reference compounds. For protonated 2DMP, both the possibility of protonation at the pyridine ring and protonation at $N(CH_3)_2$ are considered. Fluorescence data indicate that both forms may be present at low pH [97]. Quantum mechanical calculations were performed as a further aid to assigment and to verify the reliability of the method adopted.

4.2 Experimental

Materials Tripelennamine hydrochloride (TRP), mepyramine maleate (MEP), 2–(*N,N*–dimethylamino)pyridine (2DMP), 2–aminopyridine (2AP) and *N,N*–Dimethylaniline (DMA) were purchased from Sigma Aldrich and used without further purification. Aqueous solutions were prepared by dissolving the antihistamine salts and the reference compounds in Milli–Q water. Measurements were performed at room temperature in a quartz cuvette of 1 cm path length. UV absorption spectra were recorded at an analyte concentration of 4 μM and

UVRR spectra at 0.3 mM. Self–association of the studied antihistamines starts to be important in aqueous solution at much higher concentrations than the ones used in this study [93]. The neutral and the mono–protonated form of 2DMP, 2AP and DMA were obtained by pH adjustment with analytical grade 5 mM NaOH and 5 mM HCl, respectively. For the antihistamines more alkaline or acidic pH's were obtained with (1–10) mM NaOH and HCl (1–10) mM.

Instrumentation UV electronic absorption spectra were measured on a Varian Cary 50 Bio UV–Vis spectrophotometer. The UVRR setup was described in detail previously [96].

Resonant excitation at 229 nm and 257 nm is achieved by a frequency–doubled Argon ion laser, Innova FreD 90C (Coherent, Utrecht, the Netherlands). In order to avoid photodecomposition the quartz cell was held in a moving object and the laser power reaching the sample was kept low at 4.5 mW. No effects of photodegradation of the samples were observed. A 3600 lpm line grating was used to disperse the spectra on a cooled (–50°) Andor technology Model DV420–OE CCD camera (Belfast, Northern Ireland) in the range (500–2000) cm^{-1}. All the spectra presented in this Chapter have the blank subtracted and are normalized relative to ring mode 8a.

Vibrational Calculation Simulated vibrational spectra of 2AP, DMA and 2DMP along with their mono–protonated forms were calculated with the Gaussian 03 software package [99]. Geometries of the neutral and protonated molecules were optimized without imposing any geometrical constraint at two levels of theory: Hartree–Fock (HF) and density functional theory (DFT) using the standard 6-31G++(d) basis set. The DFT method employed was with exchange correlation functional B3LYP. Since diffuse functions allow orbitals to occupy a large region of space they become important for calculations involving molecules with lone paired electrons [100]. Absence of imaginary wavenumbers indicated that the stationary points corresponded to true minima for the optimized geometries. The calculations of vibrational wavenumbers with the two methods were used to establish which kind of calculation agrees best with the experimental data.

In our case the DFT method appears to provide the more accurate vibrational data. Therefore B3LYP/6-31++G(d) results are presented, where wavenumbers have been scaled with a standard common scaling factor of 0.96 to achieve better correspondence between the theoretical and experimental data. The normal modes of vibration of the benzene and pyridine rings were labeled according to the convention adapted from the Wilson notation for benzene [75]. Below 1700 cm^{-1} the ring modes are described by six in–plane stretches (ν) (8a, 8b, 19a, 19b, 14, and 1), three in plane bends (δ) (12, 6a, and 6b), three out of plane bends (4, 16a, and 16b), six in–plane bends of the CH's (9a, 9b, 18a, 18b, 3, and 15) and six out of plane CH bends (17a, 17b, 10a, 10b, 11, and 5). A further description of the notation used in this Chapter can also be found in [101].

4.3 Results and Discussion

4.3.1 UVRR spectra of 2AP, DMA and 2DMP

In this section we discuss the UVRR spectra of the various reference compounds 2AP, DMA and 2DMP, and their protonated forms.

Selective Excitation To gain insight into the expected resonance effects at 229 nm and 257 nm excitation, the electronic absorption spectra of 2DMP and the reference structures in aqueous solution are shown in Figure 4.2. Since in 2DMP two protonable nitrogens are present, in the pyridine ring and in the $–N(CH_3)_2$ group, one point of interest was to find out effects of protonation on vibrations associated with these moieties. In the absorption spectra of 2AP and $2APH^+$ (see Figure 4.2(a)) two absorption bands can be discerned originating from the close lying n–π^* and π–π^* states of the amino substituent and the pyridine ring. Upon protonation of the pyridine ring there is a bathochromic shift of the 287 nm band to 300 nm and an intensity increase due to enlargement of the conjugated system. At the 257 nm laser line the extinction coefficients

of both 2AP and $2APH^+$ are very weak. Furthermore, the transition at 229 nm coincides with the S_0–S_2 transition which has a strong π–π^* character, as is known from literature [89]. Therefore, UVRR at 229 nm will provide information about the way the pyridine ring vibrations are affected by protonation.

In DMA only the $-N(CH_3)_2$ group can be protonated. From Figure 4.2(b) it is evident that in the neutral molecule the $-N(CH_3)_2$ group is strongly conjugated with the benzene ring and two electronic transition bands can be discerned, presumably related to the n–π^* transition at longer wavelengths and the benzene π–π^* at shorter wavelengths [88]. The 257 nm laser line is in overlap with both these bands, whereas the 229 nm line will only excite the π–π^* transition. Differences between spectra taken at these wavelengths will be indicative of the $-N(CH_3)_2$ vibrations of DMA. Upon protonation the conjugation is lost, which changes the absorption spectrum rather dramatically: the molar absorbivity of $DMAH^+$ becomes too weak to be discernible at these concentrations, and therefore for $DMAH^+$ resonance enhancement of the vibrations is expected to be very small. We note that only in DMA the n–π^* is weak and almost forbidden. The reason these bands are much stronger in 2AP and 2DMP is geometrical. The orbitals are no longer perpendicular, leading to considerable mixing between the states in those two compounds.

The absorption spectrum of 2DMP (see Figure 4.2(c)) also shows the two characteristic bands, at 240 nm the transition of the pyridine aromatic system and furthermore the charge transfer transition at 310 nm. Introduction of the exocyclic dimethyl group instead of the hydrogen atoms as in 2AP causes a bathochromic shift of both the neutral and mono–protonated absorption spectra originating from increased electron donating properties of the substituent. This is partly regarded as being due to a favorable coplanarity of 2DMP caused by smaller steric effects [88].

In view of the absorption spectra of 2DMP and $2DMPH^+$, it should be expected that at 257 nm excitation the $-N(CH_3)_2$ vibrations should be more enhanced than at 229 nm excitation. At 229 nm the vibrations of the protonated and non–protonated pyridine ring will be relatively stronger.

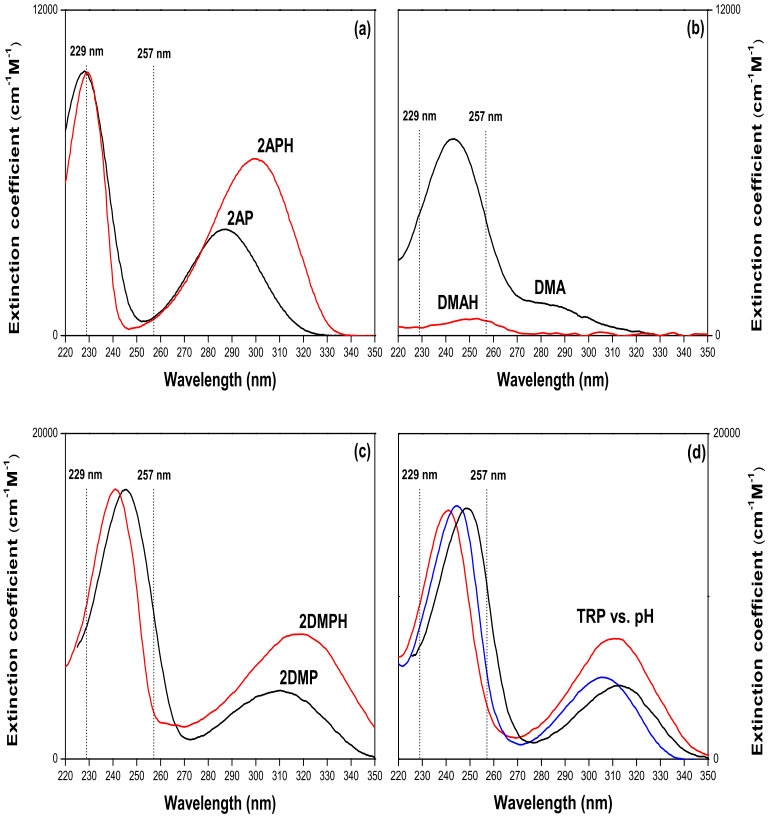

Figure 4.2: UV absorption spectra of (a) 2AP —— and $2APH^+$ ——; (b) DMA —— and $DMAH^+$ —— ; (c) 2DMP —— and $2DMPH^+$ —— ; (d) TRP —— at pH 13.0, TRP —— at pH 7.0 and TRP —— at pH 3.0

The electronic absorption properties of the aminopyridine moiety of TRP and MEP in its neutral (alkaline pH) and di–protonated form (acidic pH) are

well described by 2DMP and $2DMPH^+$ [97]. At 229 nm the absorption from the anisole chromophore and the maleate counter–ion contribute to the MEP spectral profile. Therefore in order to show pure AP vibrations, RR spectra of TRP and MEP are presented at 257 nm. In Figure 4.2(d) the UV absorption spectrum of TRP is shown at different pH values. Similar results were recorded for MEP [97]. The UVRR spectra of all reference compounds in their neutral and mono–protonated form are shown in Figure 4.3 and 4.4.

UVRR spectra of 2AP and $2APH^+$ UVRR spectra of 2AP and $2APH^+$ at 229 nm are shown in Figure 4.3 (a1). The wavenumbers of the observed (R and RR) and calculated wavenumbers are summarized in Table 4.1. Assignment of the bands in 2AP was achieved by matching the spectrum with Raman wavenumbers reported by Carmona *e*t al. [98] which are also shown in Table 4.1 for comparison.

Again vibrational calculations of 2AP and $2APH^+$ were used to verify the experimental assignment proposed in [98] and to correlate the RR bands of $2APH^+$.

Theoretical investigation led to assignments for 2AP which are in agreement with those of Carmona *e*t al. [98] apart from an exchange between pyridine ring modes 3 and 14, which is in accordance with the Raman assignment of pyridinium salt [102]. In addition mode 12 and 1, which were related in [98] to the Raman bands at 1048 cm^{-1} and 997 cm^{-1}, are now ascribed to RR bands at 1000 cm^{-1} and 850 cm^{-1}, respectively. Our results are in line with a more recent theoretical and experimental investigation of 2AP [103, 104].

Significant changes were found in the enhancement pattern of $2APH^+$. The wavenumber of the characteristic C=C stretch of the ring (8a) increases by 31 cm^{-1}, similarly to what was observed in the Raman spectrum of pyridinium salts [101]. This is likely due to the bond order changes following reduced conjugation of the nitrogen lone pair to the ring after protonation. The molecule becomes less aromatic, and get more single/double bond character. The bonds involved in this vibration get more double bond character, and consequently the wavenumber increases.

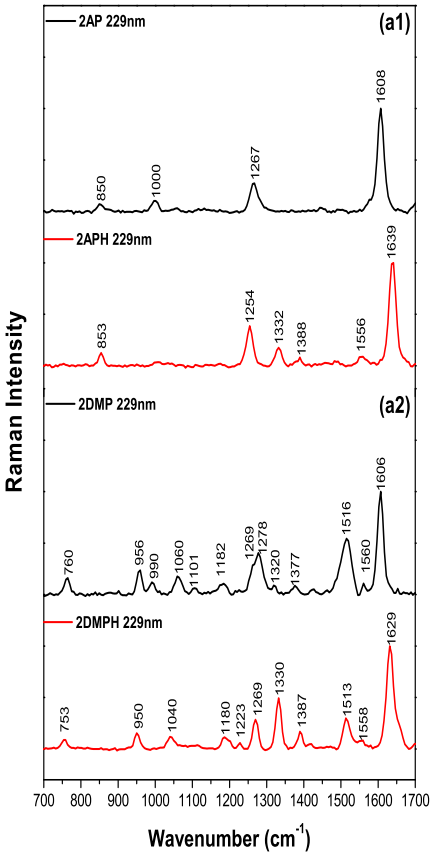

Figure 4.3: Experimental UVRR spectra recorded at 229 nm of 2AP —— and $2APH^+$ —— (a1); 2DMP —— and $2DMPH^+$ —— (a2).

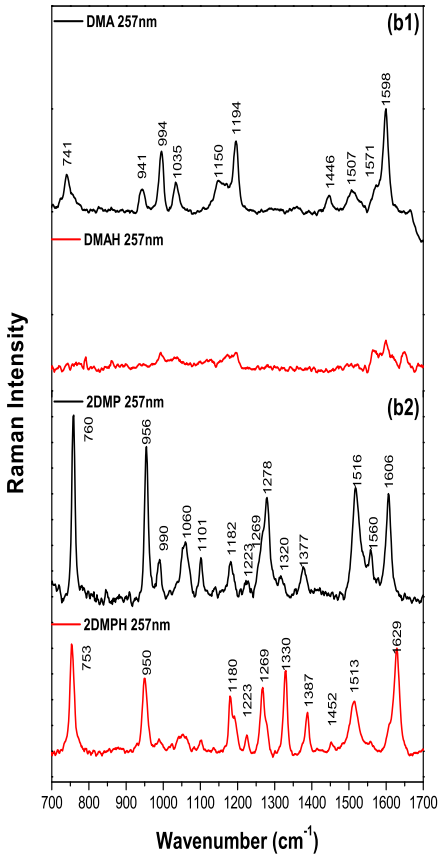

Figure 4.4: Experimental UVRR spectra recorded at 257 nm of DMA —— and $DMAH^+$ — – (b1); 2DMP —— and $2DMPH^+$ —— (b2).

2AP			$2APH^+$		
R Exp.	RR Exp.	R Calc.	RR Exp.	R Calc.	Assignment
1606(m)	1608(s)	1606	1639(s)	1648	ν_{ring} 8a + δ_{NH^+}
1570(m)		1558	1556(w)	1601	ν_{ring} 8b
1333(m)		1306	1332(w)	1360	δ_{CH} 3
1314(sh)		1289	1388(vw)	1382	$\nu_{(N-ring)}$
1261(m)	1267(m)	1276	1254(m)	1301	ν_{ring} 14 + δ_{NH^+}
997(s)	1000(w)	960		968	δ_{ring} 12
866(sh)	850(w)	825	853(w)	823	ν_{ring} 1

Table 4.1: Raman (R), Resonance Raman(RR) and calculated wavenumbers (cm^{-1}) of 2AP and $2APH^+$ in aqueous solution. Experimental Raman wavenumbers of 2AP are taken from [98]. Abbreviations: (s) strong; (m) medium; (w) weak; (vw) very weak; (sh) shoulder. Notations: ν stretch; δ bend.

Two new bands are weakly intensified in the RR spectrum of $2APH^+$ at 1332 cm^{-1} and 1388 cm^{-1} and attributed respectively to ring mode 3 and to an N–ring stretch vibration. The resonant enhancement of the $\nu_{(N-ring)}$ in $2APH^+$ at higher wavenumbers with respect to the position of the mode in the neutral base reflects a shortening of the bond length, typical of double bond character [105]. In the work of Cook [101] concerning the Raman spectrum of pyridinium ion, the NH^+ in plane bending was ascribed to the Raman band at 1245 cm^{-1}. In the RR spectrum of 2AP we ascribed the band at 1267 cm^{-1} to ring mode 14, which indicates a contribution from the intracyclic nitrogen stretching. This is corroborated by the calculations.

The reduced wavenumber of the band in the RR spectrum of $2APH^+$ implies a loss of the electronic density in the bond as a consequence of protonation. Therefore we related the RR band of $2APH^+$ at 1254 cm^{-1} to the ring mode 14 coupled to an NH^+ in–plane bending mode. We will show below that the

same mode is active in the RR spectrum of 2DMP and of the antihistamines TRP and MEP.

UVRR spectra of DMA and $DMAH^+$ The UVRR spectra of DMA and $DMAH^+$ at 257 nm are shown in Figure 4.4 (b1). As expected for $DMAH^+$ the resonance effects (both at 229 nm and 257 nm) are too weak to record an informative Raman spectrum at the concentration used, although some of the stronger bands of DMA appear to be present in the $DMAH^+$ spectrum. The RR spectrum of DMA was recorded in aqueous solution, where the concentration of $DMAH^+$ is negligible, since in addition to its low intrinsic intensity, the pK_a=5.15 is sufficiently low for the molecule to be regarded as neutral.

The observed RR bands and the calculated wavenumbers of DMA are summarized in Table 4.2 and compared to the experimental Raman wavenumbers of DMA taken from [106].

The assignment we propose is also based on the paper of Brouwer *et* al. [107], who performed a theoretical investigation of the DMA vibrations and changed some of the assignments of [106]. In particular the assignment of the band at 741 cm^{-1} was changed since vibrational calculations indicated that it is more likely related to ring mode 6a coupled to the NC_2 stretch, rather than ring mode 1 [107].

All the RR bands of DMA correspond to active Raman bands except for two weakly enhanced bands at 1571 cm^{-1} and 1507 cm^{-1}, which apparently have no counterpart in the off–resonance Raman spectrum. Their positions match very well the ring modes 8b and 19a, which are more active in the infrared spectrum of DMA. Those modes are ring stretches whose intensities are enhanced as a consequence of the resonant character of the technique. It is noteworthy that no N–ring stretch shows up in the RR spectrum of DMA at 1348 cm^{-1} whereas the mode has medium Raman activity. We will show that this band is instead enhanced in the RR spectra of 2DMP and even more so in $2DMPH^+$, suggesting that the relative orientation between the dimethylamino substituent and the π ring in 2DMP is affected by the presence of the nitrogen in the ring, and that a more quinoidal character is recovered.

DMA			
R Exp.	RR Exp.	R Calc.	Assignment
1605 (s)	1598 (vs)	1594	ν_{ring} 8a
	1571 (sh)	1602	ν_{ring} 8b
	1507 (w)	1497	ν_{ring} 19a + $\nu_{(N-ring)}$
1450 (w)	1446 (w)	1460	ν_{ring} 19b
1195 (m)	1194 (s)	1191	δ_{CH} 9a + $\nu^{as}_{NC_2}$
1165 (sh)	1150 (m)	1166	ν_{ring} 15
1038 (s)	1035 (m)	1020	δ_{CH} 18a+ $\nu_{(N-ring)}$
995 (vs)	994 (s)	972	δ_{ring} 12
949 (m)	941 (w)	868	ν_{ring} 1 + $\nu^{s}_{NC_2}$
744 (s)	741 (m)	684	$\delta ring$ 6a+ $\nu^{s}_{NC_2}$

Table 4.2: Raman (R), Resonance Raman (RR) and calculated wavenumbers (cm^{-1}) of DMA in aqueous solution. The experimental Raman wavenumbers of DMA are taken from [106]. Abbreviations: (vs) very strong; (s) strong; (m) medium; (w) weak; (sh) shoulder. Notations: ν stretch; ν^{as} anti-symmetric stretch; ν^{s} symmetric stretch; δ bend.

UVRR spectra of 2DMP and 2DMPH$^+$ For the previous two compounds experimental data in the form of ordinary Raman spectra were already available from literature, and although the intensities will be different, the line positions do not change. They are the same for ordinary and resonance Raman spectra. The interpretation of the Raman spectra of 2DMP and 2DMPH$^+$ is therefore slightly more involved. In addition the n–π^* transition band is overlapping with the 257 nm line of the FRED laser, and consequently data on resonance with an other electronic transition can give additional information.

The UVRR spectra of 2DMP and 2DMPH$^+$ recorded at 229 nm are presented in Figure 4.3 (a2). The observed and calculated wavenumbers of 2DMP and

$2DMPH^+$, and the proposed assignments are given in Table 4.3.

At this excitation wavelength, which is in resonance with the π–π^* ring transition, the focus is on the vibrations of the (protonated) pyridine moiety of 2DMP. Similarities in the UVRR spectra of 2DMP and 2AP (*cf.* Figure 4.3 (a1)) as well as in their mono–protonated forms, are abundant, both in terms of number of bands and their position. For each enhanced pyridine band in the spectra of 2AP or $2APH^+$ there is a counterpart in the UVRR spectrum of 2DMP or $2DMPH^+$, which can then of course be related to the same mode. This is also demonstrated by the calculations, although in the wavenumber region below 1000 cm^{-1} no correspondence is observed due to the combination of ring modes 1 and 6a of 2DMP with the stretch of the dimethylamino group, similar to DMA.

Mode 8a, a stretch vibration of aromatic compounds is highly characteristic and very prominent in the spectrum of benzene and pyridine derivatives and essentially unperturbed by substituents. The UVRR spectra we recorded for DMA and 2AP all showed strong bands at 1608 cm^{-1} and 1598 cm^{-1} respectively, and without ambiguity we attributed the RR band of 2DMP at 1606 cm^{-1} to it. In the spectrum of $2DMPH^+$ this band shifted to higher wavenumbers, similarly to the behavior in $2APH^+$, strongly indicating that the first protonation site is indeed the pyridine nitrogen.

At lower wavenumbers, other characteristic pyridine modes like 8b, 19a and 19b are expected, similarly to 2AP. In the spectrum of 2DMP the two bands at 1560 cm^{-1} and 1516 cm^{-1} were attributed to modes 8b and 19a, in accordance with vibrational calculations, which also showed that in 2DMP mode 19a is strongly mixed with ν(N–ring), like for DMA. In the RR spectrum of $2DMPH^+$ the new band weakly enhanced at 1452 cm^{-1} was attributed to ring mode 19b.

In the RR spectrum of 2DMP two bands of weak intensity are visible at 1377 cm^{-1} and 1320 cm^{-1}, where the ν(N–ring) stretch and ring mode 3 are active in the Raman spectra of both DMA and 2AP. vibrational calculations confirm assignment of the band centered at 1377 cm^{-1} as the ν(N–ring) stretch of 2DMP, and the band at 1314 cm^{-1} to ring mode 3.

Since at 229 nm the laser line is in resonance with the electronic transition of the pyridine ring, RR activity of the (N–ring) vibration in 2DMP can only be explained in terms of a major coupling between ring and dimethylamino vibrations due to favourable $n - \pi$ conjugation, in contrast to 2AP where no ν(N–ring) was enhanced. That also explains why the ν(N-ring) wavenumber of 2DMP showed up in the RR spectrum at higher wavenumbers compared to the position of the same mode in 2AP. In line with this interpretation the pyridine wavenumbers of 2DMP are found at lower wavenumbers than those of 2AP, because of the electron releasing property of the dimethylamino group towards the aromatic nucleus, which would reduce the average bond order of the ring with a consequent lowering of the ring skeletal vibrations.

Interestingly, the broad band of 2DMP enhanced in the range (1230–1310) cm^{-1} is the result of two close lying bands centered at 1269 cm^{-1} and 1278 cm^{-1}, respectively. Upon protonation, the latter is strongly attenuated. Calculations give evidence that the two bands enhanced at 1269 cm^{-1} and 1278 cm^{-1} both bring in a contribution of the pyridine nitrogen, exactly as was obtained for 2AP; the former was ascribed to to ring mode 9a and the latter to ring stretch 14. Those bands were also observed in the RR spectra of the antihistamines, as discussed below.

Other ring modes of 2DMP were visible in the low wavenumbers spectral range at 1182 cm^{-1}, 1101 cm^{-1} and 1060 cm^{-1} and attributed to mode 15, 9b (uncertain) and 18a. The symmetric deformation of the pyridine ring (mode 12) showed up in the RR spectrum of 2DMP at 990 cm^{-1}. The band disappeared in $2DMPH^+$, similarly to $2APH^+$, where the protonation site is known to be the pyridine nitrogen.

The UVRR spectrum of 2DMP at an excitation of 257 nm is presented in the upper part of Figure 4.4 (b2). At this wavelength the $n - \pi^*$ transition is also in resonance with the laser line, and the focus is now on the vibrations of the $–N(CH_3)_2$ group of 2DMP. By direct comparison with the DMA spectrum (*cf.* Figure 4.4 (b1)) the group of vibrations of the dimethylamino substituent could be readily assigned. Ring mode 19a in 2DMP is coupled to the ν(N-ring)

resulting in a stronger RR enhancement of the band in the spectra of both DMA and 2DMP, when compared to 2AP.

Symmetric and antisymmetric bends of the methyl group (δCH_3) were visible in the Raman spectrum of DMA between (1400–1500) cm^{-1}, see Table 4.2. In the same spectral region the 19b fundamental of the pyridine ring is also Raman active; therefore mixing of the normal coordinates is expected. The weak bands observed for $2DMPH^+$ at 1452 cm^{-1} was attributed to mode 19b coupled to the methyl umbrella mode, in agreement with vibrational calculations. The antisymmetric stretch of NC_2 in 2DMP was ascribed to the band at 1223 cm^{-1}, which is infrared active at 1230 cm^{-1} in the spectrum of DMA. No ring modes are expected at this spectral range.

The symmetric $\nu_S NC_2$ mode of 2DMP is coupled to breathing ring mode 1 and 6a, giving rise to two bands at 955 cm^{-1} and 758 cm^{-1}, already reported for DMA.

The UVRR spectrum of $2DMPH^+$ at an excitation of 257 nm is presented in the lower part of Figure 4.4 (b2). At this excitation wavelength both the electronic transition of the pyridine ring and the charge transfer band of 2DMP and $2DMPH^+$ are expected to lead to enhancement, on the basis of the UV absorption spectra. By comparison with the UVRR spectra recorded at 229 nm (*cf.* Figure 4.3 (a2)), where mainly pure pyridine ring vibrations are enhanced, it is clear that some changes in the enhancement patterns depending on the excitation wavelength of both 2DMP and $2DMPH^+$ occur. A new band shows up in the UVRR spectra of 2DMP and $2DMPH^+$ at 1223 cm^{-1} which is ascribed to the antisymmetric stretch of of NC_2, similarly to DMA. Several ring modes in 2DMP gained in intensity at 257 nm compared to 229 nm, thus unveiling which pyridine ring modes are actually mixed with the vibrations of the dimethylamino subtituent. Strong changes are observed for the vibrations at 1516 cm^{-1} (19a), 1377 cm^{-1}, and the two bands at 956 cm^{-1} (1) and 760 cm^{-1} (6a). The enhancement pattern of the same modes in the UVRR spectra of $2DMPH^+$ when excited at 257 nm are weaker than at 229 nm, when compared to 2DMP. This is fully in line with the much weaker absorption in the charge

2DMP		2DMPH$^+$		
RR Exp.	RR Calc.	RR Exp.	RR Calc.	Assignment
1606 (m/s)	1623	1629 (s)	1625	ν_{ring} 8a
1560 (m)	1590		1596	ν_{ring} 8b
1516 (m/s)	1501	1513 (m)	1528	ν_{ring} 19a + $\nu_{(N-ring)}$
	1425	1452 (w)	1466	ν_{ring} 19b + δ_{CH_3}
1377 (m)	1361	1387 (m)	1386	$\nu_{(N-ring)}$
1320 (m/w)	1320	1330 (s)	1357	δ_{CH} 3
1278 (m/s)	1291		1316	ν_{ring} 14
1269 (m)	1232	1269 (m/s)	1243	δ_{CH} 9a + δ_{NH^+}
1223 (w)		1223 (w)	1206	$\nu^{as}_{NC_2}$
1182 (m)	1148	1180 (m)	1165	δ_{CH} 15
1101 (m)	1086		1088	δ_{CH} 9b
1060 (m)	1038		1020	δ_{CH} 18a
990 (m)	962		975	δ_{ring} 12
956 (s)	944	950 (s)	921	ν_{ring} 1 + $\nu^{s}_{NC_2}$
760 (s)	749	753 (s)	730	δ_{ring} 6a+ $\nu^{s}_{NC_2}$

Table 4.3: Raman (R), Resonance Raman(RR) and calculated wavenumbers (cm^{-1}) of 2DMP and 2DMPH$^+$ in aqueous solution. Abbreviations:(s) strong; (m/s) medium/strong; (m) medium; (m/w) medium/weak; (w) weak; (sh) shoulder. Notations: ν stretching; ν^s symmetric stretching; ν^{as} anti–symmetric stretch; δ bend.

transfer band (at 257 nm) upon protonation of the pyridine ring (Figure 4.2(c)).

4.3.2 UVRR spectra of Tripelennamine and Mepyramine

Although interesting by itself, the main purpose of the previous section was to identify the vibrational modes in order to obtain insight into the spatial

structure of the antihistamines TRP and MEP. These molecules are too large and flexible to allow for easy quantum chemical calculations, which deserve to be treated in more detail, and in combination with binding to proteins. The main goal of the present Chapter is to validate the model where the protonated alkylamino tail has an intramolecular bond with the pyridine unit, and to see if UVRR spectroscopy can be used to elucidate the inter– and intramolecular bonding of these molecules. To that end we now turn to the relevant compounds, of which the absorption spectra are also shown in Figure 4.2(d).

The UVRR spectra of TRP and MEP at different pH values are shown in Figure 4.5 and 4.6 with excitation at 257 nm, where the AP chromophore as well as the charge transfer band are resonantly excited. By comparison with the UVRR spectra of the parent chromophore, *i*.e. 2DMP and $2DMPH^+$, we could verify that all the bands resonantly enhanced at 257 nm are attributed to vibrations of the AP moiety, and not to other parts of the molecule. Furthermore, that a neutral 2DMP describes the RR enhancement of the neutral AP group of antihistamines very well, while the vibrations of $2DMPH^+$ account for the RR profiles of the protonated AP at the pyridine nitrogen.

At 257 nm the anisole chromophore in MEP is also (weakly) absorbing so that mixing of the pyridine and anisole electronic states may be responsible for the small differences in the enhancement patterns between MEP and TRP, in line with our earlier findings [97]. There is no clear evidence of anisole vibrations present in the MEP spectrum. Anisole is very weakly absorbing at that excitation wavelength, but apparently not sufficient to give rise to visible Raman lines. The UVRR spectrum of anisole at an excitation wavelength of 229 nm, at a higher concentration of 1 mM is shown in Figure 4.7.

No spectral differences between MEP and TRP are noticeable at alkaline and acidic pH. However, at neutral pH, a stronger electronic coupling between the pyridine and the anisole moiety in MEP may be responsible for the higher intensity of the band at 755 cm^{-1} and ascribed to in plane ring bend 6a, compared to TRP. It is noteworthy that the band is the only one to be shifted to lower wavenumbers compared to alkaline pH, in the UVRR spectra of both

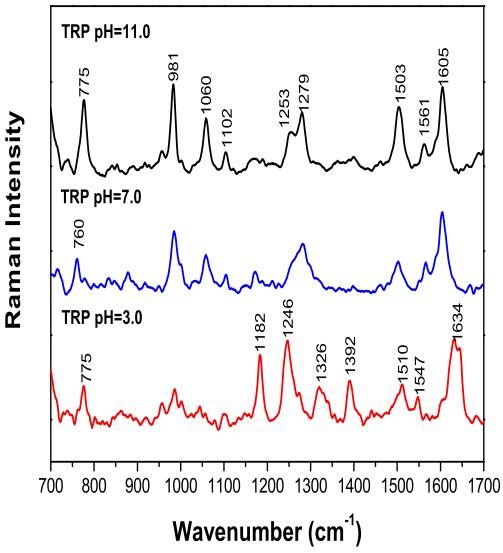

Figure 4.5: Experimental UVRR spectra recorded at 257 nm of Neutral TRP —— (pH 11.0), mono-protonated TRP —— (pH 7.0) and di-protonated TRP —— (pH 3.0).

TRP and MEP. We could refer to it as diagnostic for H-bonding but frequency calculations are needed to ascertain our hypothesis.

From Figure 4.5 and 4.6 it is clear that the UVRR spectra of TRP and MEP recorded at neutral and alkaline pH are quite similar in terms of wavenumbers, but strong changes in enhancement can be observed as a consequence of the pH change. Changes are visible at (1450–1650) cm^{-1} related to characteristic ring stretches of the pyridine ring. The attenuation of the band at 1502 cm^{-1} compared to the band at 1606 cm^{-1} in neutral aqueous solution resembles the behavior of $2DMPH^+$ when compared to 2DMP. In addition, the attenuation of

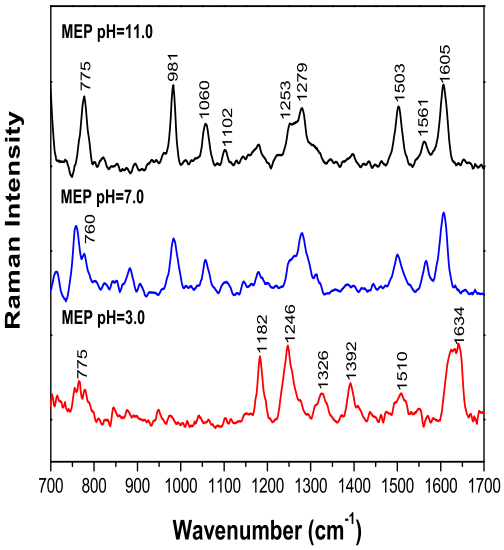

Figure 4.6: Experimental UVRR spectra recorded at 257 nm of Neutral MEP —— (pH 11.0) mono-protonated MEP —— (pH 7.0) and di-protonated MEP —— (pH 3.0). For the mono-protonated compounds, protonation is at the aminoalkyl nitrogen.

the band at 1257 cm^{-1} where ring mode 14 involving the pyridine stretch takes place, and the reduction in intensity of the ring breathing and deformation (ring modes 1 and 12 respectively) at around 1000 cm^{-1} are again in line with the behavior of $2DMPH^{+}$ when compared to 2DMP.

The modifications recorded in the resonance enhancement of TRP and MEP when going from alkaline solution to neutral pH are indicative of a perturbation of the charge distribution in the AP chromophore, originated by the protonated tail. Attenuated intensities thus reflect a more rigid environment the AP chro-

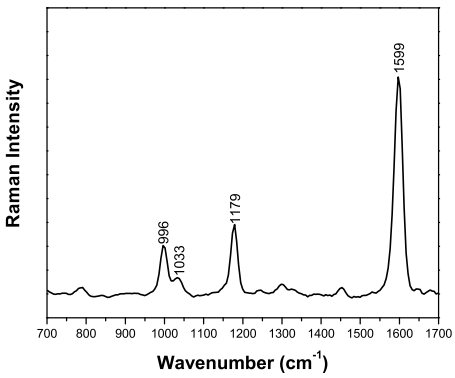

Figure 4.7: Experimental UVRR spectrum of anisole recorded at 229 nm at a concentration of 1 mM.

mophore experiences at neutral pH, compatible with a gauche conformation. In line with our interpretation, at acidic pH when the pyridine nitrogen becomes protonated and the preferred conformation is expected to change to an extended one, owing to the electrostatic repulsion between the two positive centers, a re–enhancement of the AP bands was recorded with a shift in wavenumbers, again in line with the behavior of $2DMPH^+$. The ν(N-ring) of both TRP and MEP protonated at the protonated pyridine nitrogen is now recorded at 1392 cm^{-1}, thus reflecting a more planar configuration of the ring and the dimethylamino group, No such configuration is likely at neutral and alkaline pH, and the band is not enhanced. It is unlikely, and not apparent from the spectra that at neutral physiological conditions the pyridine nitrogen is protonated. However, the fact that in aqueous solution band changes observed for the AP chromophore are consistent with the changes 2DMP undergoes upon proton addition, indicate that close proximity of the AP group with the protonated tail reduces the intensity of the breathing and stretching modes of the antihistamines.

This means that the UVRR spectra of TRP and MEP are in line with our previous investigation of their electronic properties by fluorescence spectroscopy [97]. The effect of the protonated tail on the the AP group was postulated in neutral aqueous solution. Thus, under physiological conditions one probably deals with an equilibrium mixture of stretched (trans) and bent (gauche) conformers for both TRP and MEP as depicted in Figure 4.1a.

4.4 Conclusions

The above results underline the potential of UVRR as a structure elucidation technique applicable to aqueous solutions of typically 10–100 μM analyte concentrations even for analytes exhibiting native fluorescence.

We have shown that it is possible to assign all vibrational bands of the UVRR spectra of the two antihistamines TRP and MEP, and that changes in structure as a function of pH are related to changes in vibrational patterns due to protonation of the nitrogens in the molecule. For the 'helper' molecules 2AP, DMA and 2DMP these changes can only be due to protonation at either the pyridine nitrogen or the amino nitrogen, but the behavior of TRP and MEP is more complicated due to the presence of a side chain that can also be protonated.

In the protonated state, this side chain influences the physicochemical properties of the pyridine moiety considerably. In Chapter 3 we indicated major changes in fluorescence properties, but also in the pK_a value of the pyridyl nitrogen, which shifts from its usual value of around 7, to a much lower value of 4. Consequently the group will no longer be protonated at neutral pH, but the UVRR spectra now show that changes similar to protonation nevertheless occur. We therefore conclude in line with our previous model that an intramolecular hydrogen bond, leading to the gauche conformation is indeed likely. This is also in line with theoretical calculations for histamine itself, where such a configuration was suggested [94].

Although it is in principle possible to perform quantum chemical calculations on the antihistamines themselves, the flexibility of the molecules and the number of conformations that need to be investigated, coupled to its large size, makes this a rather lengthy procedure. It turned out to be much more profitable to investigate a number of smaller molecules and relate their vibrational properties to those of the antihistamines. This is one of the advantages of the resonance technique, which in this case is extra fortuitous since the resonant chromophore is also the relevant part of the molecule determining the binding properties of the antihistamines. Despite the fact that only two laser wavelengths, *i*.e. 229 nm and 257 nm, were utilized, the selectivity created is sufficient to prove the gauche structure of TRP and MEP under neutral pH conditions.

Vibrational assignment of 2DMP was achieved by comparison to UVRR spectra of two even simpler reference structures, 2AP and DMA, chosen to differentiate those wavenumbers characteristic of the pyridine moiety in 2DMP and those related in stead to the $-N(CH_3)_2$ substituent. However, the structural similarity of 2DMP with the two reference structures breaks down if the group symmetry changes, thus affecting the number of UVRR fundamentals in the recorded spectra. At 229 nm where the laser is in resonance with the electronic transition of the pyridine ring of both 2AP and 2DMP, the number of bands enhanced in the UVRR spectrum of the latter is higher. Besides the skeletal vibrations of the pyridine ring, symmetric and antisymmetric NC_2 stretch together with $\nu_{(N-ring)}$ vibration indicate a strong interference of the local symmetries related the dimethylamino group and the pyridine ring. Similar activity has been shown to be a typical sign of an iminium character of the nitrogen bonding configuration in aromatic amines [105]. Excitation at 257 nm which overlaps with the n–π^* transition shows a number of features related to the substituent vibrations. The effect of protonation in 2DMP was also investigated by comparison to $2APH^+$. Our results gave proof that protonation of 2AP and 2DMP first takes place at the pyridyl nitrogen, which has profound effects on the ring–$N(CH_3)_2$ bond length, which shows considerable

double bond character, UVRR spectra of 2DMP and $2DMPH^+$ were shown to be dependent on the excitation wavelength used thus confirming the assumption that two electronic states are differently enhanced by resonance excitation. From the UVRR study of 2DMP and $2DMPH^+$ we provided diagnostic bands for the protonation state of the pyridyl nitrogen.

The fact that obvious changes in the vibrational structure are evident upon pH change bodes well for further investigation of binding of these ligands to proteins.

Study of the binding of H_1 antihistamines to HSA

Chapter 5

Complementary fluorescence and phosphorescence study of the interaction of brompheniramine with human serum albumin[5]

[5] The contents of this Chapter were submitted for publication by Silvia Tardioli*, Ivonne Lammers*, Jan–Hein Hooijschuur, Freek Ariese, Gert van der Zwan, and Cees Gooijer. * Both authors contributed equally.

Abstract Binding of BPA to HSA is studied by measuring quenching of the fluorescence and room temperature phosphorescence (RTP) of tryptophan. The modified Stern–Volmer equation was used to derive association constants and accessible fractions from the steady–state fluorescence data. Decay associated spectra (DAS) revealed three tryptophan fluorescence lifetimes, indicating the presence of (at least) three HSA conformations. BPA causes mainly static quenching of the long–living, solvent–exposed conformer. RTP spectra and lifetimes, recorded under deoxygenated conditions in the presence of 0.2 M KI, provided additional kinetic information about the HSA–BPA interactions. Fluorescence DAS that were also recorded in the presence of 0.2 M KI, revealed that the solvent–exposed conformer is the major contributor to the RTP signal. The phosphorescence quenching is mostly dynamic at pH 7 and mostly static at pH 9, presumably related to the protonation state of the alkylamino chain of BPA.

5.1 Introduction

Binding of drugs to the transport protein human serum albumin (HSA) has been the subject of a large number of investigations [108, 109, 110]. A wide variety of techniques has been applied for this purpose, based on separation methods on the one hand and spectroscopic methods on the other, with focus on binding constants. For instance, Martinez–Gomez and coworkers studied the binding of antihistamines [111] and other drugs [112] by monitoring the mobility in capillary electrophoresis. Yoo *et al.* used the chromatographic behavior in HSA–packed microcolumns to determine overall drug binding constants [113]. Chadborn *et al.* used tryptophan fluorescence quenching to study drug–induced conformational changes in albumins [113]. However, it is still a challenge to interpret these binding constants since various binding sites of HSA are available [114]. For pharmacokinetic modeling, the results of such studies should preferably be combined with information about the dynamics.

HSA contains only a single tryptophan and this amino acid is situated near a primary binding site, so in principle fluorescence spectroscopy at selective wavelengths can provide direct information about the effects of ligand binding if it influences the properties of that tryptophan. Unfortunately, as is well known from literature [1], even proteins with a single tryptophan residue often still show more than a single fluorescence lifetime, which can be attributed to the existence of multiple protein conformations. This is also the case for HSA. Since nearby amino acid residues can act as quenchers of tryptophan fluorescence, even slightly different protein conformations can result in different decay times. The longest lifetime (as long as 7 ns) of single–tryptophan proteins is usually observed at the red side of the emission spectrum and is attributed to water–exposed tryptophan residues. Buried tryptophans often show shorter lifetimes as a result of the above mentioned quenching effects from certain amino acids [1].

For (static) fluorescence quenching in proteins with more than one tryptophan, the Stern–Volmer plot will be nonlinear when the individual fluorophores are not equally accessible to the quencher [115, 116]. Instead, a modified Stern–Volmer equation has to be used given by

$$\frac{F_0}{\Delta F} = \frac{1}{f_a K_a [Q]} + \frac{1}{f_a}$$

represent the fluorescence intensities of the protein in absence and in presence of quencher, respectively, and [Q] is the quencher concentration [1]. From a plot of F_0/F vs $[Q]^{-1}$, one can obtain the values of the fractional accessible tryptophans fa and the quencher association constant K_a. The question needs to be addressed whether in the case of HSA, which only contains a single tryptophan but is present in more conformations, differences in accessibility also play a role. Static fluorescence quenching experiments of HSA with the antihistamine compound chlorpheniramine seem to suggest this [117]. In the present Chapter, we investigate fluorescence quenching phenomena of a similar compound, (*i.e.*, the antihistamine brompheniramine (BPA, see Figure 5.1), not only by steady–state fluorescence, but also in the time–resolved fluorescence

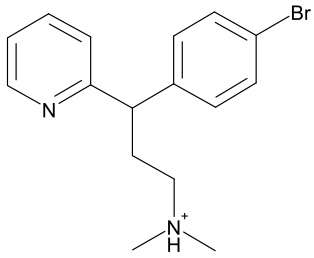

Figure 5.1: Molecular structure of BPA; the protonated form is dominant at neutral pH. A racemic mixture was used for this study

mode by recording decay associated spectra (DAS) to study these phenomena in more detail.

The tryptophan moiety is not only fluorescent but can also emit phosphorescence at room temperature (RTP), as is already known for proteins since 1974 [14]. RTP of HSA under liquid conditions is not easily detected, but Wei and coworkers [118] showed that intense phosphorescence spectra can be obtained if the samples are deoxygenated and KI is added as heavy atom reagent. Phosphorescence can provide valuable information about protein structure and dynamics in the micro– to milliseconds regime, in contrast to fluorescence phenomena, which take place on a nanosecond timescale. Proteins with a single tryptophan residue may show more than a single phosphorescence lifetime, indicating the presence of multiple conformations that are stable at the phosphorescence time–scale [119, 120]. In this work, in addition to the fluorescence data, complementary phosphorescence information about HSA–BPA binding will be obtained in the spectral as well as in the time domain.

As far as we know, for the interaction of BPA and HSA only the overall binding constant has been determined. Martinez–Gomez and coworkers [111]

determined the fraction of unbound drug at various HSA levels in a capillary electrophoresis setup at pH 7.4 and derived an association constant of $(1.8\pm0.3)\times10^3$ M^{-1}. For those experiments, the authors had to assume that there is only a single active binding site. In this Chapter, we aim at gaining insight into complex quenching phenomena, as well as binding kinetics. HSA is the major transport protein for drugs in the human body, and the results on BPA binding processes will be useful input for pharmacokinetic modeling.

5.2 Experimental

5.2.1 Chemicals

Fatty acid free albumin from human serum (96%), *L*–tryptophan, (±) brompheniramine maleate salt, boric acid, potassium iodide and sodium sulfite were purchased from Sigma–Aldrich (St. Louis, MO, USA); unfortunately, to the best of our knowledge the separate enantiomers of BPA are not commercially available. Sodium hydroxide was from Fluka (Buchs, Switzerland). Potassium dihydrogen phosphate and potassium monohydrogen phosphate were obtained from J.T. Baker (Deventer, The Netherlands). All chemicals were used as received. Water was purified with a Milli–Q system from Millipore (Bedford, MA, USA).

5.2.2 Fluorescence

Fluorescence emission spectra were recorded at room temperature on a LS50–B spectrometer, using a square quartz cuvette of 10 mm path length. All measurements were performed at an excitation wavelength of 295 nm and spectral band widths of 10 nm. Static fluorescence spectra of HSA and BPA mixtures were determined in 10 mM phosphate buffer (pH 7.2) or 10 mM borate buffer (pH 9.0), at a fixed protein concentration of 4 μM and varying BPA concen-

trations: 0.10, 0.27, 0.61, and 1.63 mM. The emission at 350 nm was used to construct Stern–Volmer plots.

Time correlated single photon counting (TCSPC) was used to determine fluorescence intensity decays. The excitation source was a Ti:Sapph laser (Coherent, Mira 900, Santa Clara, CA, USA) with a pulse width of 3 ps. The output of the laser was frequency tripled to get the excitation wavelength of 295 nm. A multichannel–plate photomultiplier (Hamamatsu, R3809U–50, Japan) collected the fluorescence emission, and data were recorded through a SPC–630 module (Becker&Hickl GmbH, Berlin, Germany) with a time resolution of 15 ps. Fluorescence decay curves were analyzed using a global fitting procedure based on the Levenberg–Marquardt algorithm. The instrument response function (determined by collecting scattered light from a suspension of silica particles) was used for deconvolution of the recorded decays and for determination of lifetimes and wavelength–dependent amplitudes. Each intensity curve was fitted with a multiexponential decay, and the goodness of the fit was assessed on the basis of and the distribution of residuals. The decay–associated spectra were constructed by distributing the total intensity per decay curve over the lifetimes that make up the total intensity according to their amplitudes obtained by the above fit procedure. The relative fluorescence intensity I$j(\tau_j)$ of lifetime component τ_j at wavelength λ with amplitude A$j(\lambda)$ can be expressed by the following equation:

$$I_{\tau_j}(\lambda) = \frac{A_j(\lambda)\tau_j}{\sum_i A_i(\lambda)\tau_i} \tag{5.2.1}$$

The sum in the denominator of this expression is equal to the steady–state emission spectrum.

5.2.3 Phosphorescence

A Cary Eclipse luminescence spectrometer (Varian, Melbourne, Australia) was used for recording the HSA phosphorescence. For enhancing the phospho-

rescence emission 0.2 M KI was added. Chemical deoxygenation was achieved by adding 2 mM Na_2SO_3 to the samples just before capping the 10 mm square quartz cuvettes. The temperature was kept at 20°C using the single–cell Peltier cooler of the spectrometer. The phosphorescence emission spectra were recorded with an excitation wavelength of 290 nm, spectral band widths of 10 nm, a delay time of 0.1 ms, and a total gate time of 5 ms. The intensities were corrected for the signal loss during the delay time by multiplication with a correction factor depending on the phosphorescence lifetimes. Time–resolved phosphorescence decay curves for the lifetime measurements were obtained with an excitation wavelength of 290 nm, an emission wavelength of 443 nm, an initial delay of 50 μs, a gate width of 50μs and a total decay time of 15 ms. Origin 8.0 was used to fit the phosphorescence decay curves with a biexponential decay function, and the goodness of the fit was assessed on the basis of and the distribution of residuals.

5.3 Results and Discussion

5.3.1 Fluorescence

In this subsection on HSA tryptophan fluorescence, we will first present static and time–resolved fluorescence data on the quenching of 4 μM HSA by various concentrations (0–1.63 mM) of BPA. Excitation was at 295 nm, which is selective for tryptophan; other amino acid residues and BPA are not excited at that wavelength. The fluorescence quenching can not be due to Förster resonance energy transfer (FRET), since the absorption spectrum of BPA does not overlap with the emission spectrum spectrum of tryptophan. Furthermore, the effect of adding KI was investigated in order to be able to couple the fluorescence with the phosphorescence results. To obtain more insight into the mechanism of fluorescence quenching, the experiments were carried out at pH 7.2 and at pH 9.0. Because of its alkylamine tail, BPA has a pK_a of 9.1 [121],

which implies that at neutral pH the fraction of unprotonated BPA is negligible, whereas at pH 9.0 it is close to 50%. Binding to HSA can be influenced by the charge of the BPA tail, and therefore the equilibrium constant is expected to be pH dependent. Measurements at higher pH with fully deprotonated BPA could not be carried out because of protein denaturation under those conditions.

When plotting the steady–state quenching data using the regular Stern Volmer equation, no linear relationship was obtained. Such behavior may be caused by differences in accessibility of the tryptophan. Indeed, at both pH values tested a modified Stern–Volmer equation resulted in a linear plot (data not shown). The results of steady state fluorescence experiments did indeed show a strong pH dependence: at pH 7.2 the equilibrium binding constant was determined to be $(2.2\pm0.3)\times10^3$ M^{-1} with f_a=0.50±0.03, but at pH 9.0 it was substantially higher: $(9.1\pm2.2)\times10^3$ M^{-1} with f_a=0.71±0.03. The fact that the protonated ligand has a lower association constant may indicate a non–polar binding mechanism.

In order to study these phenomena in more detail, time–resolved fluorescence experiments were performed. The DAS obtained for a pure HSA solution (no ligand) and in the presence of 1.63 mM BPA are shown in Figure 5.2 for pH 7.2 and in Figure 5.3 for pH 9.0. Without quencher at pH 7.2, three fluorescence lifetimes are obtained: 7.2, 2.6 and 0.4 ns. Upon increasing the pH to 9.0, these lifetimes hardly change: 6.7, 2.6 and 0.4 ns. Apparently, over the pH range from 7.2 to 9.0 the protein does not undergo any major conformational changes that involve the direct environment of the tryptophan moiety. This is in line with the findings of Amari *et al.* [122] and of Otosu *et al.* [123], who noted that the tryptophan lifetimes change significantly only at more extreme pH values. The DAS corresponding to these three lifetimes (Figure 5.2a and 5.3a) are distinctly different: the maximum wavelength of the 7.2/6.7 ns fluorescence is at about 355 nm, some 15 nm red shifted in comparison with that of the shorter–living species. These results are in accordance with other single–tryptophan proteins as discussed by Lakowicz [1].

In the following, these lifetimes will be equated with three different species,

which will be referred to as conformers I, II and III. The longer living component (conformer I) is found at longer emission wavelengths, indicating that it is exposed to a more polar environment, possibly water, whereas tryptophan residues buried inside the protein matrix (conformers II and III) have shorter lifetimes and emit at shorter wavelengths. According to this interpretation, the overall static HSA fluorescence spectrum is dominated by conformation I, in which the tryptophan is most exposed to quenching: its DAS does not only show the longest lifetime, but also the highest relative amplitude. Time–resolved fluorescence quenching by BPA was studied over the concentration range from 0.10 to 1.63 mM. The DAS at the highest BPA concentration are depicted in Figure 5.2b and Figure 5.3b.

Interestingly, the tryptophan fluorescence lifetimes are only little influenced by BPA addition: the longest lifetime is reduced from 7.2 to 6.7 ns (4%) at pH 7.2 and from 6.7 to 5.8 ns (15%) at pH 9.0. In other words, dynamic quenching of fluorescence plays only a negligible role at the BPA concentrations dealt with in this study. The DAS spectra in Figure 5.2 and 5.2 show mostly a decrease in amplitude of the long lifetime component. Therefore, the main cause of fluorescence quenching is the static quenching of tryptophan fluorescence in conformer I, while the contributions of conformers II and III are much less affected. This agrees with the hypothesis that multiple conformations with different tryptophan accessibilities exist, and supports the use of the modified Stern–Volmer equation for the steady–state quenching data. Similar results (not shown) were obtained when the experiments were repeated at λ_{exc}=288 nm (close to the absorption maximum) instead of 295 nm (red edge), confirming that the observed changes in amplitude are not due to spectral shifts of the tryptophan absorption band upon binding.

Room temperature phosphorescence measurements require the presence of KI, and in proteins containing several tryptophan residues, iodide is known to quench the fluorescence of only the solvent–exposed tryptophan moieties [15]. Therefore, we determined the effects of adding KI on the fluorescence characteristics of HSA. Figure 5.4 shows the DAS obtained in absence and presence

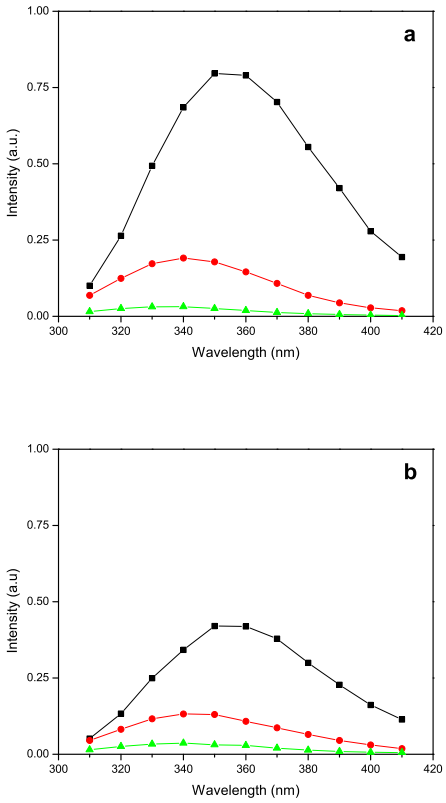

Figure 5.2: Decay associated fluorescence spectra of HSA 4 μM at pH 7.2. Frame a): in absence of BPA, 7.2 ns ■, 2.6 ns ●, and 0.4 ns ▲. Frame b): in presence of 1.6 mM BPA, 6.7 ns ■, 2.6 ns ●, and 0.4 ns ▲. The total intensity of graph a) is normalized to 1; that of graph b) is on the same scale.

of 0.2 M KI at pH 7.2; at pH 9.0 the results were similar (not shown).

Also in the presence of 0.2 M KI three lifetimes are observed, but they are significantly shortened. At pH 7.2 the longest lifetime decreases from 7.2 to

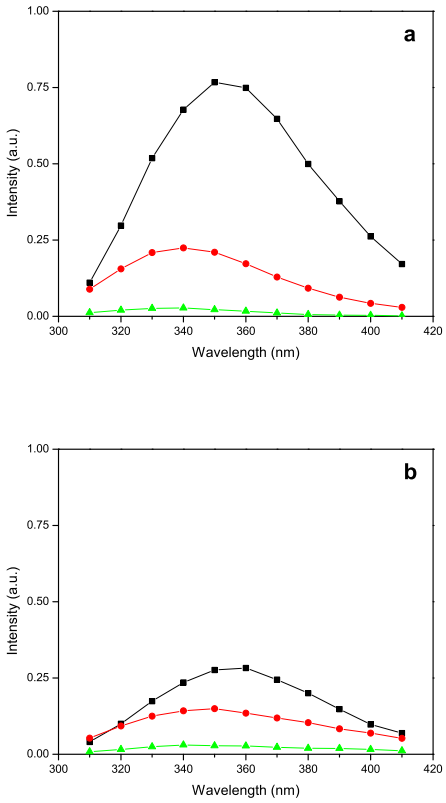

Figure 5.3: Decay associated fluorescence spectra of HSA 4 μM at pH 9.0. Frame a): in absence of BPA, 6.7 ns ■, 2.6 ns ●, and 0.4 ns ▲. Frame b): in presence of 1.6 mM BPA, 5.8 ns ■, 2.6 ns ●, and 0.4 ns ▲. The total intensity of graph a) is normalized to 1; that of graph b) is on the same scale.

4.6 ns (36%), the second one from 2.6 to 1.8 ns (31%). Similarly, at pH 9.0 the longest lifetime decreases from 6.7 to 4.5 ns (33%), the second one from 2.4 to 1.7 ns (29%). Because of the poorer precision, changes in the shortest

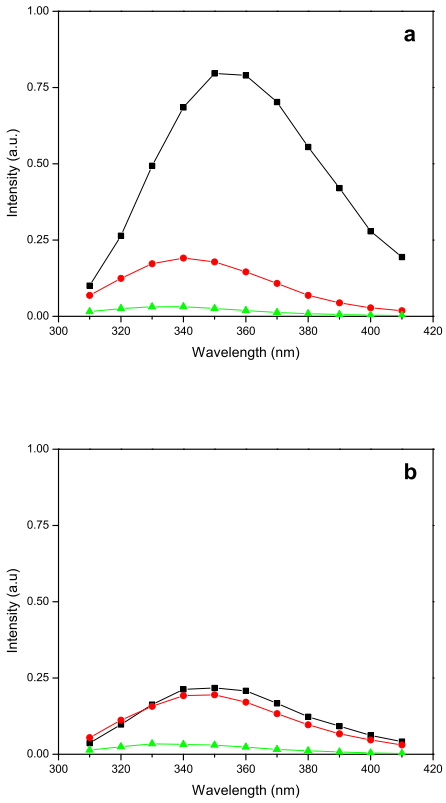

Figure 5.4: Influence of iodide on the decay associated fluorescence spectra of 4 μM HSA at pH 7.2. Frame a: in absence of KI 0.2 M, 7.2 ns ■, 2.6 ns ●, and 0.4 ns ▲. Frame b: in presence of KI 0.2 M, 4.6 ns ■, 1.8 ns ●, and 0.3 ns ▲. The total intensity of graph a) is normalized to 1; that of graph b) is on the same scale.

lifetime of 0.3 ns are not taken into consideration. These lifetime changes indicate that iodide causes a similar degree of dynamic quenching for conformer I and II. Presumably, the heavy atom iodide species —through collisional inter-

action with tryptophan— causes an enhanced inter–system crossing rate from the first excited singlet state S_1 to the triplet state T_1, and thus a reduction in fluorescence lifetime. The bimolecular rate constant for fluorescence quenching by iodide (k^+) can be calculated from the lifetime changes: for conformer I it is about $4{\times}10^8$ $M^{-1}s^{-1}$, and for conformer II it is even somewhat higher at $9{\times}10^8$ $M^{-1}s^{-1}$. As can be seen in Figure 5.4, the addition of 0.2 M KI strongly affects the fluorescence intensity of conformer I, which is reduced by a factor of 4. Apparently, for conformer I apart from dynamic quenching also steady–state quenching plays a role: the corresponding equilibrium association constant was calculated to be about $K{=}8$ M^{-1}. These results indicate that complex formation of iodide with conformer I influences the tryptophan fluorescence, whereas its association with conformers II and III is of minor importance. The lifetime of this complex can be estimated, since $K = k^+/k^-$ where k^- is the dissociation rate of the complex. Using the values found in the previous paragraph we get $k^-{=}5{\times}10^7$ s^{-1}, and thus a lifetime of the complex of about 20 ns. Obviously, this is very short compared to the phosphorescence phenomena to be discussed below.

5.3.2 Phosphorescence

Following the fluorescence experiments, we also studied the static and dynamic effects of BPA on the HSA tryptophan phosphorescence. All samples were chemically deoxygenated to prevent the quenching of phosphorescence by dissolved oxygen. Furthermore, 0.2 M KI was added to all samples to increase the phosphorescence luminescence by accelerating inter–system crossing processes. In addition, we will compare the HSA phosphorescence quenching with that of the free amino acid tryptophan. Since time–resolved phosphorescence measurements must be carried out at a much lower repetition rate than fluorescence experiments (50 Hz vs. 4 MHz) and thus show a poorer signal–to–noise ratio, the phosphorescence decays were fitted with a bi–exponential function.

Contrary to the mono–exponential decay of free tryptophan (see below),

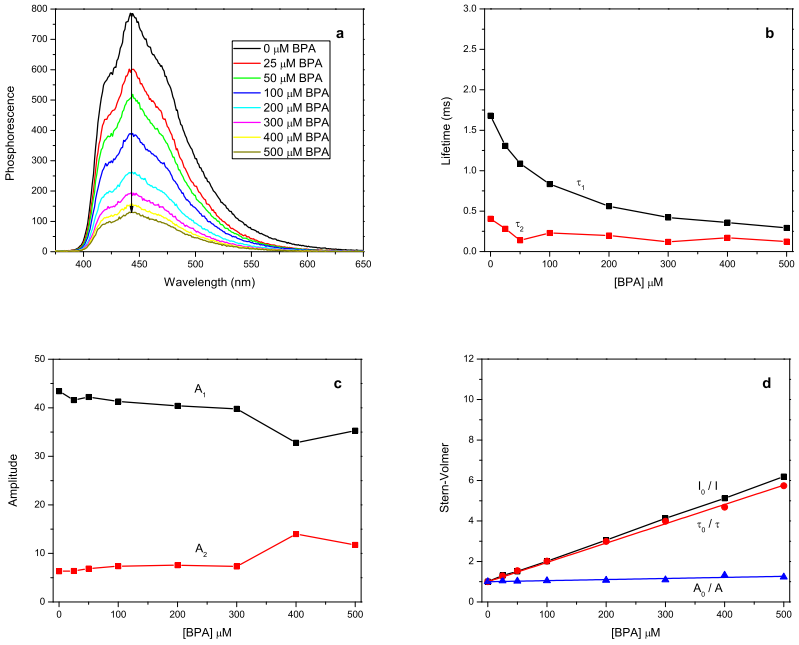

Figure 5.5: Phosphorescence quenching of 4 μM HSA by 0–500 μM BPA in 20 mM phosphate buffer at pH 7.0. All samples contained 0.2 M KI to enhance the inter–system crossing and 2 mM Na_2SO_3 for deoxygenation. (a) Phosphorescence emission spectra of HSA at increasing BPA concentrations. Time–resolved phosphorescence data (measured at 443 nm) were fitted with a bi–exponential function; frame (b) shows the phosphorescence lifetimes τ_1 and τ_2 as a function of the BPA concentration, and frame (c) the corresponding amplitudes A_1 and A_2. (d) Stern–Volmer plots based on the overall intensity I ■, in comparison with the Stern–Volmer plots based on the longest lifetime τ_1 • and the corresponding amplitude A_1 ▲. I_0, τ_0 and A_0 are the intensity, the longest lifetime and its amplitude in absence of BPA.

HSA shows at least two phosphorescence lifetimes. The observation of several lifetimes for a protein with a single tryptophan indicates that conformational heterogeneity occurs at the time–scale of the phosphorescence emission [119,

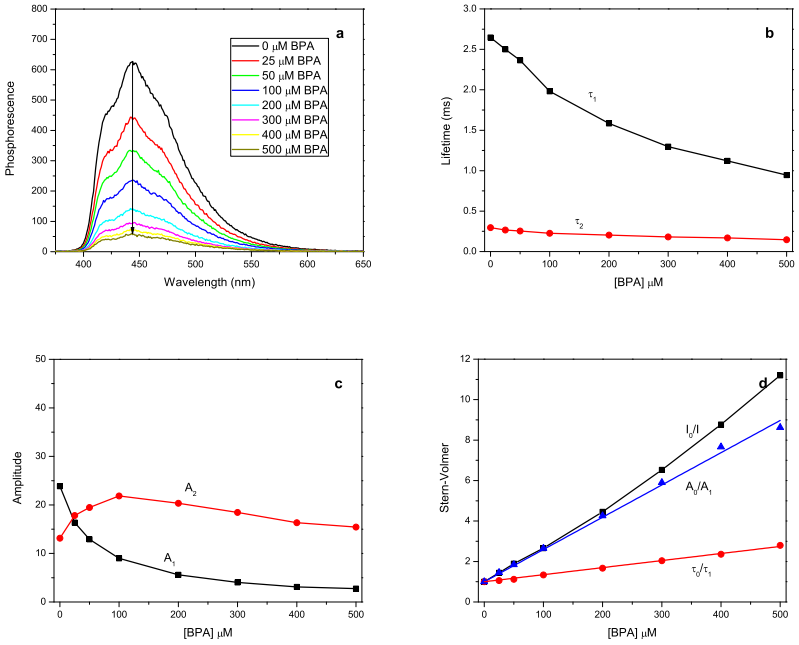

Figure 5.6: Phosphorescence quenching of 4 μM HSA by 0–500 μM BPA in 20 mM borate buffer at pH 9.0. All samples contained 0.2 M KI to enhance the inter–system crossing and 2 mM Na_2SO_3 for deoxygenation. (a) Phosphorescence emission spectra of HSA at increasing BPA concentrations. Time–resolved phosphorescence data (measured at 443 nm) were fitted with a bi–exponential function; frame (b) shows the phosphorescence lifetimes τ_1 and τ_2 as a function of the BPA concentration, and frame (c) the corresponding amplitudes A_1 and A_2. (d) Stern–Volmer plots based on the overall intensity I ■, in comparison with the Stern–Volmer plots based on the longest lifetime τ_1 • and the corresponding amplitude A_1 ▲. I_0, τ_0 and A_0 are the intensity, the longest lifetime and its amplitude in absence of BPA.

120]. These cannot be directly compared with the different conformers observed in fluorescence, since different timescales and different quenching mechanisms play a role.

At pH 7.0 in absence of BPA, two phosphorescence lifetimes of 1.7 ms and 0.4 ms are found, with relative amplitudes of 15:1. The fluorescence experiments with KI described above and the larger amplitude of the long–living species indicate that this conformer is relatively accessible to iodide. Figure 5.5a shows the RTP spectra of 4 μM HSA in the presence of BPA concentrations ranging from 0 to 500 μM. The HSA tryptophan phosphorescence is strongly quenched by BPA and the corresponding Stern–Volmer plot I_0/I is shown in Figure 5.5d. In order to evaluate the nature of the quenching mechanism, the phosphorescence lifetimes and associated amplitudes as a function of the BPA concentration are shown in Figure 5.5b and 5.5c, respectively. A decrease in phosphorescence lifetime indicates a process occurring during the lifetime of the excited triplet state (dynamic quenching), whereas a decrease in amplitude indicates the formation of a nonphosphorescent complex (static quenching). Upon addition of BPA, the lifetime of the long–living conformer is strongly decreased (Figure 5.5b), in agreement with a species in which the tryptophan is relatively accessible. The amplitude of this species hardly changes upon adding BPA (Figure 5.5c); apparently the quenching mechanism at pH 7.0 is mainly dynamic. The Stern–Volmer plot τ_0/τ for the long–lifetime–component shows a linear relationship with the BPA concentration, which corresponds with a rate constant of dynamic quenching of $(5.7\pm0.2)\times10^6$ $M^{-1}s^{-1}$ (Figure 5.5d). The associated minor amplitude change could not be determined very precisely, but the binding constant was estimated from the Stern–Volmer plot A_0/A in Figure 5.5d as $(5.3\pm3.0)\times10^2$ M^{-1}, reasonably close to the value derived from the static fluorescence experiments described in the previous section ($(2.2\pm0.3)\times10^3$ M^{-1}).

The RTP results at pH 9.0 are quite different from those at neutral pH, as can be seen in Figure 5.6. Again, two lifetimes are found; the long–living component has a longer lifetime (2.7 ms) and a lower amplitude than at pH 7.0, whereas the short–living component has a slightly shorter lifetime (0.3 ms) and a distinctly higher amplitude than at pH 7.0. By plotting t0/t for the long lifetime component as a function of the BPA concentration (Figure 5.6d) a linear

curve is obtained with a dynamic quenching constant of $(1.3\pm0.1)\times10^6$ $M^{-1}s^{-1}$, which is 4 to 5 times lower than at pH 7.0.

In a separate set of experiments, we studied the quenching effect of BPA on the phosphorescence of tryptophan free in solution (deoxygenated, in the presence of 0.2 M KI). Both at pH 7.0 and 9.0, dynamic quenching rates of about 1×10^9 $M^{-1}s^{-1}$ were obtained (data not shown). The rate constants of dynamic quenching for HSA are 2–3 orders of magnitude lower than those for free tryptophan, in line with a reduced accessability of the tryptophan moiety. In contrast to the results obtained under neutral conditions, at pH 9.0 the phosphorescence of the long–living conformer does not only undergo dynamic quenching but also significant static quenching. The formation of a non–phosphorescent complex is evident from Figure 5.6c, which shows a strong decrease in amplitude A_1 at higher BPA levels. From the Stern–Volmer plot A_0/A based on the amplitude of the long–living conformer (Figure 5.6d), the association constant was calculated to be $(1.6\pm0.1)\times10^4$ M^{-1}. Again, this value is quite close to that found with the static fluorescence quenching experiments described above ($(9.1\pm2.2)\times10^3\pm$ M^{-1}) and confirms the stronger binding of BPA to HSA at higher pH.

5.4 Conclusions

Despite the fact that HSA is a single–tryptophan protein, modeling of steady state tryptophan fluorescence quenching of HSA by BPA required the use of the modified Stern–Volmer equation, indicating the existence of an inaccessible fraction of fluorophores. This could be explained by recording the fluorescence decay associated spectra of HSA. Three fluorescence lifetimes associated with different emission spectra were found, which indicates the presence of (at least) three conformers of HSA: I, II, and III. Upon addition of BPA, mainly conformer I is amenable to static quenching, whereas complex formation with the tryptophans in conformer II and III plays a negligible role. Apparently, BPA

forms a non–fluorescent complex with the exposed tryptophan in conformer I.

In our fluorescence experiments, static quenching by BPA dominates, since at the BPA concentrations applied possible dynamic quenching processes would be too slow to be effective. At the mM quencher level, bimolecular reaction rates as high as 10^10 $M^{-1}s^{-1}$ would be needed for substantial dynamic fluorescence quenching to occur, whereas in phosphorescence the rate constants required for dynamic quenching are some four decades lower.

Applying the modified Stern–Volmer equation to the fluorescence quenching results, an association constant of $(2.2\pm0.3)\times10^3$ M^{-1} was derived, which agrees very well with the value reported by Martinez–Gomez *et al.*: $(1.8\pm0.3)\times10^3$ M^{-1} [111]. It should be realized that the latter value refers to the overall BPA–HSA binding, whereas the association constants derived from the Stern–Volmer plots refer only to a binding mode that affects the fluorescence quantum yield. Apparently, in the case of BPA other binding modes do not play a major role. Both the fluorescence and the phosphorescence quenching experiments showed a much stronger binding at higher pH, presumably related to the deprotonated (less polar) state of the alkylamino chain.

Since phosphorescence emission mostly comes from the tryptophan moiety in conformer I interacting with iodide, the HSA conformation with exposed tryptophan dominates the steady state RTP spectra. From the time–resolved RTP spectra not only the binding constants but additionally the biomolecular rate constants of quenching can be derived. These rate constants, $(5.7\pm0.2)\times10^6$ $M^{-1}s^{-1}$ at pH 7.0 and $(1.3\pm0.1)\times10^6$ $M^{-1}s^{-1}$ at pH 9.0, are 100, respectively 600 times lower than the phosphorescence quenching rate constants determined for free *L*–tryptophan. These differences can be attributed to the spatial structure of HSA: in HSA the tryptophan moiety is much less accessible than the free amino acid in solution. The lower dynamic phosphorescence quenching rate and the higher static phosphorescence quenching rate at pH 9 are most probably related to the stronger binding of deprotonated BPA. The results obtained illustrate that time–resolved fluorescence and phosphorescence spectroscopy are appropriate tools to study HSA–ligand interactions, at two

complementary timescales.

Chapter 6

pH dependent complexation of Histamine H_1 receptor antagonists and HSA studied by UV resonance Raman spectroscopy[6]

[6] The contents of this Chapter were submitted by Silvia Tardioli, Joost Buijs, Cees Gooijer, and Gert van der Zwan and accepted for publication by the Journal of Physical Chemistry B.

Abstract UV resonance Raman spectroscopy was used to characterize the binding of three first generation Histamine H_1 receptor antagonists —tripelennamine (TRP), mepyramine (MEP) and brompheniramine (BPA)— to human serum albumin (HSA) at pH 7.2 and pH 9.0. Binding constants differ at these pH values, which can be ascribed to the different extent of protonation of the ethylamino side chain of the ligands. We have shown recently [Tardioli *et al.*, *J. Raman Spectrosc.*, **42**, (2011), 1016] that for the solution conformation of TRP and MEP the side chain plays an important role by allowing an internal hydrogen bond with the aminopyridine nitrogen in TRP and MEP. Results presented in this Chapter suggest that the existence of such molecular structures has serious biological significance on the binding affinity of the those ligands to HSA. At pH 7.2 only the stretched conformers of mono–protonated TRP and MEP bind in HSA binding site I. Using UV absorption data we derive binding constants for the neutral and protonated forms of TRP to HSA. The neutral species seems to be conjugated to a positive group of the protein, affecting both the tryptophan W214 and some of the tyrosine (Y) vibrations. BPA, for which the structure with an intramolecular hydrogen bonded side chain is not possible, is H–bound to the indole ring nitrogen of W214, of which the side chain rotates over a certain angle to accommodate the drug in site I. We propose that the mono protonated BPA is also bound in site I, where the Y150 residue stabilizes the presence of this compound in the binding pocket. No spectroscopic evidence was found for conformational changes of the protein affecting the spectroscopic properties of W and Y in this pH range.

6.1 Introduction

Histamine H_1 receptor antagonists (commonly referred to as antihistamines) are particularly effective in the treatment of allergies by interacting with the H_1 receptor. The sedating effect of the first generation H_1 antihistamines has been associated with their ability to penetrate the central nervous system, which is likely related to weak serum protein binding [79]. Binding of those antihistamines to plasma proteins is therefore an important issue for their biological efficacy, since it modulates drug availability to the intended target. In the present Chapter attention is focussed on the binding of antihistamines to human serum albumin (HSA), the most abundant transport protein in blood.

in Chapter 4 we selected two antihistamines, tripelennamine (TRP) and mepyramine (MEP) as representative, for their optical properties. As many antihistamines of that class, and as indicated in Figure 6.1, they share as common feature an ethylamino chain with a strongly basic ($pK_a \approx 9$) nitrogen atom at the end. Under physiological conditions the tail is therefore protonated. Furthermore, both TRP and MEP have an aminopyridine moiety, which is largely responsible for their chromophoric properties. Both chromophore nitrogens are unprotonated under physiological conditions: the second pK_a value for these molecules is approximately 4 [97]. For comparison another antihistamine, brompheniramine (BPA) is used, which has an ethylamino tail similar to TRP and MEP, but the chromophoric properties are rather different: the aminopyridine moiety is replaced by a pyridine, with a pK_a of approximately 5.2 also unprotonated under physiological conditions, and furthermore the central atom is an optically active carbon, instead of a nitrogen.

HSA has long been at the center of attention of the pharmaceutical industry due to its ability to bind various drugs and alter their pharmacokinetic properties. HSA is a globular protein with two principal binding sites for a wide variety of ligands located in hydrophobic cavities in subdomains IIA (site I) and IIIA (site II). A single tryptophan residue in HSA (W214) is located in binding site I [124].

Several papers report methodologies on separations to determine the association equilibrium constants for binding of these antihistamines to proteins [111, 125, 126] but the elucidation of the binding mechanism has hardly been attended. For this purpose vibrational spectroscopic techniques, which provide detailed structural information, could be invoked. In particular, UV resonance Raman (UVRR) spectroscopy can in principle provide detailed data on how a ligand is bound. In view of this, complex formation between HSA and the three antihistamines was investigated in aqueous solution at two pH values 7.2 an 9.0, by means of UVRR spectroscopy. These pH values were chosen to elucidate the influence of the protonation of the ethylamino tail on the binding properties. Of course one should know also whether the protein structure is affected in this region. Although conformational changes were reported for HSA in binding experiments as a consequence of pH change [127], in the pH range between 7 and 9 so far no changes in the optical properties of the tryptophans such as aborption or fluorescence spectra have been observed [122, 123]. We confirm those findings by showing in this Chapter that no changes in the UV absorption or in the UVRR spectra are observed either.

UVRR spectroscopy is performed at 244 nm excitation, a laser line provided by the continuous wave frequency doubled argon ion laser. This is a suitable wavelength, not only because it is in resonance with the amino pyridine moiety of TRP and MEP and in between the $S_0 \rightarrow S_1$ and $S_0 \rightarrow S_2$ transitions of the pyridine part of BPA. It is also in resonance with the tryptophan and tyrosines of HSA, so that in principle difference spectra can give information about possible complexation induced changes in these amino acids as well. We recently made use of the same technique to successfully investigate the solution conformation of TRP and MEP [87]. We showed that there is a definite influence of the protonated ethylamino chain on the chemical and photophysical properties of these molecules. Most probably for TRP and MEP the HSA–ligand interaction is affected by their solution conformations, which in turn are dependent on the protonation state of the tail. It was found that the protonation state of the tail influences the chromophoric properties as well as the pK_a values

of the aminopyridine moiety. Compared to isolated aminopyridines K_a values are two orders of magnitude lower in TRP and MEP. We concluded that in addition to the normal stretched conformer also a bent conformer plays a role. The bent conformation allows interaction of the tail nitrogen with the chromophore, either by formation of a hydrogen bond, or direct interaction with the ring π–electrons. These findings explain why Ter Laak and co–workers [79] in a previous study of the binding of H_1 antihistamine to serum proteins by equilibrium dialysis coupled to UV detection found that the ionization state of MEP strongly influences its binding to serum proteins in the pH range from 6.0 to 9.0. The differences in MEP binding at different pH values indicate different affinities of the ionized and the unionized form of MEP for HSA [79].

The aim of the present study is to obtain more detailed structural information about the interaction of TRP and MEP with HSA. The bent conformer only exists when the tail is protonated, upon deprotonation only the stretched conformer is expected. For BPA such complications are not encountered, therefore it is quite suitable for comparison.

6.2 Experimental

6.2.1 Materials

Essentially fatty acid free human serum albumin (HSA), tripelennamine hydrochloride (TRP), mepyramine maleate (MEP) and brompheniramine maleate (BPA) were purchased from Sigma Aldrich and used without further purification. Binding experiment were performed at pH 7.2 and pH 9.0 by dissolving the protein and the antihistamine salts respectively in 20 mM phosphate buffer (sodium monophosphate-sodium diphosphate) and 20 mM borate buffer (boric acid-sodium hydroxide). Water was purified by passage through a Millipore Milli–Q system.

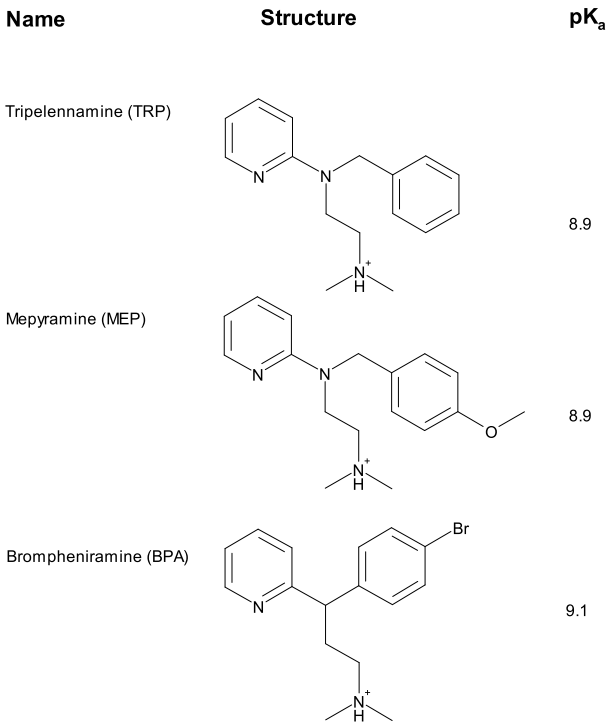

Figure 6.1: Structures of the antihistamines under physiological conditions. The pK_a value given is for the ethylamino side chain nitrogen. The other nitrogens are unprotonated under physiological conditions.

6.2.2 Sample preparation

UV titration measurements of HSA were performed in the presence of TRP and MEP at pH 7.2 and pH 9.0. The protein concentration was kept constant at

120 μM while ligand concentration was varied between (0–600) μM. The range was chosen in accordance with the values of the known association constants of the antihistamine salts to HSA [97]. The binding of BPA to HSA was not investigated by UV titration since under physiological conditions the ligand has a very low affinity ($K_a = 1.8 \times 10^3$ M^{-1}) for the protein [111].

UV Absorption spectra of the TRP and MEP in absence and in presence of the protein were recorded at room temperature using a 0.5 mm quartz cell. In the range investigated no concentration effects on the UV absorption spectra of the antihistamine salts were observed. Self–association of the compounds studied starts to be important in aqueous solution at much higher concentrations than used in this study [93]. For the binding experiments 120 μM HSA buffer solution was prepared and partly used to dissolve TRP and MEP at a concentration of 1.03 mM and 1.05 mM, respectively. Different aliquots of the ligand/protein solution were added to the protein solution so that a constant protein concentration was maintained throughout the titration. In order to record the spectra of the free ligands at the same concentrations as used in the titration, TRP and MEP were also dissolved in buffer (without the protein) at a concentration of 1.03 mM and 1.05 mM, respectively. The same volumes of TRP and MEP used in the binding experiment with HSA were added to the buffer solution.

UVRR spectra were measured at a protein concentration of 120 μM and ligand concentrations of 500 μM at pH 7.2 and of 250μM at pH 9.0, for both TRP and MEP. In virtue of the low K_a of BPA to HSA the concentration used for this compound was 1.13 mM at both pH 7.2 and pH 9.0. Na_2SO_4 50 mM was added to all samples as internal standard for Raman intensity measurements. $NaClO_4$ could not be used: it was found to aggregate with the ligands.

6.2.3 Instrumentation

UV electronic absorption spectra were measured on a Varian Cary 50 Bio UV-Vis spectrophotometer. Continuous–wave UV radiation of wavelength at 244 nm was obtained from an intracavity frequency–doubled argon ion laser, Innova FreD 90C (Coherent, Utrecht, the Netherlands). The UVRR setup was described in detail previously [128].

6.2.4 UVRR detection system

Raman scattering was collected from a vertically dropping flow of sample solution (6 mL) delivered by a peristaltic pump (Gilson Minipuls 2) coupled to a peek tube with a flow rate of 100 cc/min. The setup was specifically designed for this experiment to enable detection of the Raman scattered light from the protein solution. Previous measurements utilizing a flow through a horizontally mounted quartz capillary showed that HSA sticked to the wall cell at the spot where the laser light was focused, thus seriously hindering the Raman signal from the protein solution circulating in the capillary. The present drop-flow system gave outstanding results in terms of sensitivity even at short times of collection. A 3600 lpm line grating was used to disperse the spectra on a cooled (–50° C) Andor technology Model DV420–OE CCD camera (Belfast, Northern Ireland) in the range (500–2000) cm^{-1}. The S/N ratio was improved by repetitive scanning (45 times) during 10 s for all samples. No time dependent changes were observed from scan to scan indicating the stability of the dropping sample in the UV laser beam. Also, UV absorption spectra taken before and after the RR data acquisition showed no evidence of laser induced photo–degradation for any of the compounds investigated. The intensities of UVRR spectra of all compounds and mixtures were first normalized to the 981 cm^{-1} band of SO_4^{-2}. All spectra presented in this Chapter have the solution background subtracted.

6.2.5 Difference spectra

The pH dependencies of the UV absorption and UVRR spectra of the antihistamines investigated were determined by subtraction of the the spectrum at pH 7.2 from the spectrum at pH 9.0 at equimolar concentrations. For each antihistamine investigated in this study, the changes in spectral properties induced by complexation between the investigated antihistamines and HSA were evaluated at one point of the titration by subtracting the free ligand spectrum (no HSA) and the free HSA spectrum (no ligand) from the recorded spectrum of the complex. Such difference spectra originate from those molecular groups affected by binding. Since all passive groups are invisible, the difference spectrum exhibits details of the binding mechanism.

6.3 Results and Discussion

6.3.1 UV absorption spectra

In order to study the influence of protonation on the ligand structure and their binding to HSA by UVRR spectroscopy, UV absorption spectra should be recorded, since pH changes might affect the molar extinction coefficients and thus the resonance enhancement effect in UVRR at 244 nm. First the influence on the antihistamine spectra will be discussed, and subsequently the ligand–HSA combinations.

Antihistamines In Figure 6.2 the UV absorption spectra of TRP and BPA are presented at two pH values. For both ligands the difference spectra associated with the pH change from 7.2 to 9.0 are included as well. The UV spectral profile of MEP (not shown) resembles that of TRP, though additionally rather weak absorption bands from the anisole chromophore are observed below 230 nm and at 275 nm, which are not influenced by the pH change [97].

The UV absorption spectrum of BPA shown in Figure 6.2 has close spectroscopic resemblance to the absorption spectrum of the pyridine molecule [129].

The difference spectrum is a flat horizontal line: its chromophoric properties are not affected by a change in pH, consistent with the idea that there is no interaction between the protonated ethylamino tail and the pyridine chromophore. The negative feature below 230 nm is related to the acid–base equilibrium of the maleate counter–ion.

TRP and MEP behave quite differently from BPA; their difference spectra exhibit several positive and negative features, indicating band shifts. At pH 7.2 TRP and MEP exhibit similar bands centered at 245 nm and 306 nm. These are ascribed to electronic transitions within the aminopyridine chromophore at 245 nm and to a charge transfer transition from the amino substituent to the π-ring at 306 nm, which are conjugated [87, 97]. At pH 9.0 a wavelength shift of the two bands is recorded resulting in a difference spectrum with negative features at 240 nm and 300 nm and a positive component at 257 nm. These wavelength shifts are thought to be caused by by a difference in interaction between the tail and the amino pyridine moiety at pH 7.2 and 9.0. This interaction is significant in the bent conformation if the tail is protonated and could be hydrogen bond formation or direct interaction with the pryidine π–electrons. At pH 9.0 only 50% of the molecules will be protonated at the tail (pK_a =8.9) [97, 87].

Antihistamine/HSA complex and K_a evaluation The pH influence on the binding of TRP and MEP to HSA was first investigated by means of UV absorption spectroscopy. The UV absorption spectra of HSA, TRP and TRP/HSA complex are presented at pH 7.2 in Figure 6.3. Absorption spectra evaluated at pH 9.0 are not included. Emphasis is on the difference spectra (TRP/HSA–HSA–TRP) at pH 7.2 (a) and pH 9.0 (b). Only those features whose intensity increases upon TRP addition are labeled. We emphasize that no change in the shape and intensity of the HSA absorption spectrum itself was found when going from pH 7.2 to pH 9.0 indicating that in this pH range no conformational change influencing the absorption of the protein takes place.

In the difference spectrum at pH 7.2 complex formation induces negative features around 244 nm and 300 nm, and a weak positive band at 257 nm.

This is quite similar to the difference spectrum shown in Figure 6.2 showing the effect of pH on the structure of TRP as in absence of HSA. This similarity in difference spectra strongly suggests that upon complexation with HSA at pH 7.2 the stretched configuration of TRP is favored, even though in solution at that pH this conformation is present in only a minor amount. The difference spectrum at pH 9.0 is quite similar in shape to that at pH 7.2 apart from the region below 240 nm, although the peaks appear to be shifted slightly and the peak at 257 nm is more pronounced. When the concentration of bound TRP is plotted as a function of the TRP concentration, see insert of Figure 6.3, there is an initial linear change up to about 120 μM (the HSA concentration in these experiments), with a steeper slope at pH 9.0 than at pH 7.2. These results indicate the formation of a 1:1 complex. The association constant calculated at pH 9.0 is 9.5×10^3 M^{-1}, more than three times larger than the value at pH 7.2 of 3.1×10^3 M^{-1} (see Supplementary Information). This implies that the binding constant of the neutral component, present at about 50% in solution, is about five times larger than that of the protonated form (1.6×10^4 M^{-1}). This in turn implies that —if the difference in binding constants is attributed to the difference in protonation state— about 80% of the HSA bound drug is in its neutral form at pH 9.0. For the model, and evaluation of the binding constants, see Supplementary Information.

The difference spectra at pH 9.0 and pH 7.2 are markedly different in the wavelength region below 240 nm. Whereas at pH 7.2 the 225 nm band is positive, it is negative at pH 9.0. At pH 7.2 complex formation with TRP gives rise to a blue shift in the HSA spectrum, but at pH 9 to a red shift. The interpretation is not straightforward, since in this region a number of effects can contribute to the difference spectrum. The observed absorption can not be fully ascribed to the Bb ($\pi - \pi^*$) band of tryptophan (W214) in HSA, also the Lb ($\pi - \pi^*$) transitions of the tyrosine residues contribute to the intensity. Nevertheless the results indicate that complexation of HSA with positively charged TRP gives rise to another spectrum than complexation with deprotonated TRP. Presumably in the former the W214 bands shifts to the

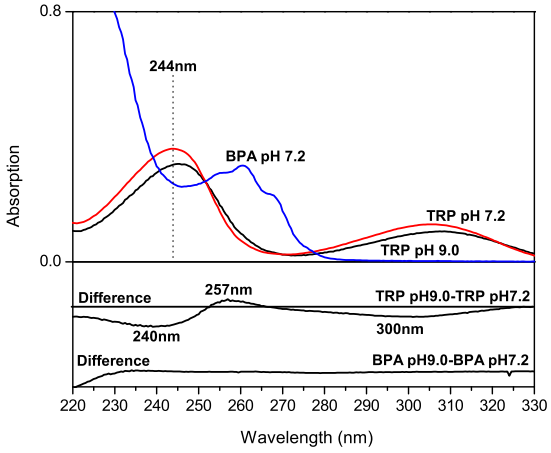

Figure 6.2: UV Absorption spectra of: TRP (500 μM) pH 7.2 ——, pH 9.0 ——, and BPA (1.13 mM) pH 7.2 ——. The associated difference spectra (pH 9.0–pH 7.2) are also shown. 244 nm is the emission wavelength of the FreD laser used to record UVRR spectra.

red, in line with the observation that interaction with a proton at the NH side of the indole ring causes a red shift in a hydrophobic environment and an intensity increase of the Bb absorption [130, 131, 132], whereas complexation of HSA with the neutral form causes shifts the spectrum to the blue.

6.3.2 UVRR spectra

UVRR spectra of all the compounds investigated and their complex with HSA are presented and discussed in this section. Excitation was performed at 244 nm, suitable for enhancement of both the protein and the ligands. The concentrations of HSA (120 μM) and the ligands (500 μM and 250 μM) gave rise to similar signal to noise ratios.

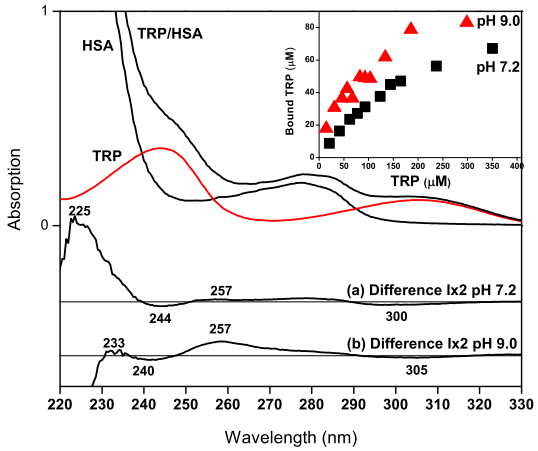

Figure 6.3: UV Absorption spectra of HSA , TRP and TRP/HSA complex at pH 7.2. (a): difference spectrum (TRP/HSA–HSA–TRP) at pH 7.2; (b): at pH 9.0. In the inset the dependence of bound TRP *vs* [TRP], measured at 255 nm, is shown at pH 7.2 ■ and pH 9.0 ▲.

The 244 nm excitation wavelength favors in HSA the resonance enhancement of the vibrations of tryptophan, tyrosine, and to a minor extent the peptide backbone [131, 133, 33]. Also, the 244 nm excitation is in resonance with the aminopyridine moiety of TRP and MEP, and with the pyridine chromophore of BPA. Due to the overlap of the UVRR spectra of the antihistamines and HSA, use was made of difference spectra to distinguish between spectral changes originating from HSA and those arising from the ligands. In Figure 6.4 we show the UVRR spectra, at pH 7.2 and in Figure 6.5 the UVRR spectra at pH 9.0, of HSA, antihistamine, antihistamine/HSA complex, and the associated difference spectra for the three ligands. In supplementary material (Figure 6.6) we provide a description of the UVRR spectra of TRP, MEP and BPA, and the difference spectra related to changes in pH and polarity, with the complete

assignments done according to [87] and [101]. In Figure 6.4 and 6.5 only those ligand vibrations modified by binding are labeled.

HSA The UVRR spectra of HSA at pH 7.2 and pH 9.0 are displayed in the top traces of Figure 6.4 and Figure 6.5, respectively. At 244 nm excitation strong enhancement is observed for the Raman bands arising from one tryptophan, 18 tyrosine, and 31 phenylalanine residues [10], in pre-resonance through their Bb (tryptophan) and Lb (tyrosine) electronic transitions. No modification of the UVRR profile of HSA was detected with pH change, thus confirming previous results from Harada and coworkers [131], who first reported the UVRR of HSA. This is in line with the observation that no observable changes are found in the optical properties of HSA upon this pH change. Observable Raman bands arising from the tryptophan (W) and tyrosine (Y) residues are listed in Table 6.1 and assigned using [131].

The UVRR bands of the single tryptophan (W214) in HSA show up at 1621 cm^{-1} (W1 overlapping with Y8a, aromatic C–C stretching), 1553 cm^{-1} (W3, C-C stretching of the pyrrole ring), 1347 cm^{-1} (W7, tryptophan doublet), 1004 cm^{-1} (W16, benzene ring breathing overlapping with F12) and 758 (W10) cm^{-1}. Those vibrations, except W1, are strongly enhanced with excitation in pre-resonance with the Bb electronic transition of tryptophan (~220 nm) [134].

The UVRR bands of the tyrosine residues are observed at 1621 cm^{-1} (Y8a), 1208 cm^{-1} (Y7a, ring–C stretching), 1174 cm^{-1} (Y9a, CH in plane bending). We also recorded the tyrosine Fermi doublet at 828/851 cm^{-1} which originates from resonance between the symmetric ring breathing Y1 and the overtone of the out-of-plane deformation mode Y16a of the ring vibration at ~ 413 cm^{-1}. Phenylalanine only contributes at 1004 cm^{-1} (F12, ring breathing) where it overlaps with W16 of tryptophan. Additional peptide vibrations occur at 1455 cm^{-1} (Pro C–N stretch, Amide II) and 1655 cm^{-1} (Amide I) [33, 135]. Those latter vibrations depend on the secondary structure of the protein.

TRP/HSA complex In Figure 6.4 the UVRR spectrum of TRP/HSA complex at pH 7.2 (trace (c)) and the associated difference spectrum

HSA		
Band (cm^{-1})	Assignment	Description
758	W18	symmetric benzene/pyrrole in phase breathing
828	2Y16a	out of plane ring deformation
851	Y1	symmetric phenol in phase breathing
1004	W16	symmetric benzene/pyrrole out-of-phase breathing
1174	Y9a	in plane CH bend, C_6H_5–C
1208	Y7a	ring–C stretch
1341	W7	pyrrole ring vibration
1455	Pro Imide II	Pro C–N stretch
1553	W3	C_2–C_3 pyrrole ring stretch
1621	W1, Y8a	phenyl mode with contribution from the pyrrole NC stretch
1655	Amide I	C=O stretch with minor contribution the out-of-phase C-N strech

Table 6.1: Vibration band assignments of HSA [131].

(Complex–HSA–TRP) (trace (d)) are presented.

Upon binding, several negative features show up in the difference spectrum which can be attributed to the aminopyridine moiety of TRP: at 760 cm^{-1} δ_{ring}, at 1283 cm^{-1} and 1505 cm^{-1} $\nu_{C-C(N)}$, and at 1607 cm^{-1} ν_{C-C}. The same vibrations also show up in the pH difference spectra for TRP as such, *c*f. Figure 6.6 (Supplementary Information). They are affected by the protonated tail in the bent conformer at pH 7.2. Similar behavior was observed in the UV absorption spectra as detailed above. The lower wavenumber component of the doublet at 760/774 cm^{-1} decreases in intensity upon binding

to HSA. This band originates from the ring stretching 6a of an H–bound AP moiety [87]. The intensity ratio of the 1257/1282 cm^{-1} doublet decreases upon binding, following the behavior we recorded for TRP from pH 7.2 to pH 9.0. For both 760/774 cm^{-1} and 1257/1282 cm^{-1} doublets, the reduction in intensity is consistent with the absence of a hydrogen bond with the aminopyridine moiety, as described in Figure 6.6 in the supplementary information. The difference spectra originate exclusively from those molecular groups affected by the binding. Thus trace (c) in Figure 6.4 indicates that the stretched and uncharged conformer dominates upon complexation witn HSA, whereas the bent conformation only plays a minor role.

Some bands originating from HSA change as well. Complexation induces in the difference spectrum a weak but significant intensity increase of the W214 bands at 1341 cm^{-1} (W7), 1553 cm^{-1} (W3), and 1621 cm^{-1} (W1). Furthermore complex formation induces an up–shift of the amide I band, which is found at 1663 cm^{-1} in the difference spectrum, and suggests a mild structural change of the protein towards an irregular α–helix [136]. The intensity increase of W7, W3 and W1 Raman bands are likely caused by the red–shift of the Bb electronic transition, in line with the differences in UV absorption spectra discussed above. The difference spectrum of the TRP/HSA complex at pH 7.2 therefore indicates that mono protonated TRP in the stretched conformation is bound (close) to W214, located in site I. The difference spectra at pH 9.0 clearly differ from those at pH 7.2. In Figure 6.5 the UVRR spectra of the TRP/HSA complex at pH 9.0 and the associated difference spectrum (Mix–HSA–TRP) are shown in traces (c) and (d) respectively. In view of the pK_a of TRP (8.9) under this condition about half of the molecules are deprotonated at the amino side chain, and half the TRP will be still protonated. In the difference spectrum we note that the intensity of those bands of W214 characterizing the complex formation between protonated TRP and HSA, at 990 cm^{-1}, 1341 cm^{-1}, 1553 cm^{-1} and 1623 cm^{-1}, which give positive signals at pH 7.2 are hardly observable anymore. Apparently at pH 9.0 complexes between the protonated form and HSA are no longer formed to any appreciable

extent. It can be concluded from the larger binding constant at pH 9.0 that the binding with the neutral form of TRP is much stronger, and an analysis shows that even though in solution still half the TRP is protonated, in the bound complex only about 20% of TRP will be protonated.

The difference spectrum at pH 9.0 shows other positive bands than the spectrum at pH 7.2. These originate from TRP and are observed at 974 cm^{-1} (ring bending), 1055 cm^{-1} (CH bending, 18a), 1280 cm^{-1} (C-CN stretch, 14), 1494 cm^{-1} (C-CN stretch, 19a), and 1595 cm^{-1} (C-C stretch, 8a). Compared to the spectrum of free TRP three vibrations ascribed to ring stretches are down–shifted: those at 974 cm^{-1} (was 984 cm^{-1}), 1494 cm^{-1} (was 1503 cm^{-1}), and 1595 cm^{-1} (was 1607 cm^{-1}). Since these are ring vibrations, it implies that the π electron cloud of the AP moiety is influenced to a certain extent by complexation. Intensities also change, the intensity increase of TRP vibrations is again in line with the blue shift of the absorption at 244 nm, *c*f. Figure 6.3.

Negative peaks related to HSA vibrations are observed at pH 9.0 at 828/853 cm^{-1} (Fermi doublet; Y1, Y16a), 1174 cm^{-1} (Y9a), and 1621 cm^{-1} (Y8a and W1). The change in W214 modes induced by complexation is only marginal at pH 9.0, the main changes originate from tyrosine modes in this case. The negative feature at 1621 cm^{-1} derives mainly from the Y8a vibration, where the C-C stretch of the phenolic ring takes place, but we do not exclude a small contribution from the W1 band of W214. Both Y8a and Y9a tend to decrease in more polar solvents [130].

MEP/HSA complex For MEP the results are quite similar to those obtained for TRP. The main difference is that the signal to noise ratio of trace (g) is distinctly lower than that of trace (d), due to the fact that binding of MEP to HSA is not strong at pH 7.2. Therefore we do not discuss Figure 6.4, dealing with MEP binding in detail. At pH 9.0 this signal to noise ratio is much better. In Figure 6.5 trace (f) the UVRR spectrum of MEP/HSA complex at pH 9.0 and the associated difference spectrum (g) (Mix–HSA–MEP) are presented. The strong resemblance with the the difference spectrum of the TRP/HSA complex at the same pH value is quite convincing and strongly suggests that

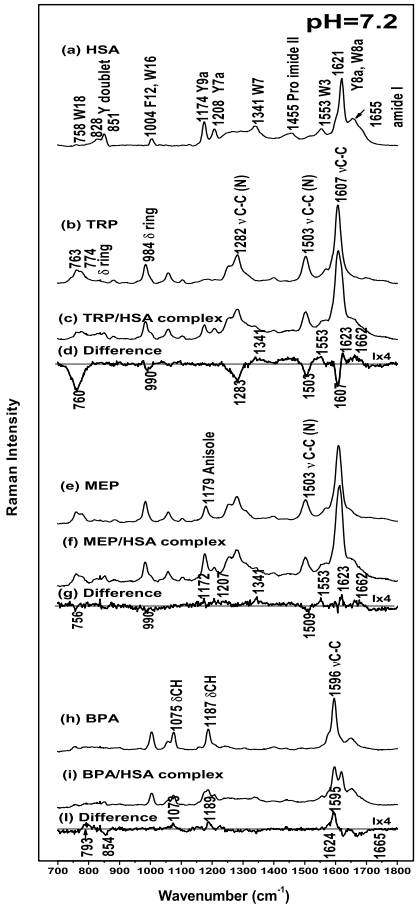

Figure 6.4: UVRR spectra at pH 7.2, 244 nm excitation: (a) HSA 120 μM; (b) TRP 500 μM, (c) TRP/HSA complex, and (d) difference (c)–((a)+(b)); (e) MEP 500 μM, (f) MEP/HSA complex and (g) difference (f)–((a)+(e)); (h) BPA 1.13 mM, (i) BPA/HSA complex and (l) difference (i)–((a)+(h)).

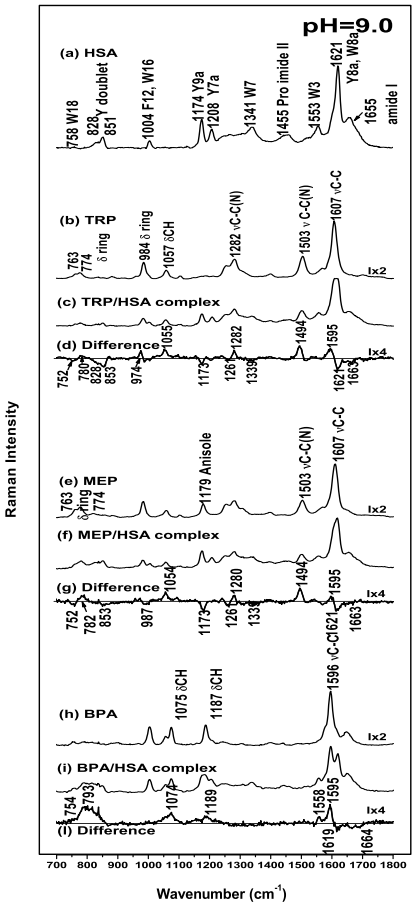

Figure 6.5: UVRR spectra at pH 9.0 244 nm excitation: (a) HSA 120 μM; (b) TRP 250 μM, (c) TRP/HSA complex and (d) difference (c)–((a)+(b)); (e) MEP 250 μM, (f) MEP/HSA complex and (g) difference (f)–((a)+(e)); (h) free BPA 1.13 mM, (i) BPA/HSA complex and (l) difference (i)–((a)+(h).

the same type of binding occur for both TRP and MEP with HSA.

BPA/HSA complex For BPA the difference spectra at pH 7.2 and 9.0 are quite similar, in contrast to the spectra of TRP and MEP, see Figure 6.4 and Figure 6.5, indicating that there is no substantial difference between the binding of protonated and unprotonated BPA. Positive peaks are observed at 1074 cm^{-1} (CH and NH bending), 1189 cm^{-1} (CH bending) and 1595 cm^{-1} (C-C stretch). They are ascribed to the pyridine moiety of BPA and probably reflect a change in environment to less polar upon binding to HSA.

The difference spectrum at pH 9.0 shows an additional positive peak at 1558 cm^{-1}. It originates form tryptophan (W3), but due to the binding it is shifted by some 5 cm^{-1}. According to literature this suggests that the dihedral angle about the bond connecting the indole ring with the C–atom of the amino backbone is changed [137].

The negative features observed upon complexation at both pH 7.2 and 9.0 originate from HSA, in particular from tyrosine residue(s): 1624 cm^{-1} (Y8a) and 1664 cm^{-1} (amide I); in addition a weak band at 854 cm^{-1} (Y Fermi doublet) is visible. A positive band is observed at 793 cm^{-1}. Since it cannot be assigned to a distinct HSA or BPA vibration, it might point to a vibration exclusively showing up in the complex.

A detailed interpretation of the BPA–HSA results accounting for these minor differences observed at different pH values is not straightforward. Nonetheless we note that the difference spectra for BPA at both pH values are quite similar to those of MEP and TRP at pH 9.0, as far as the HSA peaks are concerned. This applies to the negative 854 cm^{-1} and 1619–1624 cm^{-1} peaks from tyrosine and the 1664–1665 cm^{-1} amide I band.

To summarize the BPA results, the effect of complexation on W214 vibrations is marginal at pH 9.0 and absent at pH 7.2. Therefore it is not possible to conclude whether BPA (in its protonated and deprotonated form) enters preferably in site I or site II. To answer this question we investigated the complexation in a separate study of the BPA–HSA system by W214 phosphorescence: a strong quenching by BPA is observed which can be explained assuming a close

proximity between BPA and W214 [59].

6.4 Conclusions

This Chapter represents a first attempt to characterize the interactions of three antihistamines, TRP, MEP, and BPA, with HSA by means of UV absorption, and UVRR spectroscopy at 244 nm excitation. Using a novel experimental set–up where spectra are taken in hanging dropplets, thus avoiding coagulation of protein at the cuvet surface, we were able to obtain excellent UVRR spectra of bound complexes. Under this excitation condition tryptophan and tyrosine residues within the protein are resonance enhanced and the same holds for the pyridine chromophore of the three ligands, which are therefore used as intrinsic probes. The three antihistamines investigated present a wide-range of behavior with respect to their binding towards HSA, which is dependent on the protonation state of the amino side chain, but for TRP and MEP also on the presence in solution of stretched and bent conformers at physiological pH.

The above results make clear that for the antihistamines TRP and MEP the structure of their complexes with HSA is strongly pH dependent. In free solution at pH 7.2 where the alkylamino tail is protonated two ligand conformations play a role, *i*.e. a bent structure allowing interaction of the protonated tail with the aminopyridine moiety and a stretched conformation in which such an interaction is negligible. The UVRR spectra taken at 244 nm indicate that in the HSA complex with TRP and MEP at pH 7.2 the stretched conformer dominates, whereas the bent conformation is hardly observed. Conversely, at pH 9.0 –despite the fact that in solution about half the ligand molecules are still protonated— the HSA–TRP and the HSA–MEP complexes are primarily complexes with unprotonated stretched ligands. The protonated stretched form is not visible in the spectra. From our results we can conclude that the association constant for the neutral form is considerably larger than that for the neutral form. For MEP no accurate determination could be made at pH 7.2,

but for TRP it is about five times larger for the neutral form (1.6×10^4 M^{-1}), than that for the protonated form (3.1×10^3 M^{-1}).

For BPA, an antihistamine with a structure that shows some similarity to those of TRP and MEP, such pH effects are not observed. For this molecule, also containing the alkylamino tail, the protonated form will not give rise to a bent conformation as found for TRP and MEP. This is fully in line with the fact that protonation of the tail does not influence the UV absorption spectrum. Also in UVRR the effect of protonation is only minor: presumably also for this antihistamine the stretched deprotonated form dominates in the complexation. This interpretation is consistent with the observation that the difference spectra are quite similar —as far as the HSA vibrations are concerned— to those of MEP and TRP at pH 9.0. For all ligands it can be concluded that binding to HSA alters the protein secondary structure, since the Amide I vibration is affected. A new vibration appears at 793 cm^{-1} in the spectra of complex neutral MEP and BPA, possibly related to the formation of a new hydrogen bond with the pyridine ring.

6.5 Supplementary Information

Binding Models In the Figure below we show fits of the data at the different pH values. The curves were fitted with the function

$$[PA] = \frac{\alpha}{2}\left[[P]_0 + [A]_0 + K - \sqrt{([P]_0 + [A]_0 + K)^2 - 4[P]_0[A]_0}\right] \quad (6.5.1)$$

where $[P]_0$ is the amount of protein added to the solution, $[A]_0$ the amount of ligand added, K is the (unknown) association constant, and α gives the (unknown) relation between concentration and absorption. The resulting association constants are the ones used in the main text of the Chapter. The value of α, although not readily physically interpretable, is virtually the same in both fits (15 ± 1).

To account for this difference in binding constants, we assume a difference in binding between the neutral and the protonated form of the ligand. Thus we have the following relations. For the neutral form we have the equilibrium between protein P and ligand A:

$$P + A \rightleftharpoons PA \quad K_n = \frac{[PA]}{[A][P]} \quad (6.5.2)$$

with association constant K_n, and for the protonated form we have

$$P + A^+ \rightleftharpoons PA \quad K_p = \frac{[PA^+]}{[A^+][P]} \quad (6.5.3)$$

In addition there is an equilibrium between the neutral and the protonated form of the ligand dependent on the pH:

$$A + H^+ \rightleftharpoons A^+ \quad K_a = \frac{[A][H^+]}{[A^+]} \quad (6.5.4)$$

In an experiment of the type we performed, the following binding constant is measured:

$$K = \frac{[PA] + [PA^+]}{[P]([A] + [A^+])} = \frac{K_a K_n + [H^+]K_p}{K_a + [H^+]} \quad (6.5.5)$$

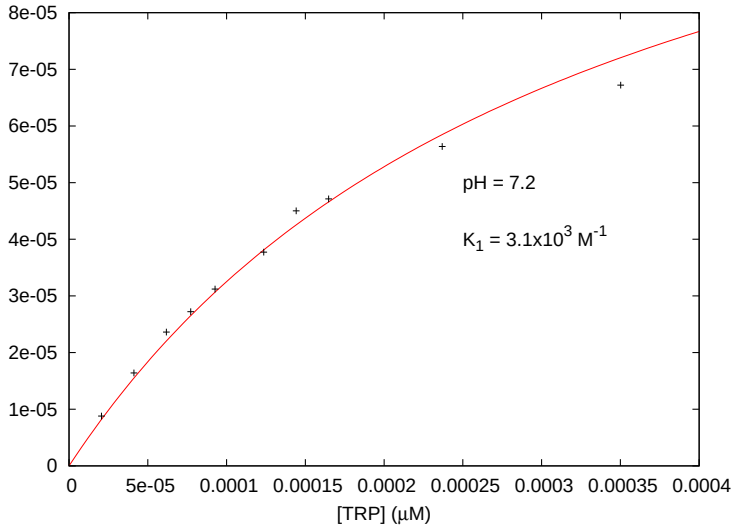

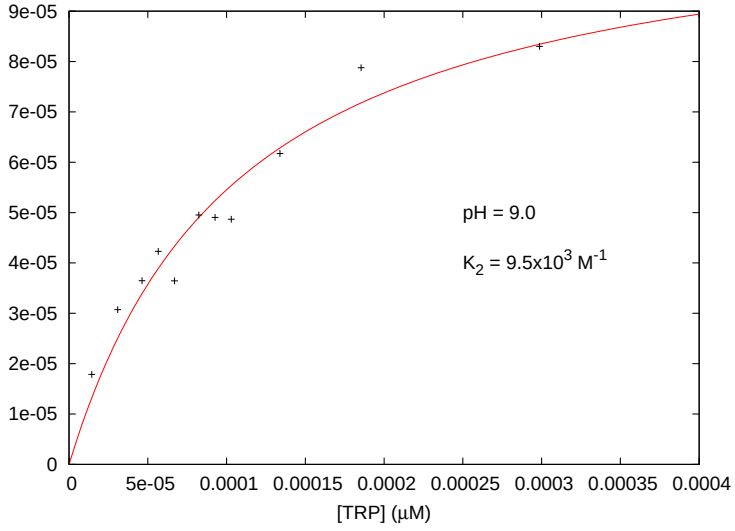

This equation can also be written in terms of the pK_a and pH values:

$$K = \frac{10^{-pK_a} K_n + 10^{-pH} K_p}{10^{-pK_a} + 10^{-pH}} \tag{6.5.6}$$

In our case the pK_a value is about 9. At a pH value of 7.2 virtually no ligand occurs in the unprotonated state, and K reduces to $K_1 = K_p$. At pH 9.0 the protonated and unprotonated form are present in approximately equal amounts, and the measured value of K, reduces to

$$K_2 = \frac{1}{2}(K_n + K_p) \tag{6.5.7}$$

From this we derive $K_n = 2K_2 - K_p = 2K_2 - K_1 = 1.6 \times 10^4$ M^{-1}. Using these binding constants it is easy to derive the relative populations of the protonated and unprotonated ligands at different pH values.

UVRR of antihistamines In Figure 6.6 the UVRR spectra of TRP, MEP and BPA at pH 7.2 are shown. In the same Figure we show the difference spectra associated with the pH change from 7.2 to 9.0 and from pH 7.2 to pH 7.2 + MeOH (2 mM).

The UVRR spectra of TRP and MEP at 244 nm excitation derive from the resonance enhancement of the aminopyridine chromophore. All vibrations are assigned according to [87]. Going from pH 7.2 to pH 9.0 (i.e. deprotonation of the tail pK_a=8.9) has a remarkable effect on several ring stretches, arising from the contribution of the pyridine nitrogen.

At pH 9.0 the changes we detect in comparison with pH 7.0 are: a strong decrease in intensity of the excitation profile of TRP and MEP as a consequence of the red shift of the pyridine absorption band in the range (230–260) nm; the up–shift of the band at 1503 cm^{-1} (in–plane C-C(N) stretch), and the change in the relative intensity ratio of the doublet at 763 cm^{-1} (6a mode in H-bond aminopyridine) and 774 cm^{-1} (6a mode in neutral aminopyridine as well as the doublet at 1254 cm^{-1} (9a) and 1282 cm^{-1} (14). The decrease of intramolecular H–bond species taking place between the protonated amino side chain and the aminopryidine chromophore is responsible for the observed spectroscopic behavior pH 9.0. A change in polarity reduces the intensity of ring modes 12, 19a (down-shifted) and 8a.

At 244 nm excitation, the UVRR bands of BPA are all ascribed to the

pyridine ring. Assignments were taken from [102, 138]. In the range (700–1580) cm^{-1} the difference spectrum of BPA is a flat line, revealing that pyridine chromophore does not experience any change as a consequence of the solution pH change (the protonation state of the tail). The $C{=}O$ stretch of the maleate counter ion was recorded at 1648 cm^{-1} in the spectrum of BPA, where enhancement of the band at the same position in the difference spectrum and at 1600 cm^{-1} (ring C-C stretch) probably originate from self–association of the ion to the pyridine ring. UVRR spectra of BPA support our assumption that bent and trans conformers are only present in TRP and MEP aqueous solution and MEP.

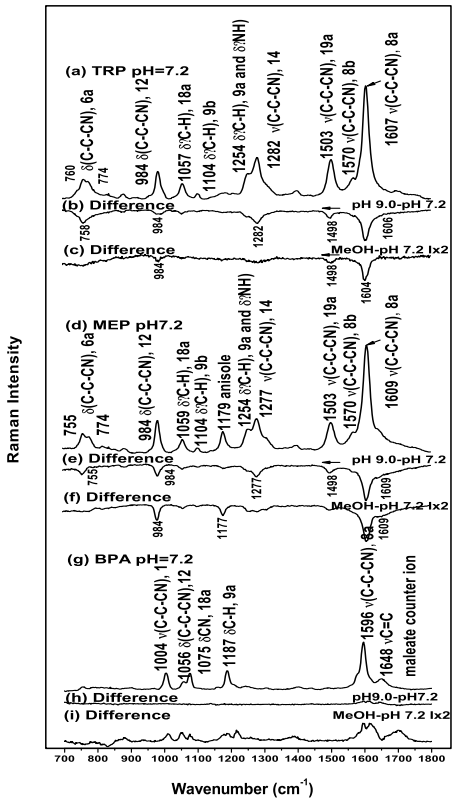

Figure 6.6: UVRR spectra at 244 nm: (a) TRP 500 μM at pH 7.2, (b) the difference spectrum associated with the pH change (TRP pH 9.0–TRP pH 7.2) and (c) the difference spectrum associated with the polarity change (TRP pH 7.2–TRP pH 7.2 + MEOH (2 mM); (d) MEP 500 μM at pH 7.2, (e) the difference spectrum associated with the pH change (MEP pH 9.0–MEP pH 7.2) and (f) the difference spectrum associated with the polarity change (MEP pH 7.2–MEP pH 7.2 + MEOH (2 mM); (g) BPA 1.13 mM at pH 7.2, (h) the difference spectrum associated with the pH change (BPA pH 9.0–BPA pH 7.2) and (i) the difference spectrum associated with the polarity change (BPA pH 7.2–BPA pH 7.2 + MEOH (2 mM).

Summary

Understanding in detail how proteins bind ligands is a formidable and fascinating challenge. Within this context, the work described in this thesis is dedicated to the spectroscopic characterization of three H_1 antihistamines —TRP, MEP, and BPA— and their binding mechanism to the human serum protein HSA. The suitability of luminescence —in particular fluorescence— in combination with UVRR spectroscopy to elucidate molecular structures and investigate aspects of protein–ligand interactions is explored for the first time with the abovementioned molecules.

H_1 antihistamines are agents used against a wide variety of human pathologies. They exert their action by interacting with the H_1 GPCR. Nevertheless, the important question on how binding occurs at the receptor site still remains unsolved. These antihistamines also act in the central nervous system, causing sedation due to their weak binding ability to HSA, the main transporter of H_1 antihistamines to the receptor, which is able to penetrate the blood–brain barrier. There is a general lack of information on the kind of interactions occurring with serum proteins. To shed light onto those fundamental topics, the aim of the research was the evaluation of the feasibility of the use of H_1 antihistamines as intrinsic optical probes in protein binding studies. Structure elucidation of the binding mechanism has obvious relevance for the development of new drugs

and therapies.

At the time the research started little information was available about the spectroscopic behavior of these H_1 antihistamines. In work dating from the 1970's anomalies concerning the luminescence behavior of TRP and MEP were reported without, however, an explanation or possible cause of those effects. In order to test the feasibility of the ligands as intrinsic optical probes detailed knowledge of their spectroscopic behavior in solution is of central importance. That is why, in the first part of this thesis, much attention is devoted to the spectroscopic characterization and elucidation of solution structures of TRP and MEP. Here the relation between the spectroscopic properties and the structures of H_1 antihistamines is derived as a function of pH. It is known from literature that ligand binding to GPCR's implicates ionic interactions with key amino acids of the receptor, leading to a strong pH dependence.

These H_1 antihistamines possess multiple (de)–protonable groups and we conclude that this property makes them suitable intrinsic optical probes since the protonation state of a particular functional group will determine the charge and the possibility of intermolecular hydrogen bond formation with the protein. At physiological pH, by the combination of fluorescence and UVRR spectroscopy, the relation between spectral properties and the solution structures was elucidated. Both TRP and MEP show complex pH–dependent effects, of which, according to our results, the reported abberations may now be interpreted in terms of an intramolecular hydrogen bond occurring at physiological pH between the protonated ethylamine side chain and the intracyclic nitrogen of the AP chromophore. Therefore those ligands exist in solution at physiological condition in two conformers: stretched, and bent with an internal hydrogen bond. This structural behavior, responsible for the anomalous spectroscopic effects and anomalous pK_a value, depends on the extent of protonation of the ethylamino side chain. The two conformers of TRP and MEP were now characterized with distinctive absorption, emission, and fluorescence maxima as well as fluorescence lifetimes, which means that by selective excitation of the ligands with respect to protein, and by monitoring their emission, it should

be in principle possible derive which of the conformers is bound to the target protein.

A very important consequence of the conformational isomerism of TRP and MEP is that ligand conformers show different activity towards the target proteins, because they cannot be equally complementary to the three dimensional structure of the protein; hence the characterization of the various conformational forms of these H_1 antihistamines represents a fundamental step in elucidating the molecular background to the biological versatility. Indeed, binding of TRP and MEP to HSA, as reported in the second part of the thesis, gives evidence that that the structural versatility of the ligands accounts for their weak binding to HSA. At physiological pH only the small percentage of the non–hydrogen bonded stretched conformers bind to HSA. In contrast BPA, which is not affected by intramolecular hydrogen bond and it is therefore supposed to bind in a stretched conformation, has a weak affinity towards the protein when the ethylamino side chain is protonated. The affinity strongly increases when the molecule is fully de–protonated.

Obviously the structural versatility of H_1 antihistamines also opens new questions on how those ligands bind to the H_1 GPCR, since, as it is known from literature, the protonated ethylamino side chain is implicated in binding with this receptor as well.

The human H_1 receptor is a protein extremely difficult to obtain in a sufficiently purified form, and impurities generally mask the intrinsic fluorescence of the receptor. For this reason exploratory binding studies with H_1 antihistamines were conducted in the presence of HSA. Not just because it is their transport protein, but also because it has only a single tryptophan, which simplifies study of specific ligand–protein interaction by means of fluorescence and UVRR spectroscopy considerably. The experience and results obtained will be helpful for the understanding of H_1 receptor–H_1 antihistamine interactions, since it is the tryptophan residue of HSA and H_1 receptor that is implicated in H_1 antihistamine binding as well. Therefore, knowledge gained from the probe system presented in this thesis may eventually represent a reference study for

future characterization of H_1 antihistamine–GPCR interactions by means of fluorescence and UVRR spectroscopy.

Samenvatting

Inzicht krijgen in de manier waarop moleculen binden aan eiwitten is een enorme en fascinerende uitdaging. Het werk dat in dit proefschrift: “Optische methodes voor de opheldering van de structuur van eiwit–ligand interacties: een fluorescentie en UV Raman spectroscopische studie” wordt beschreven, is gewijd aan een spectroscopische karakterisering van drie belangrijke antihistamines, tripelennamine, mepyrarime en brompheniramine, en het mechanisme van hun binding aan het menselijk serum albumine HSA. De mogelijkheid om met behulp van een combinatie van luminescentie, in het bijzonder fluorescentie, en Raman spectrscopie in het ultraviolet, inzicht te krijgen in dergelijke eiwit–ligand interacties is voor het eerst onderzocht met bovengenoemde moleculen.

Antihistamines zijn medicijnen die breed worden ingezet bij menselijke aandoeningen. Ze oefenenen hun werking uit door interactie met de histamine receptor. Niettemin is er nog slechts beperkte informatie over hoe de binding aan de receptor precies plaatsvindt, en wat daarvan de directe gevolgen zijn op moleculair niveau. De bestudeerde antihistamines werken ook op het centrale zenuwstelsel, waar ze slaperigheid veroorzaken, tengevolge van hun zwakke binding aan HSA. Daardoor zijn ze in staat tot de hersenen door te dringen. Ook met betrekking tot binding aan HSA is nog slechts beperkt in-

formatie beschikbaar. Om inzicht te krijgen in de soort interacties die van belang zijn voor de binding was één van de doelen van deze studie, evenals de mogelijkheid te onderzoeken of de genoemde verbindingen bruikbaar zouden zijn bij de studie van binding aan eiwitten. Dit soort informatie is van groot belang bij het ontwikkelen van nieuwe drugs en therapieën.

Toen begonnen werd met dit onderzoek was nog slechts een beperkte hoeveelheid informatie beschikbaar over de spectroscopische eigenschappen van de genoemde antihistamines. In de zeventiger jaren van de vorige eeuw zijn enkele studies gepubliceerd waarin een aantal anomalieën werden gerapporteerd, zonder dat daarvoor een goede verklaring kon worden gegeven. Moleculen gebruiken om interacties met eiwitten te bestuderen vereist grondige kennis van hun gedrag in oplossing. Daarom wordt in het eerste deel van dit proefschrift een aanzienlijke hoeveelheid aandacht besteed aan de spectroscopische karakterisering, en opheldering van de structuur, in water bij verschillende pH waarden. Het is bekend dat de bindingseigenschappen van deze antihistamines sterk van de pH afhankelijk zijn omdat ionische interacties met groepen in het eiwit een belangrijke rol spelen.

De antihistamines bevatten allen een aantal groepen waaraan protonen kunnen binden. De waarde van de pH bepaalt welke van de groepen een proton bevatten, en welke ongeprotoneerd zijn. De belangrijkste van deze groepen, die bij alle drie genoemde antihistamines voorkomt, is een zogenaamde alkylamino staart die juist in het belangrijke pH gebied een proton kan opnemen of afstaan. Bij twee van de antihistamines, tripelennamine en mepyramine kan, als de staart geprotoneerd is, een interne brug in het molecule worden gevormd die binding aan een eiwit moeilijker maakt. Bij brompheniramine kan dat niet. Door een combinatie van technieken die in dit proefschrift uitgebreid worden beschreven zijn we in staat gebleken met behulp van absorptie, emissie en Raman verstrooiing te bepalen met welke van de vorm van deze moleculen we onder de verschillende omstandigheden te maken hebben. Het zou daardoor dan ook in principe mogelijk worden te zien welke van de vormen aan eiwit bindt.

Omdat de histamine receptor zelf nog niet in voldoend zuivere vorm geproduceerd kan worden, is binding aan een ander eiwit, HSA, bestudeerd. De methodes die hierbij ontwikkeld zijn en nog verder ontwikkeld kunnen worden, zijn algemeen genoeg om als leidraad te dienen bij latere bindingsstudies aan histamine receptoren. Een belangrijk onderdeel van HSA, het aminozuur tryptofaan, dat bij de bindingsplaats voor de antihistamines zit, komt ook in de receptor voor. De gebruikte antihistamines waren in eerste instantie geselecteerd op hun optische eigenschappen, waarbij er speciaal op was gelet dat ze onafhankelijk van tryptofaan zouden kunnen worden geobserveerd. Omdat tryptofaan ook zelf fluoresceert, en een goede Raman verstrooier is, is het zinvol te zoeken naar moleculen waarvan de eigenschappen voldoende verschillen van tryptofaan, zonder dat dat de eiwitstructuur op ongeoorloofde wijze beinvloedt bij binding. Bij de studie van binding aan HSA werd aangetoond dat de aanwezigheid van meerdere conformeren inderdaad een belangrijke rol speelt in het bindingsgedrag van deze moleculen. Verder konden ook details worden opgehelderd over specifiek moleculair gedrag, zoals de vorming van waterstofbruggen, verandering van omgevingspolariteit, en, inderdaad, welke van de conformeren van de antihistamines goed aan het eiwit binden. De kennis die we met dit systeem hebben vergaard zal ongetwijfeld een belangrijke bijdrage kunnen leveren aan toekomstige studies van binding aan de receptor zelf als die in voldoende hoeveelheid, en voldoende zuiver, ter beschikking komt.

List of publications

S. Tardioli, C. Gooijer, and G. van der Zwan, Anomalous photophysics of H_1 antihistamines in aqueous solution. *J. Phys. Chem. B*, 113(19):6949-6957 (2009).

S. Tardioli, C. Gooijer, and G. van der Zwan, Structure elucidation of fluorescent H_1 antihistamines by ultraviolet resonance Raman spectroscopy. Solvent structures of tripelennamine and mepyramine. *J. Raman Spec.*, 42(5):1016-1024 (2011). Manuscript first published online: 6 Oct. 2010.

S. Tardioli, J. Buijs, C. Gooijer, and G. van der Zwan, pH dependent complexation of Histamine H_1 receptor antagonists and HSA studied by UV resonance Raman spectroscopy. *J. Phys. Chem. B*, accepted for publication.

S. Tardioli*, I. Lammers*, J.H. Hooijschuur, F. Ariese, G. van der Zwan, and C. Gooijer, Complementary fluorescence and phosphorescence study of the interaction of brompheniramine with human serum albumin. Manuscript submitted for publication. * Both authors contributed equally.

S. Tardioli, C. Gooijer, and G. van der Zwan, UVRR spectroscopy: a distinctive probe of protein-ligand binding in solution. Manuscript submitted for publication.

Additional publications:

S. Tardioli, A. Bonincontro, C. La Mesa, and R. Muzzalupo, Interaction of bovine serum albumin with gemini surfactants, *J. Colloid Interface Sci.*, 347: 96-101 (2010).

T. Cohen-Stuart, M. Vengris, S. Tardioli, I. van Stokkum, R. Van Grondelle, Monitoring energy transfer in novel Ruthenium donor–acceptor complexes containing a phenanthroline bridge and phenol coordination cavity. Manuscript submitted for publication.

Acknowledgments

I would love to express my gratitude to my promotor, Cees Gooijer, and co–promotor, Gert van der Zwan, for the great chance they gave me. The way to graduation was filled with happy and difficult moments (hours and days as well) but anyway you were there, for talk&laughs or in case of need. I really thank you for your support, your scientific skills, good advices, enormous enthusiasm —Gert's speeches sparkling with anecdotes— your lovely country and group. You made me feel very welcome.

There are also many colleagues, students, and friends who made my life so much easier and happier during those years. Many thanks to the applied spectroscopy people, Diego, Ivonne, Joost d.K., Lineke, Cecilia, Ingeborg, Maria, Alois and Evtim. A special thank goes to Freek as well. We had really a pleasant time together! I express my gratitude to Arjan and Joost B. for the knowledge of laser setups they gently shared with me and their wholehearted help in solving (my) technical problems.

Many thanks go to the really nice students I had the pleasure to work with: Anton&Lando, Marleen, Ilona, Heleen, and last but not least, Jan–Hein (waiting for you to land on Mars!).

I also want to express gratitude to the rest of the BMA group: Ferry, Lygia, Linda, Ansgar, Jon, Martin, Kim, Jeroen, Niels&Niels. How many cakes and coffees we shared!

I wish to thank my dear friends Desy&Ste, Francesca, Alvise, Cristian, Nicola, and Simone. The time spent together was legen...wait for it...dary! Guys I will never forget you!
A special thank goes to my **f**amily —Ennio, Mariella and Paolo— for having supported me along the way and for their constant presence. Many times you tried to understand... **f**.—But what do you precisely?— S.: —well... (uncomfortable silence) how to explain this?– Hopefully now it is clearer!
And then my deepest gratitude goes to Carlo for his love and precious support.

Bibliography

[1] J.R. Lakowicz. *Principles of fluorescence spectroscopy.* Number v. 1 in Principles of Fluorescence Spectroscopy. Springer, 2006.

[2] J.M. Chalmers and P.R. Griffiths. *Handbook of vibrational spectroscopy.* Number v. 1 in Handbook of Vibrational Spectroscopy. J. Wiley, 2002.

[3] J.J. Laserna. *Modern techniques in Raman spectroscopy.* Wiley, 1996.

[4] D.A. Long. *Raman spectroscopy.* McGraw-Hill, 1977.

[5] S.A. Asher. UV resonance Raman-spectroscopy for analytical, physical, and biophysical chemistry.1. *Anal. Chem.*, 65(2):A59–A66, 1993.

[6] S.A. Asher. UV resonance Raman-spectroscopy for analytical, physical, and biophysical chemistry.2. *Anal. Chem.*, 65(4):A201–A210, 1993.

[7] J. Lakowicz and I. Gryczynski. Frequency-Domain Fluorescence Spectroscopy. In J. R. Lakowicz, C. D. Geddes, and J. Lakowicz, editors, *Topics in Fluorescence Spectroscopy*, volume 1 of *Topics in Fluorescence Spectroscopy*, pages 293–335. Springer US, 2002.

[8] A.W. Fountain, T.J. Vickers, and C.K. Mann. Factors that affect the accuracy of Raman shift measurements on multichannel spectrometers. *Appl. Spectrosc.*, 52(3):462–468, MAR 1998.

[9] A.M. Ter Laak, G.J. Bijloo, M.J.E. Fischer, G.E. Donnè op den Kelder, J. Wilting, and H. Timmerman. Serum protein binding of histamine H_1-antagonists– A comparative study on the serum protein binding of a sedating H3–mepyramine and a non-sedating H_1–antagonist H3–loratadine. *Eur. J. Pharm. Sci.*, 4:307–319, 1996.

[10] T. Peters. Serum-Albumin. *Advances in protein Chemistry*, 37:161–245, 1985.

[11] J. Ghuman, P.A. Zunszain, I. Petitpas, A.A. Bhattacharaya, M. Otagiri, and S. Curry. Structural basis of the drug–binding specificity of human serum albumin. *J. Mol. Biol.*, 353:38–52, 2005.

[12] X.M. He and D.C. Carter. Atomic structure and chemistry of human serum albumin. *Nature*, 538:209–215, 1992.

[13] E.A. Burstein, N.S. Vedenkin , and M.N. Ivkova. Fluorescence and location Of tryptophan residues in protein molecules. *Photochem. Photobiol.*, 18(4):263–279, 1973.

[14] M.L. Saviotti and W.C Galley. Room-temperature phosphorescence and dynamic aspects Of protein structure. *PNAS*, 71(10):4154–4158, 1974.

[15] M.R. Eftink and C.A. Ghiron. Fluorescence quenching studies with proteins. *Anal. Biochem.*, 114(2):199–227, 1981.

[16] R. Leurs, M.K. Church, and M. Taglialatela. H_1–antihistamines: inverse agonism, anti–inflammatory actions and cardiac effects. *Clin. Exp. Allergy*, 32:489–498, 2002.

[17] F. Estelle and R. Simons. Advances in H_1 antihistamines. *New Engl. J. Med.*, 351:2203–2217, 2004.

[18] T. Shimamura, M. Shiroishi, S. Weyand, H. Tsujimoto, G. Winter, V. Katritch, V. Abagyan, R.and Cherezov, G.Won Liu, W.and Han, T. Kobayashi, R.C. Stevens, and S. Iwata. Structure of the human histamine H_1 receptor complex with doxepin. *Nature*, 475(7354):65–U82, 2011.

[19] K. Wieland, A.M. Ter Laak, M.J. Smit, R. Kühne, H. Timmerman and R. Leurs. Mutational analysis of the antagonist-binding site of the histamine H_1 receptor. *J. Biol. Chem.*, 274(42):29994–30000, 1999.

[20] K. Ohta, H. Hayashi, H. Mizuguchi, H. Kagamiyama, K. Fujimoto, and H. Fukui. Site–directed mutagenesis of the histamine H_1 receptor: roles of aspartic acid^{1}07, asparagine^{1}98 and threonine^{1}94. *Biochem. Bioph. Res. Co.* , 203:1096–1101, 1994.

[21] A. Jongejan, M. Bruysters, J.A. Ballesteros, E. Haaksma, R.A. Bakker, L. Pardo, and R. Leurs. Linking agonist binding to histamine H_1 receptor activation. *Nature Chem. Biol.*, 1(2):98–103, 2005.

[22] N. Tarcea, M. Harz, P. Roesch, T. Frosch, M. Schmitt, H. Thiele, R. Hochleitner, and J. Popp. UV Raman spectroscopy– A technique for biological and mineralogical in situ planetary studies. *Spectrochim. Acta A*, pages 1029–1035, 2007.

[23] E.V. Efremov, F. Ariese, and C. Gooijer. Achievements in resonance Raman spectroscopy: review of a technique with a distinct analytical chemistry potential. *Anal. Chim. Acta*, 606:119–134, 2007.

[24] A.M. Kelley. Resonance Raman and resonance hyper–Raman intensities: Sstructure and dynamics of molecular excited states in solution. *J. Phys. Chem. A*, 112(47):11975–11991, 2008.

[25] T.G. Spiro and P. Stein. Resonance effects in vibrational scattering from complex–molecules. *Annu. Rev. Phys. Chem.*, 28:501–521, 1977.

[26] C.M. Jones, T.A. Naim, M. Ludwig, J. Murtaugh, P.L. Flaugh, J.M. Dudik, C.R. Johnson, and S.A. Asher. Analytical applications of ultraviolet resonance Raman–spectroscopy. *Trac–Trend Anal. Chem.*, 4(3):75–80, 1985.

[27] C.Y. Huang, G. Balakrishnan, and T.G. Spiro. Protein secondary structure from deep–UV resonance Raman spectroscopy. *J. Raman Spec.*, 37(1-3):277–282, 2006.

[28] S.A. Asher and C.R. Johnson. Raman–spectroscopy of a coal liquid shows that fluorescence interference ss minimized with ultraviolet excitation. *Science*, 225(4659):311–313, 1984.

[29] S.P.A. Fodor, R.P. Rava, T.R. Hays, and T.G. Spiro. Ultraviolet resonance Raman–spectroscopy of the nucleotides with 266-nm, 240-nm, 218-nm, and 200-nm pulsed laser excitation. *J. Am. Chem. Soc.*, 107(6), 1985.

[30] S.A. Asher, M Ludwig, and CR Johnson. UV Resonance Raman Excitation Profiles of the Aromatic Amino acids. *J. Am. Chem. Soc.*, 108(12):3186–3197, 1986.

[31] J.A. Sweeney and S.A. Asher. Tryptophan UV resonance Raman excitation profiles. *J. Phys. Chem.*, 94(12):4784–4791, 1990.

[32] R.E. Littleford, D. Cunningham, P. Matousek, M. Towrie, A.W. Parker, I. Khan, D. McComb, and W.E. Smith. Surface–enhanced resonance Raman scattering using pulsed and continuous-wave laser excitation. *J. Raman Spec.*, 36(6-7):600–605, 2005.

[33] T. Kitagawa. Investigation of higher order structures of proteins by Ultraviolet resonance Raman spectroscopy. *Prog. Biophys. Mol. Bio.*, 58(1):1–18, 1992.

[34] S.A. Asher, R.W. Bormett, X.G. Chen, D.H. Lemmon, N. Cho, P. Peterson, M. Arrigoni, L. Spinelli, and J. Cannon. UV resonance Raman–spectroscopy using a new CW laser source - convenience and experimental simplicity. *Appl. Spectrosc.*, 47(5):628–633, 1993.

[35] G. Balakrishnan, Y. Hu, S.B. Nielsen, and T.G. Spiro. Tunable kHz deep ultraviolet (193–210 nm) laser for Raman applications. *Appl. Spectrosc.*, 59(6):776–781, 2005.

[36] S. Bykov, I. Lednev, A. Ianoul, A. Mikhonin, C. Munro, and S.A. Asher. Steady-state and transient ultraviolet resonance Raman spectrometer for the 193–270 nm spectral region. *Appl. Spectrosc.*, 59(12):1541–1552, 2005.

[37] S.H. Song and S.A. Asher. Internal intensity standards for heme protein UV resonance Raman studies – excitation profiles of cacodylic acid and sodium selenate. *Biochemistry*, 30(5):1199–1205, 1991.

[38] J.M. Dudik, C.R. Johnson, and S.A. Asher. Wavelength dependence of the pre–resonance Raman cross-sections of $CH3CN$, $SO4^{-2}$, $CLO4^{-}$, and $NO-3$. *J. Chem. Phys.*, 82(4):1732–1740, 1985.

[39] S.P.A. Fodor, R.A. Copeland, C.A. Grygon, and T.G. Spiro. Deep-ultraviolet Raman excitation profiles and vibronic scattering mechanisms of phenylalanine, tyrosine, and tryptophan. *J. Am. Chem. Soc.*, 111(15):5509–5518, 1989.

[40] C.R. Johnson, M. Ludwig, S. Odonnell, and S.A. Asher. UV resonance Raman–spectroscopy of the aromatic–amino–acids and myoglobin. *J. Am. Chem. Soc.*, 106(17):5008–5010, 1984.

[41] J.M. Dudik, C.R. Johnson, and S.A. Asher. UV resonance Raman studies of Acetone, Acetamide, And N–Methylacetamide Models For The Peptide–Bond. *J. Phys. Chem.* , 89(18):3805–3814, 1985.

[42] R.P. Rava and T. Spiro. Resonance enhancement in the Ultraviolet Raman spectra of aromatic amino acids. *J. Phys. Chem.*, 89:1856–1861, 1985.

[43] M. Ludwig and S.A. Asher. Ultraviolet resonance Raman excitation profiles of tyrosine - dependence of Raman cross–sections on excited–state intermediates. *J. Am. Chem. Soc.*, 110(4):1005–1011, 1988.

[44] M. Matsuno and H. Takeuchi. Effects of hydrogen bonding and hydrophobic interactions on the ultraviolet resonance Raman intensities of indole ring vibrations. *B. Chem. Soc. JPN*, 71(4):851–857, 1998.

[45] T. Miura, H. Takeuchi, and I. Harada. Tryptophan Raman bands sensitive to hydrogen bonding and side–chain conformation. *J. Raman Spec.*, 20:667–671, 1989.

[46] I. Harada, T. Miura, and H. Takeuchi. Origin of the doublet at 1360 and 1340 cm^{-1} in the Raman spectra of tryptophan and related compounds. *Spectrochim. Acta*, 42A:307–312, 1986.

[47] D.E. Schlamadinger, J.E. Gable, and J.E. Kim. Hydrogen bonding and solvent polarity markers in the UV resonance Raman spectrum of tryptophan: application to membrane proteins. *J. Phys. Chem. B*, 113:14769–14778, 2009.

[48] P.G. Hildebrandt, R.A. Copeland, T.G. Spiro, J. Otlewsky, M. Laskowsky, and F.G. Prendergast. Tyrosine hydrogen-bonding and environmental-effects in proteins probed by ultraviolet resonance Raman–spectroscopy. *Biochemistry*, 27(15):5426–5433, 1988.

[49] G.K. Pieridou and S.C. Hayes. UV resonance Raman spectroscopy of TTR(105-115): determination of the pK_a of tyrosine. *Phys. Chem. Chem. Phys.*, 11(26):5302–5309, 2009.

[50] S. Hashimoto, T. Yabusaki, H. Takeuchi, and I. Harada. Structure and ligand-binding modes of human serum albumin studied by UV resonance raman spectroscopy. *Biospectroscopy*, 1:375–385, 1992.

[51] X.J. Zhao, D.J. Wang, and T.G. Spiro. A UV resonance Raman monitor of histidine protonation in proteins: Bohr protons in hemoglobin. *J. Am. Chem. Soc.*, 120(33):8517–8518, 1998.

[52] J. Bandekar. Amide modes and protein conformation. *Biochim. Et Biophys. Acta*, 1120(2):123–143, 1992.

[53] A. Ianoul, M.N. Boyden, and S.A. Asher. Dependence of the peptide amide III vibration on the ϕ dihedral angle. *J. Am. Chem. Soc.*, 123(30):7433–7434, 2001.

[54] S.A. Asher, A.V. Mikhonin, and S. Bykov. UV Raman demonstrates that α-helical polyalanine peptides melt to polyproline II conformations. *J. Am. Chem. Soc.*, 126(27):8433–8440, 2004.

[55] V.A. Shashilov, V. Sikirzhytski, L.A. Popova, and I.K. Lednev. Quantitative methods for structural characterization of proteins based on deep UV resonance Raman spectroscopy. *Methods*, 52(1):23–37, 2010.

[56] S.H. Song and S.A. Asher. UV resonance Raman studies of peptide conformation in poly(L-Lysine), poly(L-Glutamic Acid), and Model Complexes - The Basis for Protein Secondary Structure Determinations. *J. Am. Chem. Soc.*, 111(12):4295–4305, 1989.

[57] S.P.A. Fodor and T.G. Spiro. Ultraviolet resonance Raman-spectroscopy of DNA with 200-266-nm laser excitation. *J. Am. Chem. Soc.*, 108(12):3198–3205, 1986.

[58] Z.H. Chi, X.G. Chen, J.S.W. Holtz, and S.A. Asher. UV resonance Raman–selective amide vibrational enhancement: quantitative methodology for determining protein secondary structure. *Biochemistry*, 37(9):2854–2864, 1998.

[59] S. Tardioli, J. Buijs, C. Gooijer, and G. van der Zwan. pH dependent complexation of Histamine H_1 receptor antagonists and HSA studied by UV resonance raman spectroscopy. *Accepted for publication, J. Phys. Chem. B.*

[60] J. Clarkson and D.A. Smith. UV Raman evidence of a tyrosine in apo-human serum transferrin with a low pK_a that is elevated upon binding of sulphate. *FEBS Letters*, 503(1):30–34, 2001.

[61] R. Tuma. Raman spectroscopy of proteins: from peptides to large assemblies. *J. Raman Spec.*, 36(4):307–319, 2005.

[62] P.R. Carey and P.J. Tonge. Unlocking the secrets of enzyme power uding Raman–spectroscopy. *Accounts Chem. Res.*, 28(1):8–13, 1995.

[63] V.W. Couling, P. Fischer, D. Klenerman, and W. Huber. Ultraviolet resonance Raman study of drug binding in dihydrofolate reductase, gyrase, and catechol O–methyltransferase. *Biophys. J.*, 75(2):1097–1106, 1998.

[64] F.H. Vaillancourt, C.J. Barbosa, T.G. Spiro, J.T. Bolin, M.W. Blades, R.F.B. Turner, and L.D. Eltis. Definitive evidence for monoanionic binding of 2,3–dihydroxybiphenyl to 2,3-dihydroxybiphenyl 1,2–dioxygenase from UV resonance Raman spectroscopy, UV-Vis absorption spectroscopy, and crystallography. *J. Am. Chem. Soc.*, 124(11):2485–2496, 2002.

[65] J.G. Harman. Allosteric regulation of the cAMP receptor protein. *BBA-Protein Struct. M.*, 1547(1):1–17, 2001.

[66] N. Fujimoto, A. Toyama, and H. Takeuchi. Binding modes of cyclic AMP and environments of tryptophan residues in 1:1 and 1:2 complexes of cyclic AMP receptor protein and cyclic AMP. *Biopolymers*, 67(3):186–196, 2002.

[67] JM Benevides, S.A. Overman, and GJ Thomas. Raman, polarized Raman and ultraviolet resonance Raman spectroscopy of nucleic acids and their complexes. *J. Raman Spec.*, 36(4):279–299, 2005.

[68] T.G. SPIRO. Resonance Raman spectroscopic studies of heme proteins. *Biochim. Biophys. Acta*, 416(2):169–189, 1975.

[69] T.G. SPIRO. Resonance Raman–spectroscopy as a probe of heme protein-structure and dynamics. *Adv. Protein Chem.*, 37:111–159, 1985.

[70] N. Haruta, M. Aki, S. Ozaki, Y. Watanabe, and T. Kitagawa. Protein conformation change of myoglobin upon ligand binding probed by ultraviolet resonance Raman Spectroscopy. *Biochemistry*, 40(23):6956–6963, 2001.

[71] X.J. Zhao and T.G. Spiro. Ultraviolet resonance Raman spectroscopy of hemoglobin with 200 and 212 nm excitation: H-bonds of tyrosines and prolines. *J. Am. Chem. Soc.*, 29(1):49–55, 1998.

[72] K.R. Rodgers, C. Su, S. Subramaniam, and T.G. Spiro. Hemoglobin R–T structural dynamics from simultaneous monitoring Of tyrosine and tryptophan time-resolved UV resonance Raman signals. *J. Am. Chem. Soc.*, 114(10):3697–3709, 1992.

[73] S.C. Huang, J. Huang, A.P. Kloek, D.E. Goldberg, and J.M. Friedman. Hydrogen bonding of tyrosine b10 to heme-bound oxygen in Ascaris hemoglobin - Direct evidence from UV resonance Raman spectroscopy. *J. Biol. Chem.*, 271(2):958–962, 1996.

[74] Z.Q. Wen, A. Armstrong, and G.J. Thomas. Demonstration by ultraviolet resonance Raman spectroscopy of differences in DNA organization and interactions in filamentous viruses Pf1 and fd. *Biochemistry*, 38(10):3148–3156, 1999.

[75] E.B. Wilson. The normal modes and frequencies of vibration of the regular plane hexagon model of the benzene molecule. *Phys. Rev.*, pages 706–714, 1934.

[76] R.J. Middleton and B. Kellam. Fluorophore–tagged GPCR ligands. *Curr. Opin. Chem. Biol.*, 9:517–525, 2005.

[77] D.L. Wilson, D.R. Wirz, and G.H. Schenk. Fluorescence and phosphorescence of antihistamines having the 2–aminopyridine chromophore. Effect of pH on fluorescence. *Anal. Chem.*, 45:1447–1455, 1973.

[78] N.S. Ham. Solution conformation of antihistamines. *J. Pharm. Sci.*, 60:1764–1765, 1971.

[79] A.M. Ter Laak, A.M.G.M. Donné–Op den Kelder, A. Bast, and H. Timmerman. Is there a difference in the affinity of histamine H_1 receptor antagonists for CSN and peripheral receptors? An *in vitro* study. *Eur. J. Pharm.*, 232:199–205, 1993.

[80] A.R. Katritzky and R.E. Reavill. Applications of proton resonance spectroscopy to structural problems. 21. Cations of thiopyridones and aminopyridines. *J. Chem. Soc.*, 71:3825–3827, 1965.

[81] P. Forsythe, R. Frampton, C.D. Johnson, and A.R. Katritzky. Acidity function and the protonation of weak bases. Part VII. The protonation behavior of dimethylaminopyridines and their N–Oxides. *J. Chem. Soc. Perkin Transactions II*, 5:671–673, 1972.

[82] A. Weisstuch and A.C. Testa. A fluorescence study of aminopyridines. *J. Phys. Chem.*, 78:1982–1987, 1968.

[83] A. Weisstuch and A.C. Testa. Fluorescence study of 2–(N,N–dimethylamino)pyridine and related molecules. *J. Phys. Chem.*, 74:2299–2303, 1970.

[84] T.M. Krygowski, H. Szatylowicz, and J.E. Zachara. How H–bonding modifies molecular structure and π–electron delocalization in the ring of pyridine-pyridinium derivatives involved in H–bond complexation. *J. Org. Chem.*, 70:8859–8865, 2005.

[85] R.S. Byrn, C.W. Graber, and S.L. Midland. Comparison of solid and solution conformations of methapyriline, tripelennamine, diphenydramine, histamine and choline. Infrared–X–Ray method for determination of solution conformations. *J. Org. Chem.*, 41:2283–2288, 1976.

[86] A Kania, BM Nowak-Wydra, Szafran, and ZD Szafran. UV,^{1}H and ^{13}C NMR spectra and AM1 studies of protonation of aminopyridines. *J. Mol. Struct.*, 322:223–232, 1994.

[87] S. Tardioli, C. Gooijer, and G van der Zwan. Structure elucidation of fluorescent H_1 Antihistamines by ultraviolet resonance Raman spectroscopy. *J. Raman Spec.*, 42:1016–1024, 2011.

[88] H.B. Klevens and J.R. Platt. Geometry and spectra of substituted anilines. *J. Am. Chem. Soc.*, 71:1714–1720, 1949.

[89] A.C. Testa and U.P. Wild. Inversion of close lying n-π and π-π^{**} states in 2–Aminopyridine by protonation. A CNDO Study. *J. Phys. Chem.*, 85:2637–2639, 1981.

[90] K. Kimura, H. Tsubomura, and S. Nagakura. The vacuum ultraviolet absorption spectra of aniline and some of its N–Derivatives. *Bull. Chem. Soc. Japan*, 37:1336–1346, 1964.

[91] C.R. Cantor and P.R. Schimmel. *Biophysical Chemistry. II. Techniques for the Study of Biological Structure and Function.* W.H. Freeman and Company, San Fransisco, 1980.

[92] A. Jongejan. Personal communication.

[93] D. Attwood and O.K. Udeala. Aggregation of antihistamines in aqueous solution. Self–association of some pyridine derivatives. *J. Phys. Chem.*, 79:889–892, 1975.

[94] E.D. Raczynska, M. Darowska, T. Rudka, and M. Makowski. Tautomerism of neutral and monoprotonated histamine–a comparison of semi-empirical and *ab initio* quantum mechanical predictions for "'essential"' and "'scorpio"' conformations. *J. Phys. Org. Chem.*, 14:770–777, 2001.

[95] NS Ham. Solution conformations of histamine and some related derivatives. *J. Med. Chem.*, 16:470–475, 1973.

[96] J. Neugebauer, E.J. Baerends, E.V. Efremov, F. Ariese, and C. Gooijer. Combined theoretical and experimental deep–UV resonance Raman studies of substituted pyrenes. *J. Phys. Chem. A*, 109:2100–2106, 2005.

[97] S. Tardioli, C. Gooijer, and G. van der Zwan. Anomalous photophysics of H_1 antihistamines in aqueous solution. *J. Phys. Chem. B*, 113:6949–6957, 2009.

[98] P. Carmona, M. Molina, and R. Escobar. Studies on aminopyridines in aqueous solution by laser Raman spectroscopy. *Spectrochim. Acta*, 49A:1–9, 1993.

[99] M. J. Frisch, G. W. Trucks, H. B. Schlegel, G. E. Scuseria, M. A. Robb, J. R. Cheeseman, J. A. Montgomery, Jr., T. Vreven, K. N. Kudin, J. C. Burant, J. M. Millam, S. S. Iyengar, J. Tomasi, V. Barone, B. Mennucci, M. Cossi, G. Scalmani, N. Rega, G. A. Petersson, H. Nakatsuji, M. Hada, M. Ehara, K. Toyota, R. Fukuda, J. Hasegawa, M. Ishida, T. Nakajima, Y. Honda, O. Kitao, H. Nakai, M. Klene, X. Li, J. E. Knox, H. P. Hratchian, J. B. Cross, V. Bakken, C. Adamo, J. Jaramillo, R. Gomperts, R. E. Stratmann, O. Yazyev, A. J. Austin, R. Cammi, C. Pomelli, J. W. Ochterski, P. Y. Ayala, K. Morokuma, G. A. Voth, P. Salvador, J. J. Dannenberg, V. G. Zakrzewski, S. Dapprich, A. D. Daniels, M. C. Strain, O. Farkas, D. K. Malick, A. D. Rabuck, K. Raghavachari, J. B. Foresman, J. V. Ortiz, Q. Cui, A. G. Baboul, S. Clifford, J. Cioslowski, B. B. Stefanov, G. Liu, A. Liashenko, P. Piskorz, I. Komaromi, R. L. Martin, D. J. Fox, T. Keith, M. A. Al-Laham, C. Y. Peng,

A. Nanayakkara, M. Challacombe, P. M. W. Gill, B. Johnson, W. Chen, M. W. Wong, C. Gonzalez, and J. A. Pople. Gaussian 03, Revision B.04. Gaussian, Inc, Wallingford CT 2004,.

[100] J.B. Foresman and A. Frisch. *Exploring chemistry with electronic structure methods 2nd edition*. Gaussian, Inc, Pittsburgh,PA, 1996.

[101] D. Cook. Vibrational spectra of pyridinium salts. *Can. J. Chem.*, 39:2009–2024, 1961.

[102] J.H.S. Green, W. Kynaston, and H.M. Paisley. Vibrational spectra of monosubstituted pyridines:. *Spectrochim. Acta*, 19:549–564, 1963.

[103] J. Lorenc, I. Bryndal, M. Marchewka, W. Sasiadek, T. Lis, and J. Hanuza. Crystal and molecular structure of 2–aminopyridinium-4–hydroxybenzenosulfonate - IR and Raman spectra, DFT calculations and physicochemical properties. *J. Raman Spec.*, 39:569–581, 2008.

[104] P.J. Sujin and S. Mohan. Vibrational spectra and normal co-ordinate analysis of 2–aminopyridine and 2–amino picoline. *Spectrochim. Acta A*, 64:240–245, 2006.

[105] O. Poizat, V. Guichard, and G. Buntinx. Vibrational studies of reactive intermediates of aromatic amines. Radical cation time resolved resonance Raman investigation of N,N–Dimethylaniline and N,N–Diethylaniline derivatives. *J. Chem. Phys.*, 90:14697–4703, 1989.

[106] V. Guichard, A. Bourkba, M.F. Lautie, and O. Poizat. Vibrational spectra of N,N–Dimethyl/Diethylaniline, N,N,N',N'–Tetramethyl/Tetraethyl–p–Phenylenediamine and N,N,N',N'–Tetramethyl/Tetrahethylbenzidine Derivatives. *Spectrochim. Acta*, 45A:187–201, 1989.

[107] A.M. Brouwer and R. Wilbrandt. Vibrational spectra of N,N–Dimethylaniline and its radical cation. An interpretation based on quantum chemical calculations. *J. Phys. Chem.*, 100:9678–9688, 1996.

[108] A. Varshney, P. Sen, E. Ahmad, M. Rehan, N. Subbarao, and R.H. Khan. Ligand binding strategies of human serum albumin: how can the cargo be utilized? *Chirality*, 22(1):77–87, JAN 2010.

[109] M. Dockal, D.C. Carter, and F. Ruker. The three recombinant domains of human serum albumin - Structural characterization and ligand binding properties. *J. Biol. Chem.*, 274(41):29303–29310, 1999.

[110] A. Sulkowska. Interaction of drugs with bovine and human serum albumin. *J. Mol. Struct.*, 614(1-3, Sp. Iss. SI):227–232, SEP 2 2002.

[111] M.A. Martinez–Gomez, M.M. Carril–Aviles, S. Sagrado, R.M. Villanueva–Camanas, and M.J. Medina–Hernandez. Characterization of antihistamine-human serum protein interactions by capillary electrophoresis. *J. Chrom. A*, 1147(2):261–269, 2007.

[112] M.A. Martinez–Gomez, S. Sagrado, R.M. Villanueva–Camanas, and M.J. Medina–Hernandez. Characterization of basic drug-human serum protein interactions by capillary electrophoresis. *Electrophoresis*, 27(17):3410–3419, 2006.

[113] M.J. Yoo, J.E. Schiel, and D.S. Hage. Evaluation of affinity microcolumns containing human serum albumin for rapid analysis of drug–protein binding. *J. Chrom. B*, 878(20):1707–1713, 2010.

[114] G. Sudlow, D.J. Birkett, and D.N. Wade. Spectroscopic techniques in study of protein-binding– Fluorescence technique for evaluation of albumin binding and displacement of warfarin and warfarin–alcohol. *Clin. Exp. Pharmacol. P.*, 2(2):129–140, 1975.

[115] D.B. Calhoun, J.M. Vanderkooi, and S.W. Englander. Penetration of small molecules into proteins studied by quenching of phosphorescence and fluorescence. *Biochemistry*, 22(7):1533–1539, 1983.

[116] M.R. Eftink and L.A. Selvidge. Fluorescence quenching of liver alcohol-dehydrogenase by acrylamide. *Biochemistry*, 21(1):117–125, 1982.

[117] J. Gonzalez–Jimenez, G. Frutos, I. Cayre, and M. Cortijo. Chlorpheniramine binding to human serum-albumin by fluorescence quenching measurements. *Biochimie*, 73(5):551–556, 1991.

[118] Y. Wei, C. Dong, D. Liu, S. Shuang, and C.W. Huie. Enantioselective quenching of room-temperature phosphorescence lifetimes of proteins: bovine and human serum albumins. *Biomacromolecules*, 8(3):761–764, MAR 2007.

[119] P. Cioni, E. Gabellieri, M. Gonnelli, and G.B. Strambini. Heterogenity of protein conformation in solution from the lifetime of tryptophan phosphorescence. *Biophys. Chem.*, 52(1):25–34, 1994.

[120] B.D. Schlyer, J.A. Schauerte, D.G. Steel, and A. Gafni. Time-resolved room-temperature protein phosphorescence - nonexponential decay from single emitting tryptophans. *Biophys. J.*, 67(3):1192–1202, 1994.

[121] M.J. Telepchak, G. Chaney, and T.F. August. *Forensic and clinical applications of solid phase extraction*. Forensic science and medicine. Humana Press, 2004.

[122] M. Amiri, K. Jankeje, and J.R. Albani. Characterization of human serum albumin forms with pH. Fluorescence lifetime studies. *J. Pharm. Biom. Anal.*, 51:1097–1102, 2010.

[123] T. Otosu, E. Nishimoto, and S. Yamashita. Multiple conformational state of human serum albumin around single tryptophan residue at various pH revealed by time–resolved fluorescence spectroscopy. *J. Biochem.*, 147:191–200, 2010.

[124] X.M. He and D.C. Carter. Atomic structure and chemistry of human serum albumin. *Nature*, 538:209–215, 1992.

[125] M.E. Capella–Peiro, A. Bossi, and J. Esteve–Romero. Optimization by factorial design of a capillary zone electrophoresis method for the sSimultaneous separation of antihistamines. *Anal. Biochem.*, 352:41–49, 2006.

[126] M. Rambla–Alegre, J. Peris–Vicente, J. Esteve–Romero, M.E. Capella–Peiro, and D. Bose. Capillary electrophoresis determination of antihistamines in serum and pharmaceuticals. *Anal. Chim. Acta*, 666(1-2):102–109, 2010.

[127] K. Yamasaki, T. Maruyama, K. Yoshimoto, Y. Tsutsumi, R. Narazaki, A. Fukuhara, U. Kragh–Hansen, and M. Otagiri. Interactive binding to the two principal ligand binding sites of human serum albumin: effect of the neutral–to–base transition. *Biochim. Biophys. Acta*, 1432:313–323, 1999.

[128] J. Neugebauer, E.J. Baerends, E.V. Efremov, F. Ariese, and C. Gooijer. Combined theoretical and experimental deep–UV resonance Raman studies of substituted pyrenes. *J. Phys. Chem. A*, 109:2100–2106, 2005.

[129] R.J.L. Andon, J.D. Cox, and , E.F.G. Herington. The ultraviolet absorption spectra and dissociation constants of certain pyridine bases in aqueous solution. *Trans. Faraday Soc.*, 50:918–927, 1954.

[130] Z.H. Chi and S.A. Asher. UV Raman determination of the environment and solvent exposure of tyr and trp residues. *J. Phys. Chem. B*, 102:9595–9602, 1998.

[131] S. Hashimoto, T. Yabusaki, H. Takeuchi, and I. Harada. Structure and ligand–binding modes of human serum albumin studied by UV resonance Raman Spectroscopy. *Biospectroscopy*, 1:375–385, 1992.

[132] M. Matsuno and H. Takeuchi. Effects of hydrogen bonding and hydrophobic interactions on the ultraviolet resonance Raman intensities of indole ring vibrations. *B. Chem. Soc. Jpn*, 71:851–857, 1998.

[133] R.P. Rava and T. Spiro. Resonance enhancement in the ultraviolet Raman spectra of aromatic amino acids. *J.Phys. Chem.*, 89:1856–1861, 1985.

[134] J.A. Sweeney and S.A. Asher. Tryptophan UV resonance Raman excitation profiles. *J. Phys. Chem.*, 94:4784–4791, 1990.

[135] Z.H. Chi, X.G. Chen, J.S.W. Holtz, and S.A. Asher. UV resonance Raman–selective amide vibrational enhancement: quantitative methodology for determining protein secondary structure. *Biochemistry*, 37:2854–2864, 1998.

[136] N.J. Cho and S.A. Asher. UV resonance Raman and absorption studies of angiotensin II conformation in lipid environments. *Biospectroscopy*, 2:71–82, 1996.

[137] T. Miura, H. Takeuchi, and I. Harada. Tryptophan Raman bands sensitive to hydrogen bonding and side–chain conformation. *J. Raman Spec.*, 20:667–671, 1989.

[138] F.P. Urena, M.F. Gomez, J.J.L. Gonzalez, and E.M. Torres. A new insight into the vibrational analysis of pyridine. *Spectrochim. Acta A*, 59(12):2815–2839, 2003.